UNIVERSITY OF CALIFORNIA
SANTA CRUZ

EXPLORATION OF *SCHISTOSOMA MANSONI* HAMMERHEAD RIBOZYME CATALYSIS AND STRUCTURE: TOWARDS DIRECT OBSERVATION OF CLEAVAGE AND LIGATION, AND A 1.55 Å FULL-LENGTH MG^{2+}-BOUND CRYSTAL STRUCTURE

A dissertation submitted in partial satisfaction of the requirements for the degree of

DOCTOR OF PHILOSOPHY

in

CHEMISTRY AND BIOCHEMISTRY

by

Michael Harrison Anderson

December 2012

The Dissertation of Michael H. Anderson
is approved:

_____
Professor William G. Scott, Research Advisor

_____
Professor Glenn L. Millhauser, Chair

_____
Professor Roger G. Linington

_____
Tyrus Miller
Vice Provost and Dean of Graduate Studies

TABLE OF CONTENTS

LIST OF FIGURES

LIST OF SCHEMES

LIST OF TABLES

EXPLORATION OF *SCHISTOSOMA MANSONI* HAMMERHEAD RIBOZYME CATALYSIS AND STRUCTURE: TOWARDS DIRECT OBSERVATION OF CLEAVAGE AND LIGATION, AND A 1.55 Å FULL-LENGTH MG^{2+}-BOUND CRYSTAL STRUCTURE

Michael Harrison Anderson

ABSTRACT

As a relatively simple and well-studied molecule, the hammerhead ribozyme is an ideal system to study RNA catalysis and structure. A deeper understanding of the hammerhead catalytic mechanism and the role of divalent ions in catalysis lends support to the exploration of more complex RNA machinery such as the ribosome, and ultimately may assist in the design of new medical therapies. Kinetic study of the hammerhead ribozyme to date has largely derived from bulk assays monitoring millions of molecules. In contrast to such studies, which necessarily report average rates, the magnetic tweezers assay undertaken here reveals the heterogenous characteristics of individual RNA molecules in real time. The crystal structure described in the later portion of this study advances a secondary aim concerning the study of the same full-length *Schistosoma Mansoni* subject; unmasking the role of physiologically relevant metal ions in full-length hammerhead catalysis.

The single molecule study presented reveals that supercoiled DNA embedded with a nucleolytic ribozyme acts in much the same way as supercoiled DNA.

Because the ribozyme is embedded in long DNA handles, the product strands of the ribozyme cannot dissociate, and the ligation rate consequently becomes more significant. This permits us to suggest that in their natural context, hammerheads may well favor the ligated state, and may cleave in response to some form of structural perturbation. This assay also conforms with a growing corpus of evidence suggesting RNA utilizes greater conformational freedom to overcome limited chemical diversity.

The crystal structure described in Chapter 3 represents the highest-resolution structure of any reported hammerhead ribozyme to date (1.55 Å resolution). With this improved resolution, new local rearrangements and hydrogen bonding interactions within the loop/bulge region are clear. In addition, the new structure demonstrates that a divalent metal ion does indeed occupy the A9/G10.1, in addition to two peripheral sites in Stem I and III. Crystal soaking experiments were not able to detect a metal ion at these sites in the 2006 structure. These findings suggest that physiologically relevant divalent ions like Mg^{2+} may stabilize global folding of the full-length hammerhead and provide charge neutralization during the cleavage reaction.

I dedicate this dissertation to:

My loving and supportive family

ACKNOWLEDGMENTS

My dissertation committee: Prof. Scott, thank you, I am grateful for your support and guidance. Prof. Millhauser, thank you for being my chair and providing many insights over the years. Roger, I am happy to see your lab flourish since your lab initiated 5 years ago.

To my labmates: Eric, Jaime, Nate, Eric S, Brandon, Chad, Salina. Thanks for all your support over the years.

xx

Family: Mom, Dad and Megan, I love you all. I am thankful for my wonderful immediate and extended family. Thank you for all the support.

CHAPTER 1

Introduction to Hammerhead Ribozyme Catalysis and Structure

1.1 Catalytic RNA

The discovery of messenger RNA in the 1950s established its importance as an information carrying intermediate, yet it was another decade before the field considered its catalytic potential (Volkin and Astrachan, 1956) (Crick, 1968; Orgel, 1968; Woese, 1967). The RNA era was born in 1982 with the nearly simultaneous discovery of catalytic RNA in RNaseP and the pre-ribosomal RNA (group I intron) of *Tetrahymena* by Sidney Altman and Thomas Cech, respectively (Guerrier-Takada et al., 1983) (Kruger et al., 1982). Prior to these discoveries, it was assumed that proteins were the only biopolymers that contained sufficient chemical heterogeneity to catalyze biochemical reactions. In the last twenty-five years, the importance of RNA to all of biology has become increasing evident as new specimens of catalytic RNAs are discovered and insights into their mechanistic strategies are unraveled.

Many of the natural ribozymes analyzed to date are quite simple in structure and function, and even in the absence of cofactors and metal ions are often able to perform complex chemical reactions. Indeed, the ability of RNA enzymes to achieve this level of catalytic enhancement could reflect fundamental aspects of catalysis common to all enzymes, including proteins.

The observation that RNA acts as a genetic storage medium, a catalytic machine, and is responsible for catalysis of polypeptide chains led to an elegant hypothesis that considers RNA the original self-replicating biomolecule. Similarly, it has been suggested that proteins have slowly been replacing their RNA counterparts

throughout evolution, benefiting from a more expansive set of residues and a wider range of functional pKa values.

Ribozymes take part in a variety of biochemical reactions including peptidyl transfer, tRNA maturation, self-splicing, regulation of translation in Gram-positive bacteria, and processing of replication intermediates in plant pathogenic RNAs via rolling-circle replication. (Steitz et al, 2003; Kruger et al, 1982; Prody et al., 1986). In the rolling-circle mechanism, hammerhead and hairpin ribozymes self-cleave the long multigenomic RNA strand into single genomes. The hammerhead then serves to recircularize these single genomes to continue the replication cycle. The hammerhead has also been proposed to function as the RNA ligase where it reacts in *cis* on a linear RNA to give the circular genome. (Buzayan, 1986). It is also possible that a host protein or proteins assists in this ligation reaction under physiological conditions.

The hammerhead ribozyme belongs to the group of small catalytic RNAs that includes the hairpin, VS, and HDV ribozymes. First identified in avocado sunblotch viroid (ASBVd) and in a satellite RNA (Hutchins et al, 1986; Prody et al., 1986), the hammerhead ribozyme belongs to a category of single stranded RNA particles that infects plants and appear to have no coding capacity. Hammerhead ribozymes have also been found embedded in the genomes of thousands of complex organisms such as humans, primates, blood flukes, salamanders and crickets, although the function of the ribozymes in many of these organisms remains unknown (Epstein and Gall, 1987; Ferbeyre et al., 1998; Rojas et al., 2000; M de la Peña, 2010).

The hairpin, VS, hammerhead, and HDV ribozymes all catalyze the same cleavage reaction where nucleophillic attack of the 2'-OH at the cleavage site phosphate leads to products containing a 2',3'-cyclic phosphate and a 5'-OH. The minimal hammerhead ribozyme consists of a three-helix junction that folds into a Y-shaped structure surrounding a 15-nucleotide catalytic core where 11 of these nucleotides are conserved in all hammerhead sequences. This minimal hammerhead has been extensively studied by biochemical, biophysical, and structural techniques, and efficient cleavage activity in vitro is achieved only at relatively high levels of Mg^{2+} ions (cleavage rate constants of ~1.0 min-1 at 10 mM Mg^{2+}).

Recently, it has been shown that many, if not all, hammerheads present in natural RNAs have additional, non-conserved, structural elements that are essential for cleavage in vivo (Khvorova et al., 2003) or in vitro (Garret et al., 1996). In many cases, such as in the satellite RNA of tobacco ringspot virus (sTRSV), this added element is a specific tertiary interaction between hairpin loops at the ends of helix I and helix II, which are spatially close in the X-ray crystal structures of minimal hammerheads (Pley, 1994; Scott, 1995). In other cases, such as with the hammerhead from *Schistosoma mansoni*, a tertiary interaction between a hairpin loop at the end of helix II and an internal loop in helix I is required for rapid cleavage (Osborne, 2005). In vitro cleavage of these extended hammerheads indicates that the tertiary interaction permits more rapid cleavage than minimal hammerheads at the lower magnesium ion

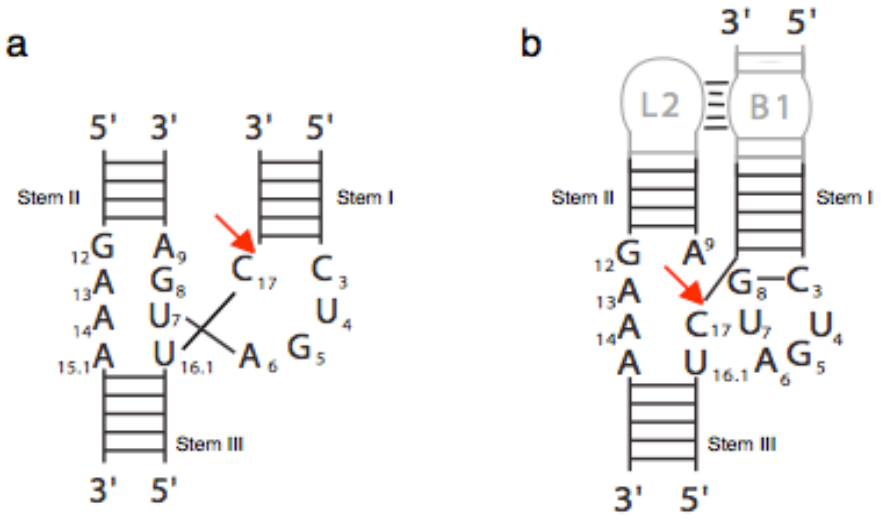

Figure W.G. Scott.

Figure 1.1 Secondary structures of the minimal and full-length hammerhead. The minimal (A) hammerhead contains 12 conserved core residues, the cleavage site, and three flanking A-form RNA helices. The full-length hammerhead (B) contains an additional tertiary contact depicted in grey which enhances catalysis 1000-fold but does not contain any obvious sequence conservation.

concentrations present within cells (Canny and Jucker, 2004).

Base-pairing between the "enzyme" and "substrate" strands of the hammerhead RNA ensures that enzyme-substrate and enzyme-product complexes are energetically stable entities. To a reasonable approximation, a simple two- state equilibrium between enzyme-substrate (*ES*) and enzyme-product (*EP*) complexes will exist, and the ratio K*int* = [*EP*] / [*ES*] characterizes the internal equilibrium.

The simplicity of the hammerhead secondary structure lends itself to the design of two-piece constructs. However, even under single turnover conditions, where the enzyme strand concentration exceeds the substrate concentration, it is impossible to demonstrate that individual enzyme strands regenerate a catalytically

competent complex following cleavage. This is especially true of highly active natural ribozymes. Thus, some have argued that the hammerhead ribozyme may not be a true catalyst in that it may be incapable of performing multiple-turnover cleavage and ligation reactions.

1.2 The Schistosoma mansoni ribozyme

The hammerhead ribozyme from the *Schistosoma mansoni* satellite DNA is perhaps the best characterized of the natural hammerhead systems, with data on the local and global structure by EPR, global folding by FRET, cleavage kinetics, and cross-linking studies. In 2006, Martick and Scott provide an X-ray structure of *S. mansoni* hammerhead containing the natural loop-loop tertiary interaction (Figure 2). Together, these studies have shown that the formation of the loop-loop tertiary interaction alters the structure, populations of active conformations, global folding, and cleavage kinetics of the natural hammerhead, leading to a ribozyme that is readily cleaved under physiological conditions.

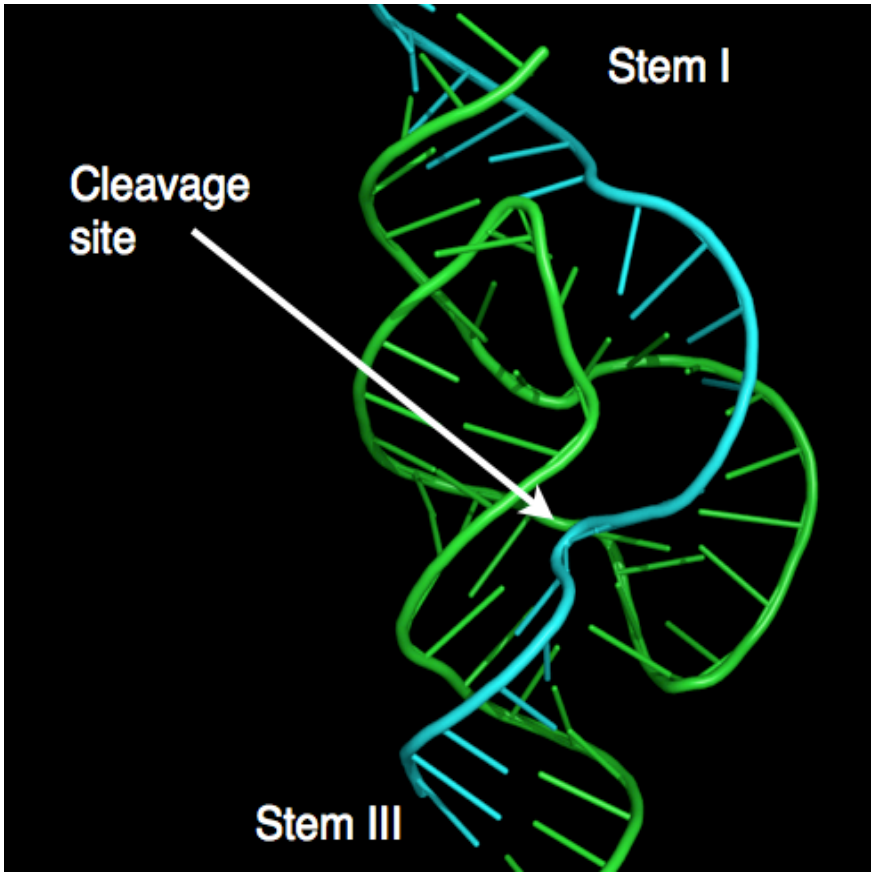

Figure 1.2 "Front" view of the Schistosomal hammerhead. Stems I (top) and III (bottom) are each comprised of both enzyme (green) and substrate (turquoise) strands. The distal end of the Stem I helix is coaxial with Stems II and III. A tertiary interaction between Stem I and II stabilizes the catalytic core in a conformation amenable to cleavage and re-ligation.

The 2006 crystal structure provides perhaps the most convincing explanation of the structure-function relationship of the *S. mansoni* hammerhead. Finally, it was shown that all 5 invariant residues are necessary to stabilize the active site core. Compared to the minimal hammerhead ribozyme, the structure additionally demonstrates large conformational changes in stem I and the catalytic core that reconcile decades of conflicting structural and biochemical data. Specifically, the tertiary contact in *Sma 1* unwinds stem I, allowing its catalytic core more frequent

access to the active conformation (Figure 3). In the study described in Chapter 2, we attempt to directly unwind stem I of the ribozyme in an attempt to accelerate the rate of cleavage relative to its overwound state. A new crystal structure of the full-length hammerhead described in Chapter 3 confirms the majority of the structural details of the 2006 structure, yet offers a novel role for divalent ions in the folding and catalysis of this ribozyme.

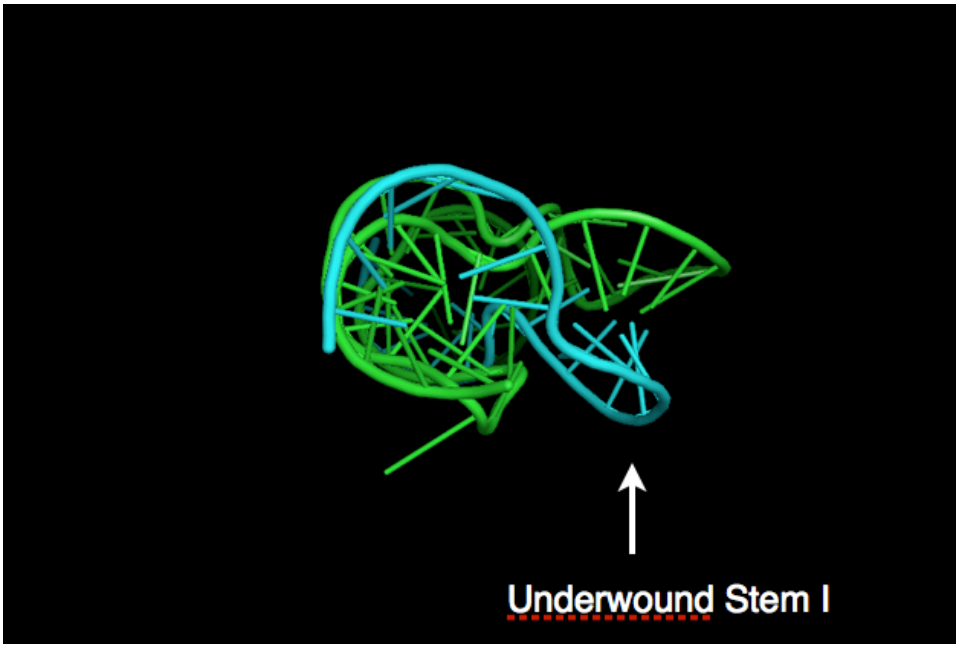

Figure 1.3 "End-on" view looking down Stem I. A significant local unwinding of Stem I results in a distortion of A-form helix, forming a bulge in otherwise continuous double-stranded RNA helix.

The *Schistosoma (Sma 1)* construct is an efficient ligase and yields up to 23% ligated product starting from the fully cleaved substrate. This is the highest level of ligation reported for any unmodified hammerhead. Additionally, this ribozyme shows a K_{int} between 2 and 3 at physiological Mg^{2+} concentrations. The loop-loop tertiary

interaction therefore leads to a ribozyme that is both an efficient nuclease and ligase in vitro.

That K_{int} of Sma 1 favors cleavage in most hammerheads is somewhat surprising, given that the enthalpy change for forming the strained 2′,3′-cyclic phosphate from a phosphodiester is quite unfavorable (Prody et al., 1987). The large favorable entropy change upon hammerhead cleavage overcomes the unfavorable enthalpy and has led to the suggestion that an increase in hammerhead dynamics helps to drive the equilibrium in the direction of cleavage (Prody et al., 1986). However, subsequent experiments have revealed that weaker binding of a divalent metal ion to the cleaved hammerhead also contributes significantly to the equilibrium. In contrast to protein enzymes which require very sophisticated experimental approaches to measure the internal equilibrium (Burbaum & Knowles, 1989), the slow rates of hammerhead cleavage and the tight binding of substrates and products make these measurements relatively straightforward in bulk. Even so, bulk measurements have traditionally relied on truncated hammerhead constructs, as product dissociation becomes rate limiting as stems I and III are extended.

The *Schistosomal* hammerhead favors cleavage to a lesser extent than the highly nucleolytic satellite tobacco ringspot virus (sTRSV) hammerhead, and is thus more ligase-like. Comparing the crystal structures of the two types of hammerheads reveals that a significantly different Stem I helical twist exists in what are otherwise mostly superimposable structures. Based on this and previous experiments in which tethering Stem I to Stem II is observed to change the hammerhead internal

equilibrium, one may suggest that, in a single ribozyme, directly altering the helical twist of Stem I relative to the rest of the ribozyme will alter the balance between nuclease and ligase activities.

1.2.1 Substrate and Product Dissociation in Natural Constructs

For natural *Schistosomal* hammerheads, product strands may exhibit dampened dissociation relative to truncated versions employed in typical kinetics experiments. These natural "embedded" constructs are pre-bound and thus pre-positioned for the back reaction to take place, likely altering the internal equilibrium. A single molecule assay for hammerhead catalysis employing long dsDNA handles and an embedded hammerhead may be well positioned to address this question, with important consequences for a growing repertoire of recently discovered natural embedded molecules.

Indeed, the discovery of embedded gene-regulating ribozymes in bacteria raised the question of whether such ribozymes also exist in eukaryotic mRNAs. The identification of numerous ribozyme switches functioning as metabolite sensors in primitive cells suggest that modern cells indeed retain some of these ancient control systems. (Breaker et al., 2004). In 2008, Martick and Scott verified this inference, describing three hammerhead ribozymes in the 3' UTRs of known rodent mRNAs. All three examples were found embedded in the transcripts belonging to a group of phylogenetically related sequences within the natural killer receptor gene complex of chromosome 6 and 4. (Martick et al., 2008). In contrast to previously identified

continuous hammerheads, the invariant regions of these ribozymes occur as two fragments separated by hundreds of nucleotides (Figure 4). Thus, the discontinuous molecule identified in 2008 provides one example of a molecule stabilized by hundreds of base pairs extending from both stems I and III.

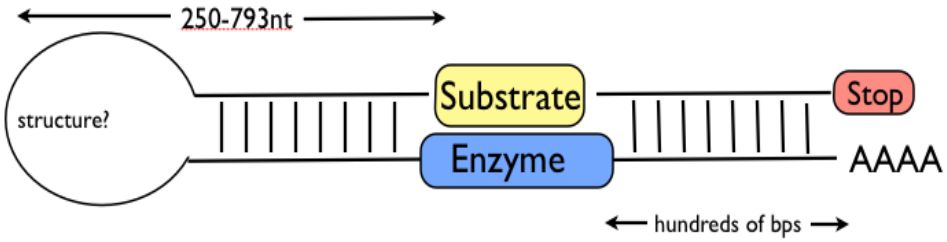

Figure 1.4 Hammerhead ribozyme in 3' UTR of mammalian C-type lectin type II (CLEC2) gene. Invariant region occurs as two fragments, (substrate in yellow and enzyme in blue), separated by hundreds of nucleotides. The pair assembles to form an active hammerhead ribozymes between the translation termination and polyadenylation signals within the 3' UTR.

In 2010, De La Peña and colleagues demonstrated that hammerhead are widespread in the genomes of most life beings. Among eukaryotes, hammerhead ribozymes are detected in the genomes of water molds, 20 plant species ranging from unicellular algae to vascular plants. Like the discontinuous hammerhead, most of the ribozymes uncovered were flanked by long base paired regions, often embedded within dimeric repeats of 1-3 kb. While the majority of natural hammerheads contain such extended stems, there has been no assay to date that has systematically studied the ribozyme in this context (with a few exceptions discussed later in section 3.2.2). Indeed, complex folding effects have likely hampered consistent structural

and kinetic studies of the molecule, and as a consequence the field has focused on a truncated version of the hammerhead in nearly every study to date.

1.2.2 Motif

Hammerhead ribozymes catalyze a specific phosphodiester bond isomerization, similar to RNA enzymes of the same class. In contrast to ribozymes in its class, however, hammerhead ribozymes use sequence and structure in a unique manner. Specifically, the motif is composed of a cluster of 12 conserved active site residues flanked by three helices, which, in natural sequences, are extended far beyond the minimal catalytic set of nucleotides and often contain loops and bulges. Since many naturally occurring hammerheads are embedded in a single strand of RNA, their secondary structure is typically composed of two helices closed by loops with the remaining third helix open-ended. Within the three-helix junction, eleven residues are strictly conserved while the other five positions are occupied with slightly more variability. For instance, the cleavage-site nucleotide, which resides just 5' of the labile bond, is typically a pyrimidine, rarely an adenosine and never a guanosine. The type of nucleotide in position 7 does not seem to be strictly conserved either, although often it is a uridine. Nucleotide pairs 11.1 and 10.1, as well as 15.2 and 16.2, are typically C-G base pairs.

Traditionally, hammerhead ribozymes were defined by the smallest constructs (as small as ~45nt) that could support catalysis. This means that in many experiments the helical sequences outside of the conserved core were modified and the stem length truncated to a minimal length supporting activity. These types of sequences are referred to as "minimal" hammerheads hereon.

1.2.3 Global structure

The hammerhead ribozyme needs to fold into a particular tertiary structure in order for catalysis to occur. The final tertiary fold is acquired through the relative positioning of the three helical stems, in contrast to the secondary structure which is defined by the three-helix junction. The early x-ray crystallography studies using minimal hammerhead motifs constructed from two strands showed that the three helices form the shape of a slingshot with Stem III as the "handle" and Stems I and II positioned in proximity to each other (Pley et al., 1994; Scott et al., 1995). Stem II and Stem III are coaxially stacked. The strand connecting Stems I and II is composed of the CUGA sequence, which forms a U-turn, a motif also present in transfer RNAs. The global conformation observed in the crystal structures of the minimal self-cleaving hammerhead sequence was supported by fluorescence resonance energy transfer (FRET), nuclear magnetic resonance (NMR) and other solution studies

(Amiri and Hagerman, 1994; Bassi et al., 1997; Bondensgaard et al., 2002; Heus and Pardi, 1991).

For decades, hammerhead ribozyme research focused almost exclusively on such minimal constructs. However, biochemical data on chemically modified hammerheads often seemed incongruent with crystal structure data, where functional groups seemingly unimportant for activity in the crystal structure reduced the activity observed in biochemical experiments (McKay 1996). The resolution to this puzzle came with the solution of the full-length crystal structure, where a significant local unwinding of Stem I between the cleavage site and the tertiary contact resulted in a repositioning of these critical residues in a manner consistent with biochemical predictions (Martick and Scott, 2006). Despite this unwinding, the rest of the ribozyme is an approximately coaxial helix, a fact we drew upon in designing the single molecule study described in Chapter 2 (Figure 3).

1.2.4 Mechanism of the chemical step

As in all nucleolytic riboymes, the mechanism of hammerhead cleavage occurs via an S_N2 reaction (Figure 5). Inversion of stereochemistry during transesterfication was determined using sequences containing a phosphorothioate with the sulfur atom residing in the R_p position of the scissile phosphate. Following

cleavage, only endoisomers of the 2'-3'-cyclophosphorothioates were detected, clearly indicating that the catalysis proceeds via in-line attack on the phosphorus center (Koizumi and Ohtsuka, 1991; Slim and Gait, 1991; van Tol et al., 1990). In the hammerhead ribozyme, the reaction is initiated by the 2' nucleophile of the nucleotide 17, attacking the active site phosphorus center and forcing the 5' leaving group oxygen of N1.1 to abandon the phosphorus center. Thus, the bond between residue 17 and 11.1 is broken leaving two new ends: 2'-3' cyclic phosphate on the N17 ribose and 5' hydroxyl on nucleotide 11.1.

1.2.5 The role of cofactors and Hammerhead ribozyme catalysis

The vast majority of known ribozymes require cations for folding and tertiary stabilization through shielding of the negatively charged phosphates (Hanna and Doudna, 2000; Sreedhara and Cowan, 2002). Although this can be achieved with any cationic agent, divalent metal ions are especially effective because they bind tighter and more specifically than monovalent ions. As discussed in Chapter 2, buffer conditions were maintained at 4 mM Magnesium and 10 mM NaCl for the single-molecule cleavage assay, respectively. This slight deviation from standard conditions was employed as a means of shifting the internal equilibrium further towards ligation, thereby increasing the chance of achieving measurable supercoiling events.

a)

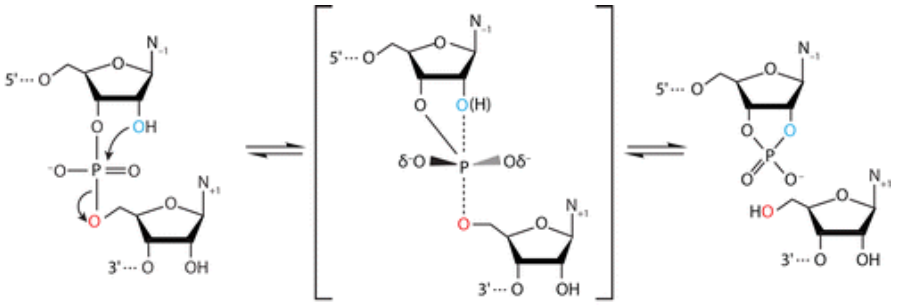

Annu. Rev. Biophys. 38:271-99

b)

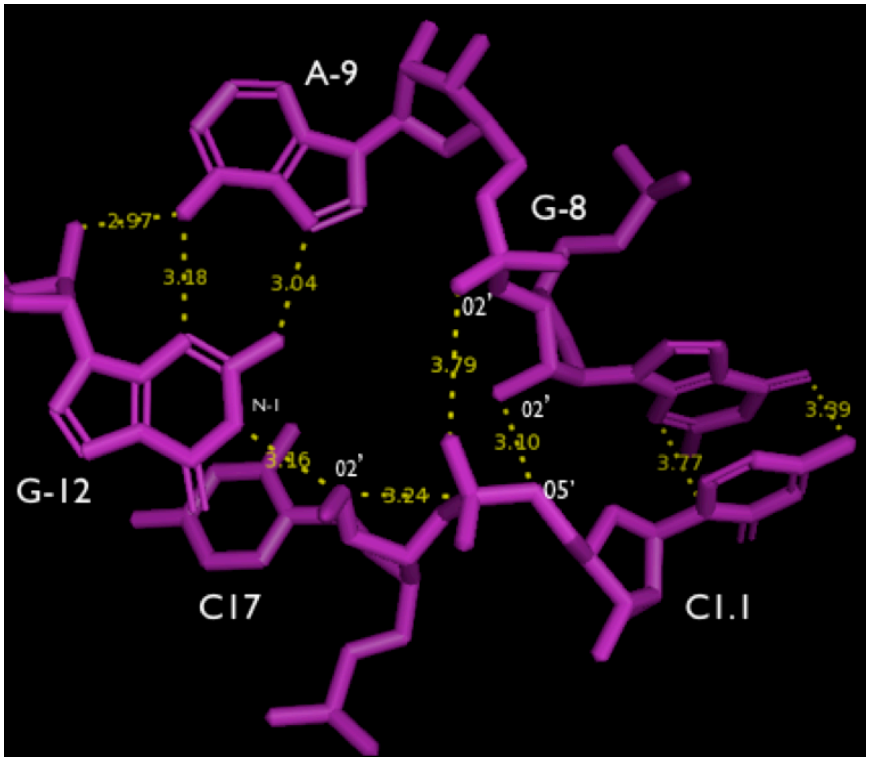

Figure 1.5 a) General mechanism of RNA SN2 transesterfication reaction. b) Schistosomal hammerhead active site core residues (2012 structure), with G-8 positioned to act as the general acid, and G-12 the general base. Interatomic distances (yellow) show that the 2'OH group of C-17 and G-12 are in near perfect alignment to initiate the phosphodiester isomerization reaction.

Some ribozymes utilize metal ions directly in catalysis by positioning them to perform specific actions in the chemistry of the reaction. These types of ribozymes are called metalloenzymes and appear to include most of the larger catalytic RNAs such as RNaseP, group I and group II introns. The smaller ribozymes tend to rely less on divalent metal ions as catalytic tools suggesting that catalysis can be driven by the functional groups of RNA themselves. Conventional wisdom holds that the hammerhead ribozyme may be such an enzyme.

The minimal hammerhead requires positive monovalent or divalent ions for folding into the active structure. In the presence of divalent metal ions, folding proceeds via a two step process, the first step having a much lower ion concentration requirement (~ 1mM) than the second step (10-20mM) (Bassi et al., 1999; Bassi et al., 1995; Rueda et al., 2003). The second step is correlated with the presence of cleaving activity (Dahm and Uhlenbeck, 1991). Substituting the divalent ions with monovalent ions facilitates folding in a similar manner (Bassi et al, 1997; Murray et al., 1998a; Rueda et al., 2003).

Several Mg^{2+} binding sites were identified in the crystal structures of the minimal hammerhead ribozyme (Pley et al, 1994; Scott et al., 1995). The significance of these sites, particularly the site between A9 phosphate and N7 of G10.1 due to coordination to a conserved nucleotide, have been previously addressed using several biochemical approaches. Metal ion specificity can be tested using a thiophillic metal-ion rescue method in which thiol substitutions in the oxygen

position of the phosphates, combined with kinetic studies, can identify catalytically important metal binding sites.

Thio-substitutions in pro-R positions of A9 and N1.1 (active site) phosphates inactivate the hammerhead ribozyme. It was presumed that these modification abolished binding of a catalytically important metal ion because the effect could be reversed with the introduction of a thiophillic ion such as Cd2+ that restored ribozyme cleaving activity and, moreover, appeared to interact with both thiophosphates simultaneously. Further analysis suggested that the metal binding site involved in this apparent bridging effect is the previously identified A9/G10.1 site in the crystal structures (Wang et al., 1999). Thus, the divalent metal ion initially appeared to play both a structural and catalytic role. These results were surprising because, in the crystal structure of the minimal hammerhead, the A9 phosphate and N1.1 (active site) phosphate are separated by 10 Å. The full-length structure of 2006 helped to resolve this disparity; A9 and N1.1 reposition to a distance capable of coordinating Mg^{2+} or other metal ions.

The role of the divalent metal ions in hammerhead catalysis was further tested, and subsequently resolved, using *in vitro* kinetics assays in metal-free solutions. In a series of titration experiments it was shown that the Mg^{2+} ions could be replaced by Na+ or Li+ ions and the ribozyme catalysis effectively reconstituted. These results supported the view that divalents are not required for catalysis either by inner or outer sphere coordination (Murray et al., 1998a).

The possibility therefore remained that the minimal hammerhead ribozyme may assume the active conformation solely through organization of RNA structure. Although the thio-substitution experiments suggest that the core region is flexible and assumes an active conformation upon binding of a divalent ion, the role of this ion may be simply to stabilize the pre-arranged conformation. In the single-molecule study reported, we explore minimal hammerhead cleavage under solvent conditions of varying ionic strength.

The 2006 full-length structure suggested that divalent ions do not directly participate in the catalytic reaction, despite the fact that the hammerhead ribozyme cleavage rates are directly proportional to the divalent ion concentration. However, the absence of a metal ion bridge between the A-9 and scissile phosphate groups in the full-length structure may be attributable to the low concentration of Mg^{2+} and high concentration of NH4+. Chapter 3 outlines our efforts to test this hypothesis by analyzing whether and how many alternate divalent metal-ion binding site(s) exist in the full-length structure under more favorable Mg^{2+}-binding conditions

1.3 Tertiary Contacts Enhance Catalysis

Studies of different natural variants of hammerhead ribozymes have revealed that the hammerhead catalytic potential has been greatly under-explored. It has recently been revealed that the majority of natural hammerheads contain peripheral contacts that serve to enhance the rate of both the forward and reverse reactions.

These contacts were unnoticed until 2003 due to their weak sequence conservation, and because the forward rate of minimal hammerheads proceeded at a rather reasonable rate of ~1/min.

1.3.1 Truncation of natural hammerhead sequence alters its activity

RNA folding is a hierarchical process in which secondary structure elements, formed by base pairing interactions, fold into higher order structures through additional, mainly nucleobase-mediated, interactions. Because the secondary structure elements are relatively domain-like, the approach of analyzing different domains in isolation has often been applied. For ribozymes, this frequently constituted truncation to a minimal sequence that supports catalysis. Although rather successful in protein enzyme research, such a method has sometimes led to unfavorable changes in ribozyme activity. It appears that global RNA structure, more often than not, relies on distal interactions for structure stabilization (Lescoute and Westhof, 2006). A classic example is an alteration of activity observed in the hairpin ribozyme that has been simplified for biochemical experiments. The hairpin, also a nucleolytic enzyme, is composed of two major helices, radiating from a four-way junction, that fold close to each other and interact via the intra-helical loops to form an active site. Because the four-way junction is located quite distantly from the active site, it initially was replaced by a simple phosphodiester linkage in order to facilitate the experiments at hand (Berzal-Herranz et al., 1993; Ahuang et al., 2000). This

seemingly innocent alteration nevertheless resulted in a drastically reduced folding efficiency. As a result, the shortened ribozyme requires a 1000 times higher Mg^{2+} concentration for folding and activity than what has been observed for its natural form (Wilson and Lilley, 2002; Zhao et al., 2000).

The hammerhead ribozyme is another classic example of practical miniaturization. The original characterization of hammerhead ribozymes was concerned with minimal natural sequences required for activity. These were found to be about 40-50 nucleotide-long strands that would fold into hammer-shaped structures and cleave in cis and co-transcriptionally (Forster and Symons, 1987). Naturally, these sequences contained two loops capping helices 1 and 2. The activity was fast, since it happened during transcription, or, if measured using renaturation methods, was complete within a minute. In order to render the hammerhead ribozyme more amiable for detailed kinetic analyses, the sequences were split into two or three strands inevitably disrupting the essence of the helix-capping loops (Haseloff and Gerlach, 1988; Jeffries and Symons, 1989; Koizumi et al., 1988; Uhlenbeck, 1987). In addition, variable sequences in flanking helical regions were often shortened or lengthened in order to stabilize the trans-cleaving complex formation. The altered ribozymes, in this text referred to as minimal hammerheads, became easier to manipulate due to decreased activity rates. Thus, the small trans-cleaving ribozyme became the gold standard for kinetic and structural analyses while the activity of the natural cis-cleaving sequences, apart form appearance in a few

studies (Ambros and Flores, 1998; Beaudry et al., 1995), remained poorly characterized.

Recently, the originally observed fast cleavage rates of cis-acting sequences were revisited almost twenty years after the discovery of the hammerhead ribozyme. A careful reanalysis of naturally occurring hammerhead sequences confirmed that construct minimization has led to a gross underestimation of the ribozyme's catalytic power. Indeed, inclusion of naturally occurring peripheral sequences in helices 1 and 2 results in an astounding ~10^3-fold cleavage rate enhancement (Canny et al., 2004; De la Pena et al., 2003; Khvorova et al., 2003). Moreover, extended hammerhead ribozymes have a significantly lower divalent and monovalent ion requirement for catalysis. While the minimal hammerhead requires millimolar divalent metal ion concentration for respectable activity, the extended version is able to function in the micromolar, and therefore physiological , Mg^{2+} concentration range (Khvorova et al., 2003; Osborne et al., 2005). The specific cause of the enhanced rates was found to be the tertiary interaction between the secondary structure elements residing in Stems I and II, and about five base pairs away from the conserved catalytic core region.

1.3.2 Structural characteristics of the distal interaction

1.3.2.1 Sequence conservation

It is now known that most natural hammerhead sequences contain loops capping the Stem II and loops or interhelical bulges in Stem I (Figure 6). In satellite

RNAs and viroids, most of the hammerhead structures have helices I and II capped by loops with the remaining stem III open-ended, while the newt and *Schistosoma* hammerheads have, instead, helices II and III capped by loops.

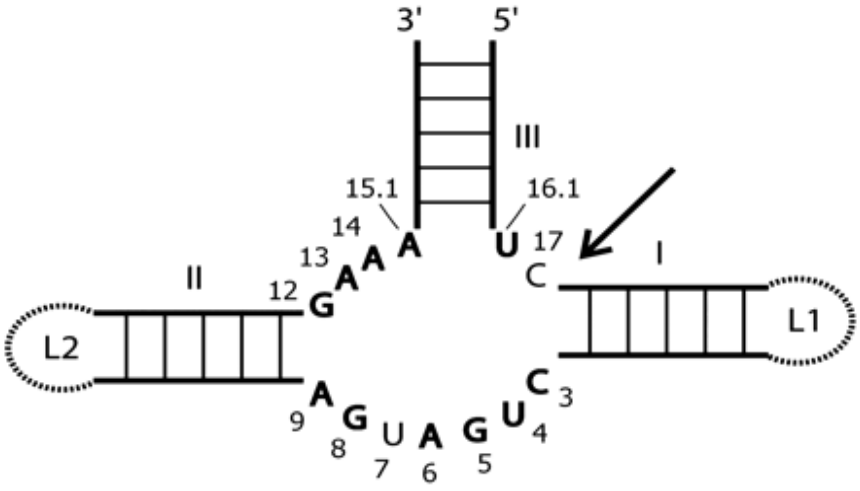

The Plant Cell July 2005 vol. 17 no. 7 1877-1885.

Figure 1.6 Orientation of stem I, II and III and the catalytic core. Most hammerheads have helices I and II capped by loops with the remaining stem III open-ended. The cleavage site (arrow) is surrounded by 11 ultra-conserved residues (bold). Ribozymes lacking loops at the ends of Stem I and II require millimolar Mg^{2+} for robust activity, while the interacting loop sequences in full-length hammerheads result in folding and cleavage in the micromolar Mg^{2+} range.

A more rare variation occurs in avocado sunblotch viroid (ASBVd) and rice yellow mottle satellite RNA (sRYMV) where the hammerhead motif forms with two helices open-ended (Flores et al., 2001). Investigation of the known hammerhead sequences suggests that the distal interactions may require two structural elements: specific lengths of helices 1 and 2, as well as a specific nucleotide sequence in the distal interacting regions (De la Pena et al., 2003). The loop sequences often contain a tandem UG sequence in a 5' portion of the Stem I loop/bulge. This always coincides with an adenosine in the 3' most position in the loop capping Stem 2. Other

trends include an adenosine triplet in the Stem II loop. The lengths of the Stem I and II also show conservation. Stem 1 is predicted to consist of 6 Watson-Crick base pairs in most of the naturally occurring sequences, while Stem II is generally 4-6 Watson-Crick base pairs long.

1.3.2.2 The effect of stem lengths

The significance of helix lengths has been addressed biochemically within the context of minimal hammerhead and the results agree well with the conservation of lengths of Stems I and II, thus supporting their involvement in catalysis. Recent FRET studies revealed marked structure dynamics differences between the minimal hammerheads containing short Stems I and II (7bp and 5bp, respectively), and hammerheads designed with longer, uniformly helical, stems (12bp and 13bp, respectively). The smaller hammerhead, an *in vitro* designed HHα, exhibited more Stem I- Stem II flexibility than the extended one. This was partially attributed to the AU rich sequence in Stem I near the core region, but also agreed well with additional evidence for importance of short lengths of Stem I and Stem II (Clouet-d'Orval and Uhlenbeck, 1997; Rueda et al., 2003). For example, increasing helix 1 length from 5 to 8 base pairs in an otherwise identical context reduced the rate by 3-fold. Similar helix length dependencies were assigned to Stem II, but not Stem III. The rate was slowed 5-fold when Stem II was extended from 4 to 6 base pairs (Clouet-d'Orval and

Uhlenbeck, 1997). It is tempting to infer that the inhibitory effect of helix lengthening was due to an inhibitory interaction between the helices. Interestingly, the effects of lengthening one helix were not dampened by shortening the other, thus suggesting alternative explanations: either there is a repulsion by the phosphate backbones resulting in increased angle between the stems which would disrupt the structure of the catalytic core or, a sequence independent interaction between the termini of the two short stems allows a catalytically favorable conformation. In either case, enhanced rates of ligation associated with extended stems suggest natural embedded hammerheads may exhibit rates that are significantly diminished relative to their truncated counterparts employed in the vast majority of kinetics studies to date.

1.3.3 Relative position of Stems I and II

It has been found that a previously engineered covalent crosslink between two ribose 2'-oxygen atoms of nucleotides residing in two sequentially distant but spatially proximal locations in the ribozyme crystal structure (residues 2.6 in Stem I and 11.5 in Stem II) shifts the cleavage-ligation equilibrium significantly in such a way that the hammerhead ribozyme becomes a ligase (Figure 7). This shift corresponds to an overwinding of stem I. Our central hypothesis draws on this observation, arguing that if one directly overwinds stem I, we will observe a decrease in the rate of cleavage (or increased rate of ligation). Further investigation has

revealed that a second, similar crosslink (between residues 11.5 and 2.5) produces a hammerhead RNA that still strongly favors cleavage in its shortest form, but remarkably produces a hammerhead RNA that begins to favor ligation similar to the other crosslink, only when the length of the crosslinking moiety is increased (Figure 7). These results indicate that subtle structural effects, such as the angle and/or relative phase between helical Stem I and Stem II, are likely involved in switching the activity of the hammerhead ribozyme from cleavage to ligation and back, as must be required in the replicative cycle of the satellite RNAs that contain hammerhead RNA sequences.

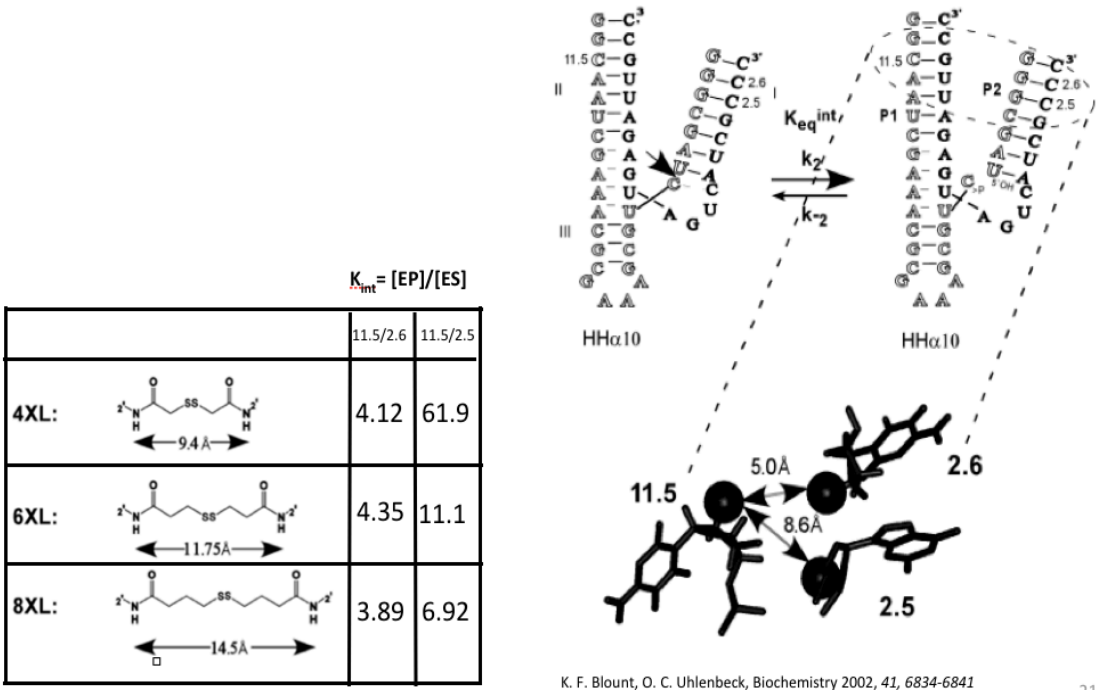

Figure 1.7 Crosslinking & the minimal hammerhead. Crosslinking between residues 2.6 in Stem I and 11.5 in Stem II shifts the cleavage-ligation equilibrium significantly in such a way that the hammerhead ribozyme becomes a ligase. A second crosslink between residues 11.5 and 2.5 produces a hammerhead RNA that still strongly favors cleavage in its shortest form, but begins to favor ligation when the length of the crosslinking moiety is increased. These results indicate that subtle structural effects, such as the angle and/or relative phase between helical Stem I and Stem II, are likely involved in switching the activity of the hammerhead ribozyme from cleavage to ligation and back.

The hammerhead ribozyme internal equilibrium is defined as the ratio of the concentrations of enzyme-product complex [EP] to enzyme-substrate complex [ES], ie, Kint = [EP] / [ES]. An efficient nuclease will have a very large Kint, whereas an efficient ligase will have a Kint approaching zero. The cleavage- ligation equilibrium of the hammerhead cross-linked between 11.5 and 2.6 is remarkably unaffected when the 11.75 Å cross-link is either decreased to 9.4 Å or increased to 14.5 Å. Not only are the cleavage and ligation rates unaffected, but also the enthalpic and entropic components of the cleavage-ligation equilibrium are virtually unchanged among the three cross-linked hammerheads. Since the length of the cross-link is expected to influence the modes of motion available to the cleaved hammerhead, these results argue against a conformational dampening model. That is, even though all three linker lengths are longer than the 5 Å distance between the 2′-positions of 11.5 and 2.6 in the structure, varying the linker length from 9.4 to 11.5 Å should still significantly alter the conformational flexibility of the hammerhead, with a resultant effect on the cleavage-ligation equilibrium. Because varying the linker lengths does not affect the cleavage-ligation equilibrium, a conformational dampening model seems insufficient to explain the effect of the cross-link.

In any event, tethering and constraining the relative motion of stem I and II can clearly shift the internal equilibrium of the hammerhead ribozyme away from cleavage and toward ligation. A series of crystal structures of a tethered minimal hammerhead, published in 2003, revealed a possible structural basis for the shift in

equilibrium. The tethered hammerhead that favored ligation revealed a change in helical twist in Stem I relative to the remainder of the ribozyme molecule, as compared to the unrestrained hammerhead. Untethered minimal hammerheads typically have an internal equilibrium constant that greatly favors cleavage product formation. The aformentioned full-length hammerheads with tertiary contacts between Stem-loops I and II impart an effect similar to tethering and constraining the helices. Although the internal equilibrium in a hammerhead ribozyme derived from the satellite RNA of tobacco ringspot virus (sTRSV) appears to strongly favor product formation, the internal equilibrium of the *Schistosomal* (Sma 1) hammerhead has a Kint ~3/1; i.e, it has significant ligase activity.

The orientation of Stem I relative to stem II changes by a small but significant extent upon cleavage of the hammerhead RNA in the crystal. It is possible that the extent of this change is much greater in solution, where crystal lattice packing does not constrain the position of Stem I. However, the observed change in helical conformation is most likely required for cleavage to take place because further constraint by tethering prevents cleavage from occurring. It is therefore quite likely that the base-pair-mediated tether formed between Stem I and Stem II in the Sma 1 structure, which restricts both helical motion and cleavage activity, may mimic, at least in part, the same interactions between Stem I and II produced by chemical crosslinks. Thus, the structural interaction between Stem I and II may constitute a biochemical switch that controls whether the hammerhead motif will function as a nuclease or a ligase.

A comparison of the 2006 Sma 1 structure and the more recent sTRSV hammerhead structure reveals a change in Stem I helical twist in otherwise very similar tertiary structures. This change is similar to what we had observed in the case of the tethered hammerhead, permitting us to hypothesize that differences in the two types of tertiary contacts in these full-length hammerheads give rise to different internal equilibrium constants via conformational changes propagated through the Stem I helix.

1.3.4 Functional characteristics of the full-length ribozyme

The aforementioned minimal hammerhead studies provide a strong correlation between the inter-helical relationship of Stem I and II and catalysis. Thus, the full-length hammerhead, containing natural Stem I and II tertiary interactions, offered an opportunity to directly investigate this correlation. To address this, biochemical approaches were aimed at determining the full-length hammerhead folding pathways, response to pH changes and Mg^{2+} binding characteristics. During the process of this analysis, the requirements for optimal hammerhead ribozyme catalysis were completely redefined in the context of the extended sequences and appear to be more attenuated than in the context of the minimal ribozyme. Nevertheless, parallels emerged between the minimal and the extended ribozyme functions suggesting that the catalytic mechanism is similar, if not exactly the same, in both forms.

1.3.4.1 Folding

Folding and ion binding are strongly correlated in the full-length hammerhead, as in the minimal. Both sequences need divalent or monovalent ions to fold into the active global shape. However, whereas the minimal hammerhead requires 1-20mM Mg^{2+} to assume an active structure via a two-step process, the full-length ribozyme folds in just 160uM Mg^{2+} , completing the process in a single step. Moreover, low millimolar concentrations of monovalent ions out-compete bound metals as evidenced by FRET analysis. Full-length *Schistosoma mansoni* hammerheads, Fluorescein-Cy3-labeled on the Stem III and I termini, show an increase in FRET efficiency upon addition of < 100mM Na+ ions, indicating that the Mg^{2+}-induced folding is reversed as Stem 1 drifts away from Stem II. Although folding into a functional form, albeit in two-step fashion, is supported only by a higher monovalent concentration, such as $[Na^{+}]$ = 230mM (Penedo et al., 2004). From these observations it is clear that the distal tertiary interaction enhances folding, circumventing the need for high concentrations of divalent ions that would otherwise be needed to stabilize the global structure.

1.3.4.2 Cleavage and ligation reaction

The presence of cations affects not only folding of the hammerhead ribozyme, but catalysis. However, a ~130-fold weaker affinity of the divalent cation is associated with catalysis (Canny et al., 2004; Kim et al., 2005). Furthermore, the cleavage rate dependence on divalent ions does not reach saturation (Canny et al., 2004; Nelson et al., 2005; Osborne et al., 2005). Taken together, the data indicate that the main cation contribution to hammerhead cleavage activity is of a structural nature.

If tested in standard conditions optimal for the minimal hammerhead cleavage (pH 7.5, 10mM $MgCl_2$, 25C) the extended sequence cleaves at a rate of 38 min^{-1}, which reflects a 40-fold enhancement over the rate of the minimal hammerhead sequence. Given super-optimal conditions, such as very high pH and elevated divalent ion concentration, the full-length ribozyme cleaves the substrate with a rate of >14 $second^{-1}$, approaching the speeds thought to be reserved for protein ribonucleases and a few select ribozymes such as the Varkud satellite ribozyme (Canny et al., 2004; Zamel et al, 2004).

Consistent with predictions from the cross-linking studies, the native sequences that include the distal tertiary interactions exhibit enhanced ligation rates. For a hammerhead derived from sTRSV (satellite RNA of tobacco ringspot virus), inclusion of loops caping helix I and II resulted in > 1000-fold increase in the ligation rate as compared to a similar hammerhead without the Stem I loop sequence. The

pre-ligated complex appeared to bind divalent ions with a higher affinity than the minimal hammerhead , and the ligation showed a saturation behavior, indicating that divalent metal ions may play a more direct role in ligation than in the cleavage reaction (Nelson et al., 2005).

1.3.4.3 General acid-base catalysis conjecture

The pH dependence of the full-length hammerhead activity parallels that of the minimal hammerhead. A log-linear relationship with a slope of ~1 is observed at both 100uM and 10mM magnesium concentrations, suggests on-pathway cleavage may be limited by a chemical step (Canny et al., 2004). The pH dependence profile plateaus at around 8.5-9 and thus is suspiciously indicative of protonation-deprotonation of a functional group with a high pKa. Direct evidence for involvement of such a group came from a kinetic analysis in the minimal hammerhead context. In this study, some of the essential guanosines were replaced with nucleobase variants of lower pKa and the effect of pH on the rate of catalysis was monitored. The 2,6-diaminopurine substitutions at positions 8 and 12 converted the pH dependence profile from a log-linear incline with the plateau at pH 8.5-9 (highest measured) to a bell-shaped curve with a peak at pH ~7. Such a change in the curve would be expected if the functional groups at the substituted positions were

directly involved in acid-base catalysis. The N1 pKa of guanosine is 9.6, while that of 2,6-diaminopurine is 5.1. Consistent with this, the peak of the curve is shifted to a lower pH, although notably not lower than 7. Interestingly, a single substitution at either position 8 or 12 resulted in a curve that has a sharp rise within pH5.5 and pH6.0 range and a horizontal profile in the range of pH > 6.0. The latter observation is consistent with a prediction that one group with a low pKa, i.e. 2,6-diaminopurine, and one with a high pKa, such as G8 or G12, are involved in catalysis (Bevilacqua, 2003; Han and Burke, 2005).

Therefore, if the hammerhead mechanism involved a general acid-base catalysis using two guanosine nucleotides, then one would expect the rate to increase with pH until the approximate pKa of guanosine is reached. The nucleotide substitution results were consistent with the experiments in which the G8 and G12 were successfully trapped within the crosslinking distance of C17 and N1.1, two nucleotides spanning the active site (Heckman et al., 2005), even though in the minimal hammerhead structures the active site phosphate is located ~16Å and ~23Å away from the G8 and G12 phosphates, respectively. Although evocative of the nucleobase-catalyzed mechanism, these results could not definitively exclude other possibilities such as structural effects or involvement of functional groups other than nucleobases.

1.4 The 2006 crystal structure of the full-length hammerhead ribozyme

Two structural models of the *Scistosoma* hammerhead were obtained by Martick & Scott in 2006. First, the *de novo* structure was solved using multiple anomalous dispersion methods. The second structure was determined in order to gain insight into how the extended hammerhead ribozyme binds to divalent metal ions.

The full-length *Schistosoma* hammerhead structure reported was 50% larger than a typical minimal hammerhead. The region of this structure corresponding to the minimal motif is similar to the minimal hammerhead fold - three helices form a junction resembling a slingshot in which Stem II aligns coaxially with Stem III. However, the remaining portion of the *Schistosoma* ribozyme, composed of the extended Stem I and II, rejoins in a conformation resembling a lower case gamma, creating a helical bubble-like structure. This has an effect of stacking the terminal section of Stem I coaxially upon Stems II and III, while distorting the lower part of Stem I (Figure 8).

One of the most prominent features of the full-length hammerhead ribozyme structure is the Stem II loop -- Stem I bulge interaction that appears to induce the structural organization of the catalytic core. The loop/bulge interaction is composed of an intricate network of interhelical non-canonical base pairs and stacks, interdigitating the Stem II loop into Stem I. This has the effect of kinking Stem I in such a way as to coaxially align its distal helix on top of the Stem II -- Stem III coaxial arm.

Most importantly, the tertiary contacts between the loop and bulge regions appeared to induce structural changes affecting the catalytic core. This interaction imparts a severe bend upon, and partial unwinding of, Stem I, compared to the more canonical A-form Stem I helix observed in minimal hammerhead crystal structures. This bend forms the foundation of one hypothesis discussed in Chapter 2. Specifically, we conjecture that directly unwinding Stem I with a magnetic tweezers device will increase the rate of cleavage. Reversing the direction of spin should correspondingly dampen the rate of activity.

The distortion in Stem I appears to accommodate G8 and U7 in the catalytic pocket, and in turn stabilize the rearrangement of the augmented Stem II helix that enables G8 to form the Watson-Crick base pair with C3 in the catalytic pocket (Figure 8). Concurrently, an over-winding or right-handed twist of stem II positions the conserved G12, A13, and A14 precisely against the catalytic site C17, helping to lock the latter in a catalytically active conformation in which C17 is oriented for in-line attack. The non-canoncial L6-B5 base pair involves adenosine and uridine, respectively, that are conserved throughout the natural full-length hammerhead sequences. Therefore, one would expect this interaction to be important for ribozyme structure and catalysis. Moreover, since this is one of the few interactions involving the substrate strand, it was postulated that it might be of importance for substrate positioning in the active site.

Surprisingly, however, hammerhead cleavage activity is only subtly affected by mutations of these two bases. Replacing L6 with a uridine reduces the rate by

only a factor of two (Kobs = 0.28 at pH 5.6, 10mM $MgCl_2$), with a similar effect observed if B5 is simultaneously replaced with an adenosine to simulate a compensatory change (Kobs = 0.20) (Ellington 2009). Disrupting this interaction has a weaker effect on catalysis than, for example, removing the loop and bulge elements all together (Clouet-D'Orval and Uhlenbeck, 1996; Murray et al., 2002) indicating that much of the loop/bulge interaction is supported by the base stacking between B2,B3, B4, L2, and L3. However, conservation of adenosine in L6 and uridine in B5 may suggest a role in the loop-bulge docking process, substrate binding for the ligation, or the ligation mechanism itself.

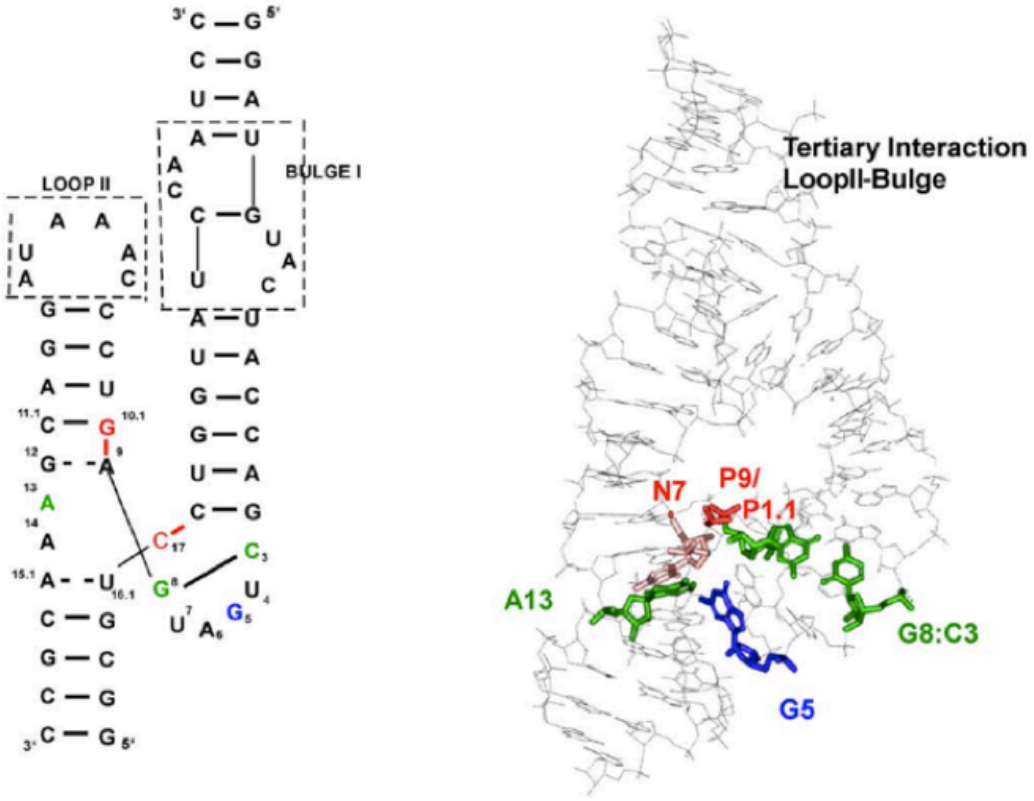

Uhlenbeck et al. Molecular Cell 23, 447–450, August 18, 2006

Figure 1.8 Secondary Structures (Left) and 2006 Crystal Structures (Right) of Schistosomal Hammerhead. The formation of loop II-bulge I tertiary interaction results in an overwound helix II and and underwound helix I. Rearrangements (relative to minimal HH) include a disruption of the noncanonical pair between A13 and G8 in domain 2 and a new Watson-Crick base pair between G8 and C3. Also the phosphodiester bond at the cleavage site (red, P1.1) is poised for in line cleavage. The putative metal binding pocket (red) is comprised of N7 and G10.1 and phosphates P9 and P1.1. The base 3' of the site of cleavage is show in pink. G5 stabilizes the active core in the full-length construct whereas its Watson-Crick face is solvent exposed in the minimal structure.

The minimal and full-length hammerhead constructs differ significantly in structures at both the cleavage site and the invariant uridine turn. In the full-length hammerhead ribozyme, the invariant nucleotides implicated in catalysis form base-pairings and extensive hydrogen bonding networks in a rather compact arrangement, whereas in the minimal hammerhead structures, these same nucleotides are distributed widely across the three-helix unction, making very few contacts with one

another. The cleavage-site base, C17, resides outside of the uridine turn in the full-length structure, positioned almost perpendicular to G5 and A6, whose exocyclic functional groups are oriented toward the ribose. G5 and A6 appear to be wedged between C17 and Stem I, splaying apart C17 and C1.1. As in the minimal hammerhead uridine turn, G5 and A6 stack upon one another, but, unlike in the minimal hammerhead, these bases in the full-length ribozyme are both oriented toward the exposed ribose of C17 and are involved in an extensive hydrogen bonding network that helps to position C17. The resulting orientation of C17 brings the attacking 2'-oxygen within about 3 A of the scissile phosphorus and to within 17 degrees of perfect in-line geometry, indicating that the hammerhead ribozyme is closely approaching the expected trigonal bipyramidal transition-state phosphate configuration in which the attacking nucleophile and leaving group oxygens occupy the axial positions of a pentacoordinated oxyphosporane.

In the full-length hammerhead, G8 occupies the position of C17 observed in the minimal hammerhead structures, forming a Watson-Crick base-pair with C3 of the uridine turn. U7, rather than U4 in the minimal hammerhead structure, stacks beneath C3. U7 and U4 thus reside close together in space but do not hydrogen bond to one another.

The endocyclic N1 of G12 is within hydrogen bonding distance of the 2'-oxygen attacking nucleophile of C17, suggesting that G12, when deprotonated, may serve as a general base that initiates the cleavage reaction. The 2'-OH of G8 appears to hydrogen bond to the 5'-oxygen of the scissile phosphate, suggesting its possible

involvement in general acid catalysis-mediated leaving group charge stabilization in the cleavage reaction.

As a result of these conformational rearrangements, the scissile phosphate adjacent to C17 becomes positioned quite close to the A9 phosphate. The closest non-bridging oxygen distance between the two phosphates is 4 A, rather than 20 A in the minimal hammerhead structure.

Chapter 3 outlines a high-resolution structure of the full-length hammerhead, wherein new contacts at the Stem I and II interface and a modest rearrangement of the active site core reinforce nearly all of the conclusions drawn above. In addition, three bound Manganese residues offer a structural explanation for a host of biochemical evidence that suggests divalent metals play a more direct role in transition-state stabilization in the full-length structure.

1.4.1 How does the full-length hammerhead activate catalysis?

The full-length hammerhead structure suggests that the Stem-Loop II - Stem I interactions stabilize or constrain a conformation within the active site that appears to position G12 for general base catalysis. G8, in pairing with C3, appears poised to

supply a 2'-proton to the leaving group as a general acid catalyst. In addition, the active site conformation stabilized by the distal tertiary interactions orients the 2'-oxygen attacking nucleophile of C17 such that it becomes aligned with the scissile phosphate and leaving group 5'-oxygen of the cleavage site. These arrangements are most clearly seen in Figure 8.

1.4.2 General base catalysis and G12

The N1 of G12 is almost certainly protonated in the crystal structure of the full-length hammerhead ribozyme, and is within approximate hydrogen bonding distance (3.26Å in Mn^{2+} -bound structure, 3.55 Å in Mn^{2+}-free structure) to the 2'-O of C17. Because C17 has been modified with a 2'-OMe to prevent the cleavage reaction, there is no 2'-H to be abstracted. If G12 functions as a general base, as its positioning and previous results (Han and Burke, 2005) suggest, it is most likely that the 2'-proton would be abstracted by a deprotonated N1. The apparent kinetic pKa of the hammerhead ribozyme reaction is 8.5, suggesting involvement of two groups with high pKas in the protonation/deprotonation events of catalysis. Indeed, substitution of G12 with groups of different pKas, such as inosine (pKa 8.7), 2,6-diaminiopurine (pKa 5.1), or 2-aminopurine (pKa 3.8), shifts the reaction rate profile in a manner consistent with G12's suggested role in general base catalysis (Ham and Burke, 2005). N1 of the guanosine nucleotide has also been proposed to play a role of a

general base in the context of hairpin ribozyme catalysis. The pH profiles of imidazole-substituted hairpin ribozymes show altered pH dependence consistent with a direct role of N1 of G in proton transfer (Wilson et al 2006). However, the apparent kinetic pKa of the hammerhead reaction, 8.5, is somewhat lower than the pKa of a guanosine (9.2).

There is limited but convincing evidence from NMR experiments suggesting that the pKa of nucleobases can be shifted in a context-dependent manner through variable electrostatic interactions such as base stacking (Acharya et al. 2002). It shows that the pKa of guanosine can be shifted 0.75 units in ssDNA and 0.5 units in ssRNA, albeit toward a more basic character (Acharya et al. 2006). This effect is highly sequence-dependent. It remains to be tested, however, if the pKa of guanosine changes in the context of more structured and complex environments such as a double-stranded RNA helix or other defined conformational spaces. The possibility that a tautomeric fluctuation participates in this catalytic scheme may also be considered.

1.4.3 General acid catalysis and G8

Donation of a proton is required to counter the accumulating negative charge on the 5'-leaving group of the hammerhead cleavage reaction, a primary alkoxide.

Previous biochemical analyses (Han and Burke, 2005) have implicated G8 as a general base or acid in the hammerhead ribozyme cleavage reaction. The simplest explanation for this observation, in the absence of structural information revealed a year later, was that G8 is a general acid, wherein the proton on the N1 of G8 is labile, and can be donated to the 5'-oxygen leaving group in the cleavage reaction as it is displaced from the scissile phosphate. However, in the 2006 crystal structure, the base of G8 is revealed to be paired with C3, and it is the 2'-OH of G8 that is observed to hydrogen bond (3.18 Å in Mn2+-free, 3.51 Å in Mn^{2+}-bound structures) to the 5'-O leaving group. Thus if G8 functions as a general acid in the cleavage reaction, either it must break its pairing with C3 and reorient toward the leaving group, or it is the 2'-OH of G8 that is the relevant functional group in acid catalysis. To test between these hypotheses, the base pair was switched to C8 and G3. Both G8 and C3 are known to be invariant; changing either nucleotide by itself abolishes activity in the minimal hammerhead (McKay, 1996). However, it was observed that the G8C + C3G double mutant (kobs = 0.22 min^{-1} at pH 7.5) rescues the deleterious effects of the single G8C mutation (kobs < 0.0001 at pH 7.5), demonstrating that the base pair, when reestablished, restores catalysis. These are perhaps the most important positive and negative controls that require replication in the single molecule context. Consistent with the formation of G8-C3 base pair is a recent observation that G8, but not G12, mutations partially inhibit ribozyme folding (Han and Burke, 2005).

1.4.4 Transition-state stabilization and the role of various solvent cations

The pentacoordinated oxyphosphorane transition state is associated with an excessive of negative charge. A transition-state stabilization interaction that would mask the electrostatic repulsive force between the oxyphosphorane and the A9 phosphate would likely contribute to catalytic enhancement. The molar concentration of ammonium cations in the crystal environment provides sufficient charge screening to enable the full-length hammerhead ribozyme to fold into the observed conformation. The observation that the full-length hammerhead ribozyme is active in molar concentrations of monovalent ammonium, both in the absence of and when supplemented with Mg^{2+}, indicates that any generic high concentration of positive charge is sufficient to stabilize the hammerhead ribozyme transition-state. A divalent metal ion, if present in a low-ionic strength solution, might help to stabilize the close approach between the A9 and the scissile phosphates.

Chapter 3 outlines experiments carried out to identify if any specific divalent metal ion binding sites exist. In prior experiments, in which 50 mM Mg^{2+} was soaked into full-length hammerhead ribozyme crystals, no Mg^{2+} ions in the 50 mM soak were observed to bind at the active site. The potential involvement of G12 and G8 in acid-base catalysis, and the ability of the RNA to fold into a structure that is unambiguously poised for catalysis in the presence of ammonium ion, together with the observation that no metal ions appear in the active site of 2006 structure, support the hypothesis, based on previous experimental observations in the context of the

minimal hammerhead ribozyme, that the hammerhead ribozyme possesses all of the chemical constituents that are strictly required for the self-cleavage reaction (Murray et al. 1998a; Scott, 1999).

1.5 Comparing the hammerhead to other self-cleaving ribozymes

The hammerhead, hepatitis delta virus (HDV), and hairpin ribozymes each catalyze the same phosphodiester isomerization reaction. However, despite some superficial similarities, each of these ribozymes deploys a unique strategy for affecting catalysis.

The HDV ribozyme, for instance, is an obligate metallo-enzyme, requiring magnesium for catalysis under all conditions (Fere-D'Amare et al, 1998; Ke et al., 2004; Murray et al., 1998a; Nakano et al., 2003; Nakano et al, 2001; Scott, 1999). In the uncleaved structure, C-75 is located nearest to the cleavage site 2'-O, and a divalent metal ion appears to make a through-water contact to the 5'-O leaving group. C75 is therefore believed to abstract the 2'-H in the (unobserved) transition-state, thus functioning as a general base in the cleavage reaction, and the hydrated divalent metal ion is though to be the general acid, supplying a proton from a coordinated water to the cleavage-site 5'-O as a negative charge develops. Thus, in sharp contrast to the hammerhead and hairpin ribozymes, a pyrimidine nucleotide base appears to play the

role of general base in the cleavage reaction, and a hydrated metal ion appears to play the role of the general acid.

Unlike the HDV ribozyme, the hammerhead ribozymes are not metalloenzymes (Curtis and Bartel, 2001; Murray et al., 1998a; O'Rear et al., 2001). All ribozymes were once thought to be metalloenzymes (Dahm et al, 1993; Dahm and Uhlenbeck, 1991; Pyle, 1993; Pyle and Cech, 1991) that use hydrated metal ions (Dahm et al., 1993) or inner-sphere-coordinated metal ions (Lott et al., 1998) in catalysis. The hammerhead and hairpin, rather than simply functioning as passive scaffolds for metal-ion binding (Yarus, 1993), are now seen to have structures in which the nucleotide functional groups are clearly positioned for acid-base catalysis.

The first structure of the hairpin ribozyme (Rupert and Ferre-D'Amare, 2001) revealed that the N1 of G8 in the hairpin ribozyme active site is within hydrogen bonding distance of the cleavage-residue 2' oxygen, suggesting its role as the base in the cleavage reaction, and the subsequent transition-state analog structure (Rupert et al, 2002) revealed an adenosine (A38) positioned near the 5' oxygen, suggesting its role as the general acid. The exocyclic amines of G8, A38, and A9 were also observed to hydrogen bond to the non-bridging oxygens, presumably helping to disperse the excess negative charge that accumulates in the transition state.

In contrast to the hairpin, the uncleaved complex of the full-length hammerhead ribozyme reveals contacts with both the attacking nucleophile (the 2'-O) and leaving group (the 5'-O). G12 in the hammerhead appears to play the same role as G8 in the hairpin, i.e., that of a general base in the cleavage reaction, whereas G8

2'-OH appears to play the role of the protonated N1 of A38 in the hairpin ribozyme transition-state analogue, i.e., that of a general acid in the cleavage reaction.

The uncleaved hammerhead structure, unlike the hairpin ribozyme, does not make contacts to the scissile phosphate non-bridging oxygen atoms, suggesting that dispersal of the accumulating negative charge, as well as screening the electrostatic repulsion between the A9 and scissile phosphates, is accomplished via nonspecific cation interactions, where ammonium, other monovalent cations, or divalent metal ion can supply a high concentration of positive charge. This is consistent with the observation that the hammerhead ribozyme requires a greater concentration of monovalent cations to be present for full activity than does the hairpin ribozyme (Murray et al., 1998a; Scott, 1999), and it also explains why the hammerhead ribozyme appears to require divalent cations under low ionic strength conditions.

Similar to natural self-cleaving hammerhead sequences in mRNAs and satellite viruses, the hairpin and HDV ribozymes can be embedded within long base-paired stretches of RNA. Natural hammerhead sequences embedded in mRNAs and satellite virus RNAs must be able to switch from favoring RNA cleavage (product formation) to RNA ligation (substrate reformation or maintenance). In other words, they must be capable of changing their internal equilibrium constant. The hairpin and HDV ribozyme similarly exhibit reversibility, yet, without a single-molecule approach to study this enzyme, an objection has persisted that these ribozymes are not true catalysts that exhibit multiple turnover. In other words, without the ability to

follow the activity of one enzyme in real time, one cannot say for certain whether the active site reforms in every case to support multiple turnover catalysis.

1.6 Magnetic Tweezers Force Spectroscopy

All biological motion, from cellular motility to replication and segregation of DNA, is driven by molecular-scale forces. Similarly, the dampening of motion through the binding of ligands or folding of complex RNA enzymes into stable three-dimensional structure involves the formation of bonds that overcome thermal and other forces. As discussed, RNA catalysts such as the hammerhead ribozyme often utilize tertiary interactions to fold into a conformation relevant for catalysis (Doty et al. 1959). In the *Schistosomal* hammerhead, tertiary contacts propagate an unwinding of stem I that would otherwise be thermally unfavorable. Indeed, folding and catalysis of the hammerhead can be thought of as thermodynamically inevitable. Under physiological conditions it is energetically favorable for the hammerhead to form Watson-Crick base pairs and thereby fold into secondary and tertiary structures that support self-cleavage. Topological properties of RNA also influences its mechanical and biochemical interactions. Despite their fundamental roles, the effects of topology and force have been difficult to ascertain. It wasn't until the development of techniques that permit measurement of force and displacement generated by single molecules that we could study these fundamental processes.

1.6.1 Magnetic Tweezers

Single-molecule force spectroscopy has emerged as a unique tool to probe the forces and motions associated with biological molecules and enzymatic activity. Along with optical tweezers and atomic force microscopy, magnetic tweezers is the most common force spectroscopy technique. The following section will introduce the customized magnetic tweezers apparatus utilized in this study and discuss issues of RNA and DNA topology in relevant to this work.

While single-molecule manipulation techniques have expanded rapidly in scope and utility in the last decade, magnetic tweezers and a variant of optical tweezers remain the two main techniques used to measure the topology of DNA molecules. (Neuman, K. C., and Nagy, A., 2008). Both techniques involve the tethering of one end of a double-stranded DNA (1-45 kb) molecule to the glass surface of a microscope flow cell, and the free end to a micron-sized particle that can be pulled and rotated.

The heart of a typical magnetic tweezers instrument is the flow cell; a 1/4 inch channel created by applying a cover slip to a glass slide fixed with double-sided tape. The flow cell allows buffer exchange and visualization of the slide surface, which contains a field of DNA molecules tethered to magnetic beads. The instrument itself consists of a pair of permanent magnets, arranged with their opposite poles separated

by a small gap (~1 mm), placed above the flow cell on an inverted microscope (Figure 9). Multiple digoxenin moieties are incorporated into the DNA molecule using ligation chemistry and PCR amplification of 'linker' segments capping each end of the molecule. Digoxenated UTP is incorporated into a standard mix of dNTPs in the PCR reaction generating a 1000 bp molecule which is subsequently digested with the appropriate restriction enzyme, resulting in 500 base pair 'linker' fragments. After the ligation reaction is performed, theses segments allow adhesion to the anti-digoxigenin-coated surface of the flow cell. The free end of the DNA is attached to a streptavidin-coated superparamagnetic bead via multiple biotin moieties. A similar preparation process is required to generate a 500 bp biotin 'linker' required for adhesion to the magnetic bead.

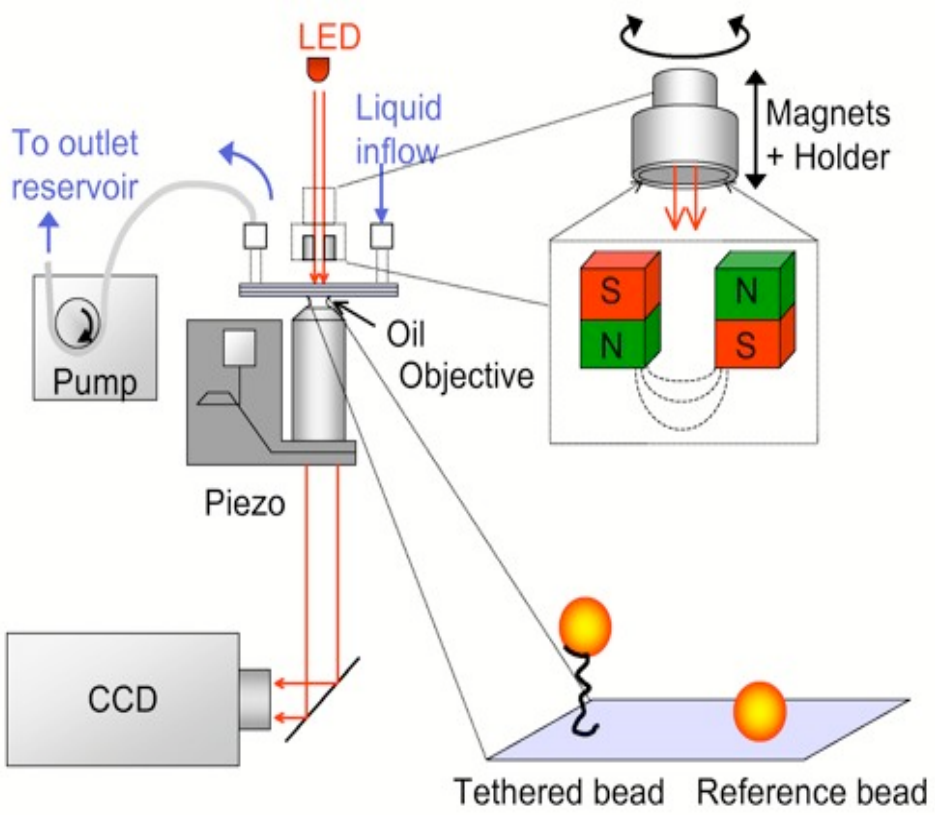

Dekker,N. [ONLINE] http://nynkedekkerlab.tudelft.nl/techniques/magnetic-tweezers/

Figure 1.9 Control of DNA topology via Magnetic Tweezers. Magnetic tweezers consist of two magnets (red and green) held above a microscope flow cell in which a magnetic bead (yellow) is tethered to the surface (light purple) by a single DNA molecule (black). The linking number of the DNA can be changed by rotating the magnets (black curved arrowI), which thereby rotates the attached beads. The upward force on the beads depends on the vertical position of the magnets (black vertical arrow).

The magnets above the flow cell impose an upward force (0.1 - 100 pN, 10^{-12}) on the magnetic bead that can be controlled by changing the vertical position of the magnets. The magnetic moment of the bead is entrained by the field of the external magnets so that it rotates in a one-to-one correspondence with magnet rotation. The three-dimensional position of the bead is obtained with 2-5-nm accuracy in real time (30-200 frames/s) by image processing with a high-magnification objective which images the bead onto a charge-couple device camera. (Lionnet, Allemand et al.

Single-Molecule Techniques: A Laboratory Manual. 2008). Changes in DNA extension can be precisely measured with this simple setup by applying well controlled pulling forces. A detailed treatment of the system employed in this work will be explored in Chapter 2.

1.6.2 DNA as a worm-like chain

The physical properties of the DNA and RNA are unlike those of any other natural or synthetic polymer. Characteristic base stacking and braided architecture lend both unusual stiffness: it takes about 50 times more energy to bend a double-stranded RNA molecule into a circle than to perform the same operation on single-stranded RNA. Furthermore, the phosphates in DNA and RNA's backbones make them two the most highly charged polymers known.

The physics of DNA in many biological contexts is usefully described using a coarse-grained treatment such as the worm-like chain (WLC) model. This model can be applied with equal utility to RNA. The WLC model characterizes a polymer using a single parameter, the flexural persistence length (A). It should be noted, however, that mechanical properties vary according to local sequence and helical structure. (Kratky, Porod. *Rec.Trav.Chim. 1949).* For forces applied (< 40pN) a fully reversible and well reproducible force-extension dependence is found. The data can be well described by both the worm-like chain model or by an approach developed by R.G.

Winkler. For the resulting persistence length, a pronounced dependence on the ionic concentration in the surrounding medium is found.

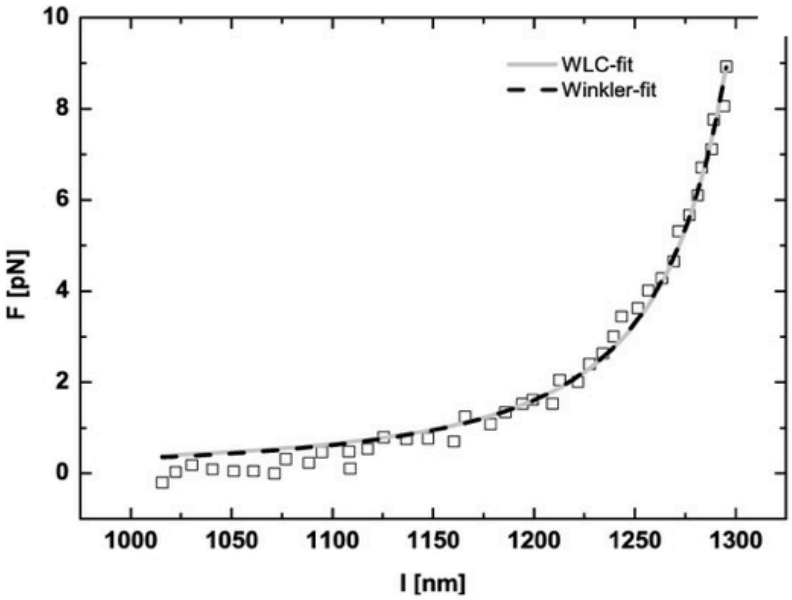

Winkler R (2003) Deformation of semiflexible chains. J Chem Phys 118: 2919-2928.

Figure 1.10 Force-extension dependence for a single ds-DNA chain of 4,000 bp. The solid line indicates a fit using the WLC model while the dashed line corresponds to Winkler's approach. The experimental uncertainty is +/- 0.5 pN

The WLC model imagines a polymer as a line that bends smoothly under the influence of random thermal fluctuations. The value of *A* defines the distance over which the direction of this line persists: correlation between the orientations of two polymer segments falls off exponentially (with decay length *A)* according to the contour length that separates them. For dsDNA in physiological buffer, A = ~50 nm.

The relationship between *A* and the bending rigidity *k* of the polymer is represented as an elastic rod[2]: $k_B TA = k$, where k_B is Boltzmann's constant and *T* is the

temperature. The energy required to bend a segment of DNA of length L through an angle theta and radius of curvature R/L is: $E(\theta) = k_B TAL/ 2R^2 = (k_B TA/2L)\theta^2$.

This data can also be described by the model of a semiflexible chain of Gaussian segments as suggested by Winkler: $F = 3k_B Tx/ [2L_o L_p(1- x^2/L_o^2)]$. The primary difference between the WLC and Winkler approach is that in the later the contour length is not fixed (In the Winkler model, the magnitude of the tangent vector is not eactly one but only its average value). (Winkler R, 2003). The force-extension dependence for a single ds-DNA chain using both the WLC and Winker model are shown in Figure 10.

According to either model, it is energetically more favorable to bend the molecule smoothly, spreading the strain over large distances rather than bending it sharply. For the *Schistosomal* hammerhead, these mechanical properties are central to tertiary interactions, which impose a severe bend in Stem I helix. (Goodman, Nash et al., 1989).

To bend RNA, like DNA, tertiary contacts must convert part of their binding energy into mechanical work. This is illustrated by an experiment concerning DNA binding proteins, in which a binding sequence was pre-bent towards the major groove by placing it in a DNA minicircle. The affinity of a transcription factor (TBP) for this binding site was found to be 300-fold higher (equivalent to a free-energy change of 3.4 kcal mol^{-1}) when the sequence was pre-bent in the same direction as TBP-induced bending, relative to pre-bending in the opposite direction. (Parvin, McCormick et al., 1995). This increase can be accounted for by the difference in

bending energy between the two initial DNA conformations, which by the equation above is predicted to be 3.2 kcal mol $^{-1}$. DNA's structure is pre-stressed by electrostatic self-repulsion, as a result of the negatively charged phosphate backbone. Therefore, asymmetric neutralization of the DNA helix (for example, by a tertiary contact or binding protein that presents a positively charged face) can lead to compression and bending of DNA towards the neutralized face.

1.6.3 Topology of RNA & DNA

The topology of DNA and RNA, which is defined by how the two complementary single strands are intertwined, has been an important consideration since the double helical structure of DNA was first proposed by Watson and Crick in 1953. Single-molecule techniques have enabled the elucidation of DNA mechanics and topology with unprecedented precision, which laid the groundwork for high-resolution measurements of topoisomerase, gyrase, RNA Polymerase and riboswitches.

DNA topology encompasses supercoiling, knots, and catenanes. For the purpose of this writing, I will restrict discussion to supercoiling as we utilize

supercoiling as a readout for enzymatic activity in the system described in Chapter 2. One may characterize the topology of closed circular DNA by the linking number (Lk), which, as the name suggests, reflects the number of links between two complementary single strands. An increase in Lk is termed positive supercoiling, whereas a decrease in Lk is termed negative supercoiling. (Neuman, 2010). This quantity is physically manifested in two geometric properties of DNA; Twist (Tw), the number of times the two strands are twisted around each other and Writhe (Wr), the geometric coiling of the double helix. DNA usually manifests an interwound (plectonemic) superhelix.

Tw is defined as positive for a right-handed helix while positive writhe corresponds to a left-handed superhelix. Changes in Lk depend on Tw and Wr according to the equation, Lk = Tw + Wr. (White J. H., 1969). For relaxed B-form DNA, the two strands twist around each other once every ~10.5 bp; therefore, the relaxed Lk (Lk0) is equal to the relaxed Tw (Tw0) ~n/10.5 for n bp. If, however, the ends of the DNA are torsionally constrained, e.g. in a closed circular plasmid, Lk can differ from its relaxed value. Supercoiling leads to changes in both Tw and Wr. For example, negative supercoiling resulting from the reduction in Lk is accommodated by reduced Tw and the formation of right-handed plectonemes corresponding to negative Wr.

Supercoiling can be easily understood by considering a length of flexible tube. If one holds one end fixed while rotating the other end the linking number changes. Initially, the tube will twist, and the torque stored in the tube will increase in

proportion to the rotation: $\tau = (C/L)\cdot\Delta\theta$, where C is the twist elasticity, L is the length of the tube, and $\Delta\theta$ is the angular rotation of the end. After a certain number of rotations, the tube will buckle, forming superhelical plectonemes, which are one possible manifestation of writhe. Further rotations increase the number of plectonemes but do not increase the twist or toque on the tube. The interconversion of twist and writhe can be appreciated by stretching the tube; writhe stored in plectonemes is converted to twist as the ends of the tube are pulled apart. The process reverses as the ends are brought back together. Although this model lacks the helicity of DNA, it describes the important features of DNA topology under tension.

1.7 Objectives

The goal of the experiments described in Chapter 2 is to understand if natural embedded hammerheads can undergo multiple successive cleavage and ligation cycles under constant force and torque, revealing for the first time whether this ribozyme is a true catalyst. A related question is if in the context of pre-bound product, whether re-ligation will become spontaneous. A more fundamental question addresses the source of the "cleavage" signal itself; what alternate sources may contribute to changes in supercoiling density of DNA in our system?

A resolution to these questions may allow us both to understand details of the nuclease-ligase switch and ligation preferences of natural embedded hammerheads.

Because the major difference between the slower-cleaving minimal hammerhead and the catalytically robust full-length molecule is an unwound portion of stem I, we proposed that directly twisting stem I will modulate the rate of ligation. Because both minimal and full-length hammerhead ribozymes respond to changes in pH and metal ion concentration, albeit to a different extent, it is also important to probe the relationship of these variables to activity in the context of a more reactive conformation.

A comparison of the crystal structures of Sma1 and sTRSV hammerheads also suggests our hypothesis is valid. Relative to the more active sTRSV molecule , stem I of Sma, immediately 3' to the cleavage site, is distorted and under-wound. Modest differences in the tertiary contacts are also apparent when the crystal structures of the two species of hammerheads are compared. We hypothesize, based upon the full-length hammerhead structures, that twisting Stem I in the negative (under-winding) direction will favor the cleavage reaction, and that imparting the opposite twist, by twisting in the positive (over-winding) direction will inhibit the cleavage reaction.

The goal of our experiments in Chapter 3 is to explore the role of divalent ions in the context of a high-resolution structure of the full-length hammerhead. Indeed, divalent metal ions are known to stimulate folding of the full-length ribozyme under low ionic strength conditions (Kim *et al*, 2005; Penedo *et al.*, 2004). However, the absence of a metal ion bridge between the A-9 and scissile phosphate groups in the full-length structure raised the question of whether this well-studied binding pocket is in fact conserved. One theory is that the absence of a metal ion in that case was due

to the low concentration of Mg^{2+} and high concentration of NH^{4+} employed. If this is the case, any high concentration of generic positive charge is likely capable of stabilizing the global structure of the molecule. However, debate persists as to whether a conserved divalent metal binding site bridges the A-9 and scissile phosphate groups.

In the early 1990s, it was proposed that these two phosphate groups, separated by 20 Angstroms, come together in the minimal hammerhead to form a single metal binding pocket (Pley *et al.,* 1994; Scott *et al.,* 1996). In strong support of this model, simultaneous phosphorothioate substitutions at each position were found to form a binding site for a single thiophillic metal ion in minimal constructs (such as Cd2+) (Wang *et al.,* 1999). Phosphorothioate metal rescue was also observed at the same sites in the full-length hammerhead at low ionic strength (Osborne *et al.,* 2005).

The possibility remains that under solution conditions more closely approximating physiological conditions the metal binding site observed in the minimal structure will occupy a divalent ion. The observation of a metal ion near this site, or anywhere else in the full-length structure, would require an in-depth examination of its structural and catalytic contribution. An examination of the detailed interactions comprising the stabilizing loop/bulge interactions may similarly enhance our knowledge regarding structure stabilization in this molecule. Given the recent discovery of hammerhead motifs throughout the tree of life, including pathogenic bacterial ribozymes, such structural details may lead to new targeting strategies and improved molecular models. (De la Peña et al., 2008). In addition, a

careful exploration of the differences between the 2006 and our high-resolution structure will address whether the 2.2 Angstrom structure represents a stable ground state, or an intermediate structure trapped along a rugged folding landscape.

CHAPTER 2

Toward Direct Observation of Cleavage and Ligation in the *Schistosoma mansoni* Hammerhead Ribozyme

2.1 Summary of Findings

The emergence of novel functional RNAs, pathogenic RNA drug targets and an expanding repertoire of RNA-based therapeutics over the past two decades has lent renewed motivation to the challenge of understanding the fundamental structural basis for RNA catalysis (DeLaPeña 2010) (Przybilski 2005). The hammerhead ribozyme represents an appropriate system to explore fundamentals aspects of RNA structure and catalysis as its canonical mechanism for cleavage and ligation are well established. Often called the "serine protease of ribozymes," it has been the subject of 20 years of exhaustive study (Hartig 2008). Here, we introduce a single-molecule magnetic tweezers assay applied to hammerhead RNA catalysis.

In order to dissect the mechanochemical cleavage and ligation cycles of the hammerhead ribozyme, we have developed a method that utilizes DNA topology as a readout for activity in a single hybrid RNA/DNA molecule. The robust nature of this system enables the real-time observation of successive cleavage and ligation cycles over the course of days. Using magnetic tweezers, a single hybrid molecule can be stretched, relaxed and supercoiled via extended DNA handles; changes in extension reflect the release of torsional constraint following catalysis and perhaps structural rearrangements (Li 2008). Here, we report an assay that can be monitored in real time, with the ability to modulate buffer conditions and force at will.

In this study, we have inserted the hammerhead ribozyme between two long dsDNA handles (~2.4 kilobases) using ligation chemistry. This was done by flanking the hammerhead construct with long DNA extensions (Figure 1a) to obtain a

ribozyme model of natural hammerheads for which substrate and product dissociation is negligible. This experimental design is similar to one used successfully to assay the activity of single DNA gyrase molecules. We have simply substituted an embedded full-length hammerhead RNA sequence (Figure 1a) for the embedded DNA gyrase binding site (Gore 2006). By comparing the supercoiling density of our construct to an all DNA molecule, we are able to calibrate our system and ensure measurement is restricted to a single molecule of DNA embedded with a single hammerhead ribozyme.

2.1.1 Canonical Cleavage in the Magnetic Tweezers Hammerhead Assay

The following work outlines the development of the hammerhead ribozyme single molecule assay. The raw data referenced in this study plots changes in the extension of a one micron magnet bead (y-axis) against time (x-axis) (Figure 5). Changes in extension ("Z-position") represent changes in the supercoiling density of a single dsDNA molecule embedded with a single hammerhead nicking enzyme (Figure 1). The agreement between the temporal spacing of successive cleavage events observed in these experiments and measured bulk rates strongly suggest that this signal represents canonical hammerhead cleavage (Figure 13). The response of the system to well-established active site mutations also reinforces the conclusion that the observed signal represents cleavage and ligation of a single hammerhead molecule (Figure 6). Finally, agreement of bulk and single-molecule responses to solution effects of pH and magnesium supports this model (Figure 7).

However, the relatively low-throughput nature of the measurement provides an obstacle to declaring this correlation to be accurate with statistical certainty. As in many prior single-molecule studies, a small proportion of tethered molecules (5-10%) exhibit the activity measured herein (Nöllmann 2007). This circumstance is tolerable in many systems when the appropriate controls are implemented; the presence of entangled DNA "braids," harsh ligation conditions, and an excess of various ligation components can reasonably be said to reduce the efficacy of any single-molecule magnetic tweezers study (Charvin 2003). A second obstacle, however, prevents us from definitively determining the source of our signal. In brief, the methylation of the 2'-OH group of C17 (the nucleophile) in our system fails to abrogate the observed signal for every molecule studied. The mutation, which is predicted to shut down cleavage activity completely, permits an average of 1% of molecules to continue successive cycles of activity. Thus, while the majority of rate calculations, sequence controls, and solution effects agree with our expectations, the low-throughput nature of our active population prohibits an unambiguously convincing statistical analysis in this system.

The following the treatment will refer to the signal observed herein as hammerhead "cleavage" and "ligation" because the attachment of those labels remains most probable and appropriate in light of our current knowledge. Alternate sources for the signal might include effects of surface attachments and the activity of ligase enzymes stalled at the DNA/RNA junction adjacent to the enzyme active site (Schlingman 2011). However, the absence of this signal in any prior study, and the

routine heat inactivation of T4 ligase render these explanations highly unlikely. In any case, the observation of a chiral impact of applied torques (Figure 21) and translational force (Figure 17) and the observation of reversibility in this system motivates continued exploration of magnetic tweezers studies as applied to nucleolytic ribozymes.

2.1.2 A Supercoiling Assay for Single Molecule Hammerhead Ribozyme Catalysis

Natural hammerhead self-cleaving sequences in mRNAs and satellite virus RNAs are in many cases embedded within long base-paired stretches of RNA (Nelson 2005). We have designed a single-molecule experimental system that exploits this arrangement by greatly extending the base-pairing regions between the enzyme and substrate strands of Stems I and III of the *Schistosomal* (Smα1) hammerhead. This was achieved by flanking the natural hammerhead construct with long DNA extensions (Figure 1a) to obtain a ribozyme model of natural hammerheads for which substrate and product dissociation is negligible.

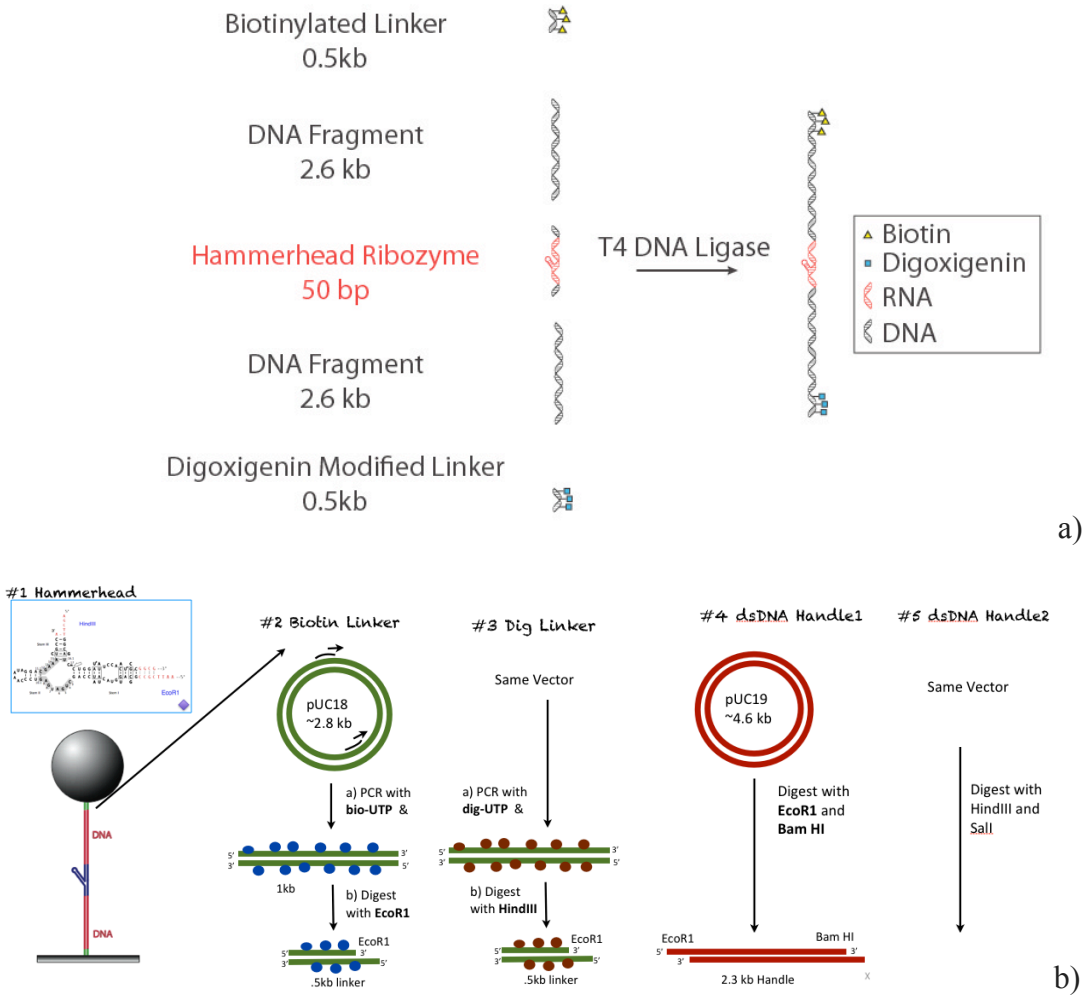

Figure 2.1 Molecular Construct a) Natural hammerhead embedded in 2.6 kb dsDNA Fragment "handles." A 46bp Hammerhead Ribozyme replaces the DNA Gyrase binding site in a prior magnetic tweezers study (Bustamante et. al, 2006). T4 DNA ligase joins functionalized "Linker" fragments to 2.6kb DNA "Handles". b) Five part molecule construction. A hammerhead ribozyme engineered with EcoR1 and HindIII overhangs (#1) is ligated to a complementary 0.5kb biotinylated linker (#2), a 0.5 kb digoxigenated linker (#3), and 2.6 kb complementary dsDNA Handles (#4, #5). Purified ~6kb constructs are adhered to a glass slide coated in anti-digoxegenin antibodies following T4 ligase heat inactivation. Streptavidin-coated magnetic beads (grey sphere, #1) are introduced to the flow chamber for 10 minutes prior to measurement under an inverted light microscope.

The experimental design utilized in this study is similar to one used successfully to assay the activity of single DNA gyrase molecules (Gore 2006). We have simply substituted an embedded full-length hammerhead RNA sequence (Figure 1b) for an embedded DNA gyrase binding site. Stems I and III of the hammerhead RNA are ligated to long flanking DNA handles. Both strands of the distal ends of the DNA handles are then tethered to an immobile surface and to a magnetic bead, respectively. If the ribozyme has not cleaved, positive or negative supercoils will be imparted simply by rotating the magnetic bead. Nucleic acid supercoiling is a powerful assay of the connectivity of the phosphate backbone (Salerno 2012). If the backbone becomes nicked, either mechanically or via cleavage of the embedded ribozyme, no supercoils can accumulate. If an intact backbone should become nicked in the course of supercoiling, any accumulated supercoils will immediately be relieved, providing a measurable readout in the form of a qualitatively identifiable optical signature for cleavage (Figures 2).

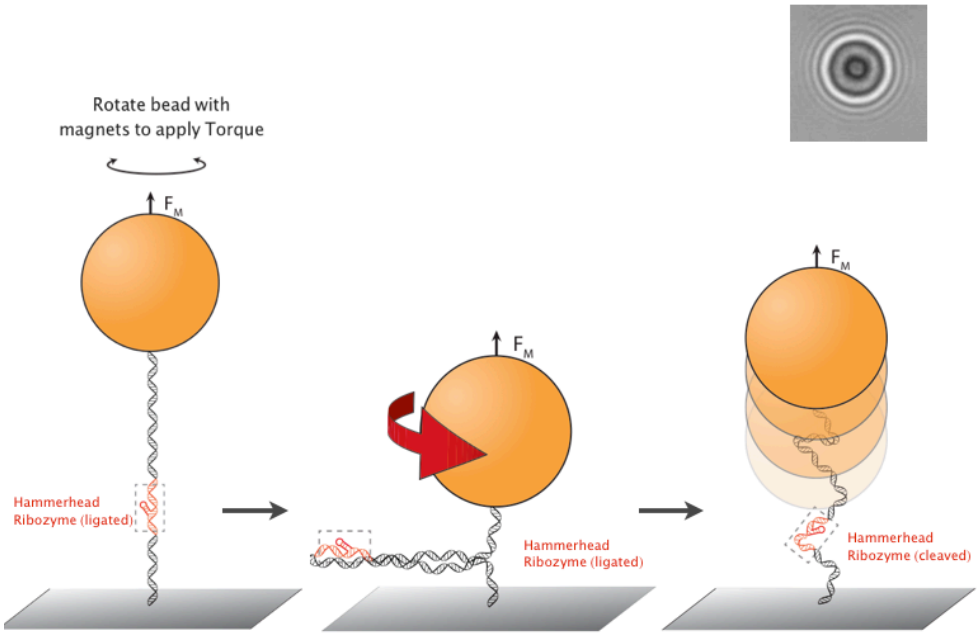

Figure 2.2 Experimental setup of hammerhead magnetic tweezers assay. A magnetic trap consists of a magnetic bead (sphere) tethered to a glass surface by one hybrid DNA/RNA molecule. The bead experiences a force proportional to the gradient of the field. (+) and (-) supercoils are formed by application of torque. The accumulation and relaxation of supercoils by an embedded hammerhead can be measured by monitoring the extension of the DNA tether in real time. If the hammerhead molecule is in the ligated state, introduction of supercoils by a pair of fixed magnets forms plectonemic DNA regions that make the DNA extension decrease (center). If the hammerhead cleaves, torsional strain is relieved. Changes in Z-position of the bead are determined by monitoring the optical signature of the paramagnetic bead (top right).

A one-micron magnetic Streptavidin bead is used to tether one end of the molecule, while the opposing end is adhered to a glass surface treated with anti-digoxegenin molecular antibodies (Figure 1b) (Shang 2007). This extension of the DNA can be determined by measuring the position of the manipulated particle in an inverted optical microscope. The accuracy of the measurement is a few nanometers (10^{-9} m) or better (Neuman 2008). The extension of DNA as a function of the linking

number difference and the applied force reveals the partitioning between *Tw* and *Wr* (Charvin 2003).

If the DNA molecule in our setup is devoid of nicks (which act as free swivels) and the attachments at both ends are rotationally constrained, rotating the particle by one full turn changes the *Lk* of the DNA by 1 unit. If, however, in the course of rotating the molecule, the ribozyme undergoes a self cleavage event, the stored torque will be released and the supercoils will unravel until either the hammerhead re-ligates, or all of the supercoiling is released. If the hammerhead religates before all of the stored torque is released ("partial relaxation"), one can determine the precise number of rotations that have occurred by measuring the Z-position of the magnetic bead (Figure 2). Because it is known that one revolution of the hammerhead about its swivel point is equivalent to roughly fifty microseconds, one can determine the rate of ligation of the molecule for partial relaxation events (Figure 3) (Vlijm 2012). The Stem I and Stem III portions of the molecule unravel in opposing directions, signified by red and green arrows in Figure 5 (DeVlaminck 2012). Notably, we observe two characteristic cleavage/ligation signals. In the most prevalent variety represented in Figure 3, the molecule spontaneously religates on the time scale of microseconds. In the second type of signal, the molecule relieves all of the imparted supercoils and fully relaxes (Figure 4).

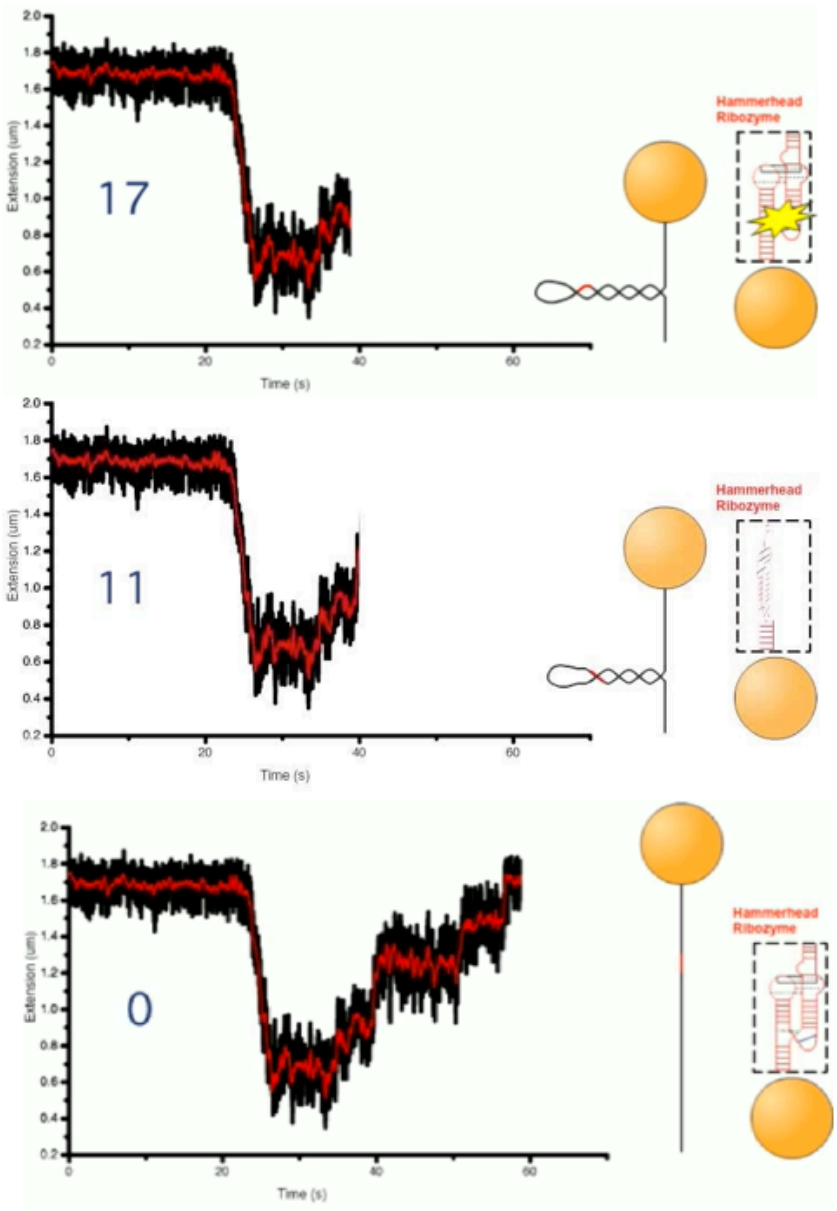

Figure 2.3 Active ligation mode: partial relaxation and fast ligation of an embedded full-length hammerhead. a) Seventeen rotations of an external magnet induces supercoiling, reducing the z-extension of the molecule relative of a reference bead adhered to the glass surface. A cleavage event (top right) results in a release of torsional strain. b) A ligation event (microsecond time scale) seals the nicked backbone following six rotations of the about the free swivel. Because dissociation is limited in the context of an embedded enzyme, the reactants are pre-positioned for ligation, resulting in an ultra-fast ligation rate. c) Three successive cleavage and ligation events release the remaining eleven supercoils.

2.1.3 A Hammerhead Embedded in Long DNA Handles Spontaneously Religates

Typical enzymology experiments performed on nucleolytic ribozymes in solution employ "ideal" constructs for which product dissociation is not rate-limiting, thus permitting identification of the turnover rate with k*cat*, the chemical step of the forward (cleavage) reaction (Osborne 2005). This is made possible in practice if the Watson-Crick base-pairing regions of Stems I and III are limited to four or five nucleotides, in which case the cleavage reaction can go nearly to completion. As base-pairing is extended, product dissociation becomes rate-limiting, and the apparent turnover rate slows, masking the chemical step of the reaction.

Our single-molecule assay relies upon very long (2.3 kb) extensions of Stems I and III, thus ensuring that product dissociation is greatly disfavored (Figure 1) (Shepotinovskaya 2008). This has two effects upon catalysis, in addition what might be expected. First, because the two product strands will fail to dissociate, they are pre-bound and pre-positioned for the back reaction to take place. The back reaction thus becomes more significant, due to the proximity and effective concentration of the back-reactants (Figure 3). Second, because the ligation reaction becomes much more favorable, we find under the conditions of our assay (an embedded ribozyme experiencing constant torque and force), unlike those in solution with an "idealized" ribozyme construct (Osborne 2005), re-ligation of a cleaved ribozyme becomes spontaneous, permitting us to suggest that in their natural context,

hammerheads may well favor the ligated state, and cleave in response to some form of structural perturbation.

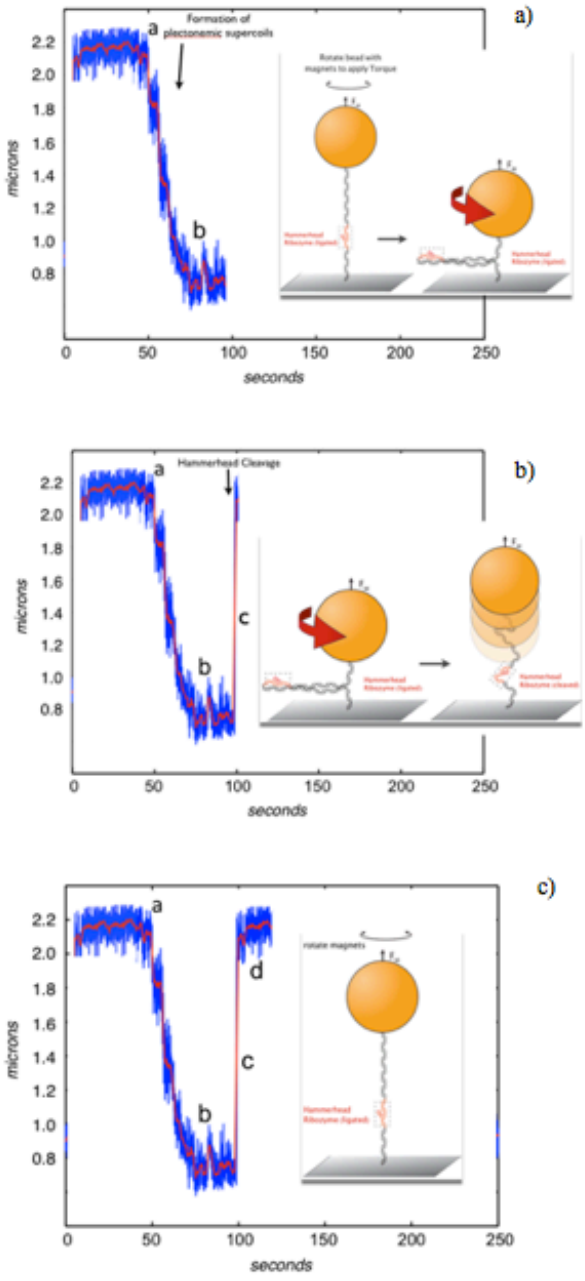

Figure 2.4 Passive ligation mode: full relaxation of an embedded full-length. a) Seventeen (+) magnet rotations induce b) supercoil formation for 30 seconds until c) hammerhead cleavage releases *all* of the stored tension before ligation can occur. d) A second cycle of magnet rotation fails to induce supercoiling because the hammerhead remains in a cleaved state.

If the hammerhead religates before all of the stored torque is released ("partial relaxation"), one can determine the precise number of rotations that have occurred by measuring the Z-position of the magnetic bead (Figure 3). Because it is

known that one revolution of the hammerhead about its swivel point is equivalent to roughly fifty microseconds, one can determine the rate of ligation of the molecule for partial relaxation events (Figure 3). Fast ligation is observed in a majority of molecules under study, however a second class of molecules exhibited slower ligation (Figure 4) (Lipfert 2011). Ligation rates on the microsecond scale have never before been reported for this molecule (Nelson 2008), however, a preference for the ligated state would facilitate both protection against endonuclease degradation and dissociation of the back reactants under physiological conditions (Celesnik 2007).

The second characteristic state is indicative of slower ligation rates (Figure 4), and demonstrates that we observe static heterogeneity in this system. It is well-documented that RNA enzymes contain rugged folding landscapes due to its numerous rotatable bonds relative to proteins (Bokinsky 2005). In our case, the cleavage and ligation rates differ moderately from molecule to molecule, yet all respond equally to force and torque. Thus, our system provides a direct observable that cannot be achieved in bulk due to averaging effects (Bokinsky 2003).

2.1.4 Apparent Cleavage and Ligation Reactions are Reversible and Processive

A single hammerhead embedded in long DNA handles can undergo multiple (hundreds of) successive cleavage/ligation cycles, revealing for the first time that the natural hammerhead sequence is indeed a genuine catalyst, or a true ribozyme (Leclerc 2010). *In vitro* enzymological characterization of hammerhead RNAs artificially divided into enzyme and substrate strands under single-turnover conditions

(wherein the enzyme strand concentration exceeds the substrate concentration) allows for the measure of the turnover (k*cat*) of the cleavage reaction, as well as K_m (Nelson 2006). However, demonstration of multiple cleavage and ligation events under such conditions is difficult, and even more so with a natural construct.

The single-molecule cleavage and ligation supercoiling assay demonstrates that a single natural-sequence hammerhead molecule indeed can undergo hundreds of successive cleavage/ligation cycles, each time regenerating a catalytically competent complex, thus putting to rest the objection that hammerheads (and presumably other self-cleaving RNAs) are not true ribozyme catalysts that exhibit multiple turnover (Leclerc 2010). Potential alternate sources of the observed signal are discussed later in this work, but the controls described herein make any of these alternative scenarios unlikely.

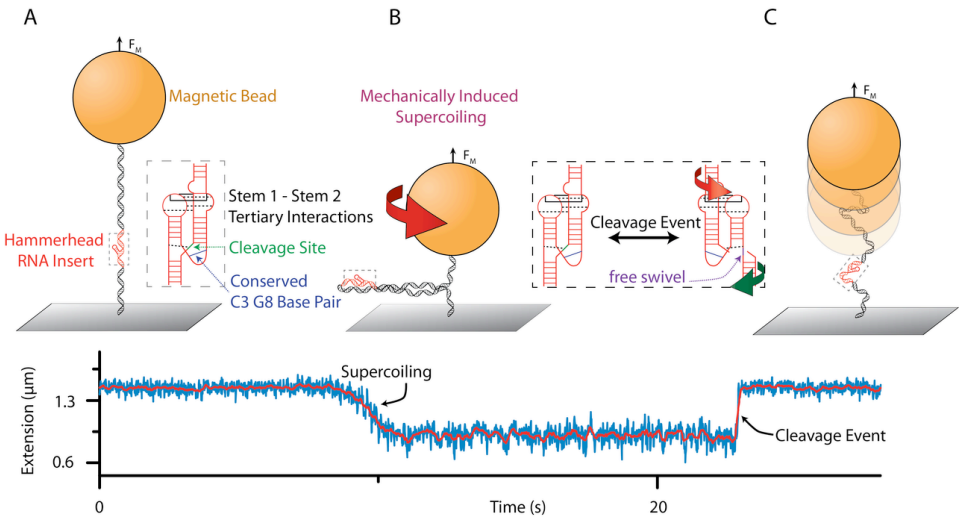

Figure 2.5 Experimental design and observation of single-molecule hammerhead cleavage. a) The full-length hammerhead contains a bulge-loop tertiary interaction between stem I and II adjacent to the C-17 cleavage site and the highly conserved C3:G8 base pair. The molecular construct is ~1.5 microns in its fully-relaxed state (bottom). b) Rotation of external magnets induces supercoiling, causing an decrease in height of the bead. c) A cleavage event results in the unwinding in opposing directions of the stem I and stem III aspects of the molecule (red and green arrows). Release of torsion results in an increase in extension of the bead.

2.1.5 Negative Control: The G8A catalytic mutation greatly reduces activity

Both minimal and full-length hammerheads possess highly conserved catalytic core sequences. In particular, residues G8 and C3, although not believed to be directly involved in the chemical step of the reaction, are absolutely invariant (Martick 2008)(Lee 2008). Crystal structures of the full-length hammerhead implicate both a structural and catalytic role for this resides (Martick 2006). G8, the putative general acid, forms a Watson Crick base pair with C3 (Figure 5a, Figure 6a).

Mutation of either residue essentially destroys activity, decreasing it by a factor of 10^{-5} (Martick 2006).

To test that the observed cleavage and ligation reactions in the single molecule assay were in fact due to standard, on-pathway hammerhead ribozyme catalysis, we created a G8U mutation and verified that its activity was indeed greatly attenuated. The G8U mutant hammerhead ribozyme construct displays about 50% reduced activity relative to the wild-type ribozyme under otherwise identical conditions.

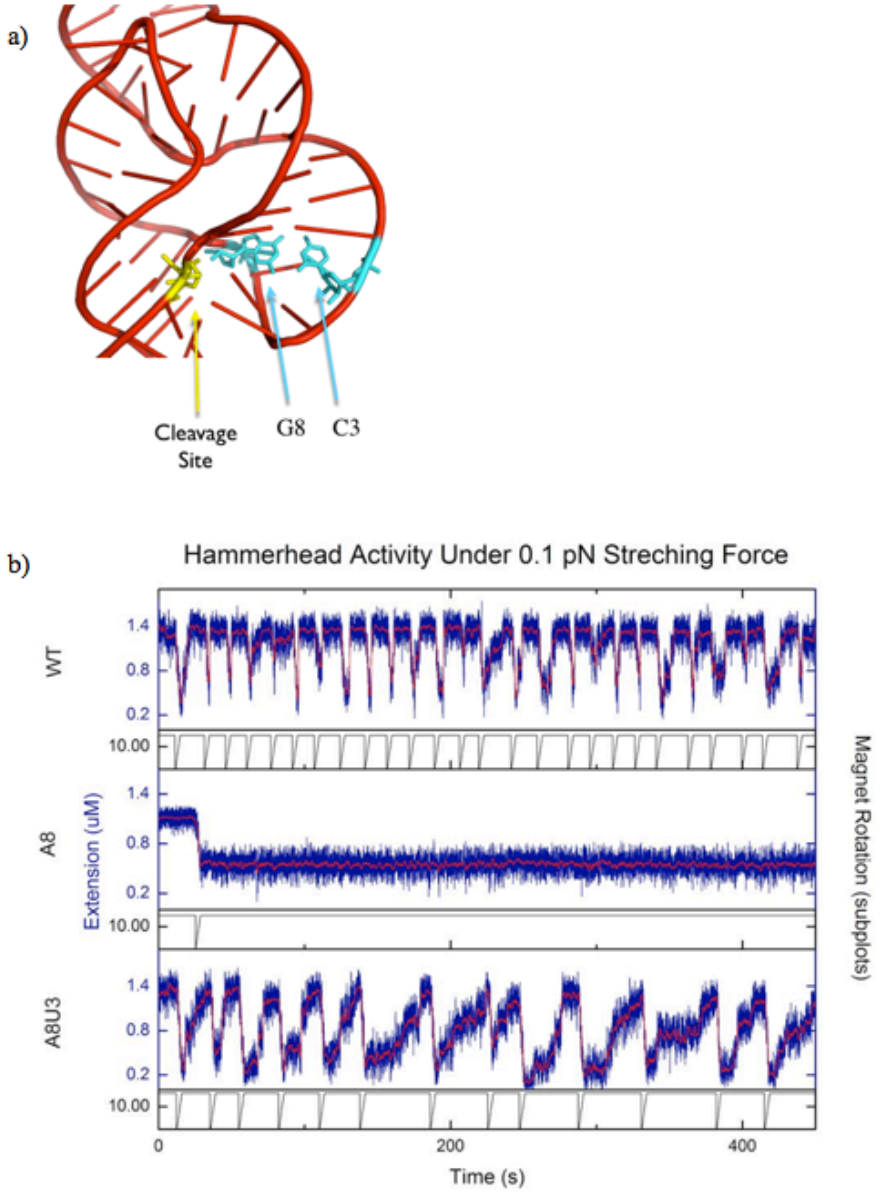

Figure 2.6 The C3U/G8A double-mutation rescues activity and changes the internal equilibrium. a) G8 and C3 form a Watson Crick base pair in the natural hammerhead crystal structure (2GOZ), positioning G8 to act as a general acid. b) Data trace of three hammerhead variants with bead extension (um) on the y-axis and time (s) on the x-axis. Magnet rotation is indicated beneath each trace (0-10 scale). Mutation of G8 to A8 (center panel) abolishes wild type activity (top). Rescue with C3U/G8A double-mutant restores activity, but the rate of ligation is restored to a greater extent than the rate of cleavage, thus shifting the internal equilibrium further toward reactants (bottom).

2.1.6 Positive Control: A C3A/G8U Double-mutation Rescues Activity

The crystal structure of the full-length hammerhead ribozyme revealed the structural basis for the deleterious effects of mutating residues C3 and G8 (Martick 2006). These are found in the full-length hammerhead to form a Watson-Crick tertiary base-pair that helps to stabilize the required conformation within the catalytic center of the ribozyme. The crystal structure lead to the prediction that if C3 were mutated to one of the other three nucleotides, a compensatory mutation in G8 that restored the ability to form a Watson-Crick base-pair should at least partially rescue catalysis (Martick 2006). Indeed, such double-mutants exhibit significantly-restored catalysis (under standard solution conditions) relative to their corresponding single mutations. Hence, as a further positive experimental control for non-aberrant hammerhead ribozyme catalysis, we constructed a C3A/G8U double- mutant and demonstrated that it rescues catalysis in the context of the single molecule construct.

2.1.7 The C3U/G8A Double-mutant Changes the Internal Equilibrium

Although all seven other possible Watson-Crick base-pairing combinations between nucleotides 3 and 8 rescue catalytic activity when compared to their corresponding single mutations, none fully restore catalysis as measured in standard

solution enzymology assays, suggesting that base-pairing might not be the only factor involved (Lee 2008). A possible explanation for these variations becomes apparent with the single molecule analysis of the C3U/G8A double-mutant. The rate of ligation is restored to a greater extent than the rate of cleavage, thus shifting the internal equilibrium further toward reactants. Hence it appears that minor differences due to sequence variations in the active site that nonetheless maintain the hydrogen-bonding structure of the active site can perturb the internal equilibrium (Canny 2007), suggesting that this may well constitute a sensitive regulatory functionality within the context of the natural hammerhead ribozyme, i.e., it may have unmasked the subtle structural fluctuations that are responsible for regulating the nuclease/ligase switch.

Notably, as the translation tension of the molecule is varied from .2pN to 1.5pN, the activity of each variant changes markedly. Alteration of translational force is achieved by changing the height of the permanent magnets positioned above the slide, controlled by a Piezo-stepping device (Oddershede 2012). In the case of both wild type and double-mutant hammerheads, an increase in translational force causes a decrease in both the cleavage and ligation rate. This observation is consistent with the findings of the only other single-molecule study of the hammerhead ribozyme which reported that undisturbed natural tertiary contacts lead to dynamic motional sampling that increasingly populate catalytically active conformations (Mcdowell 2010). In our study, it is reasonable to assume that increased translational force reorients the underwound portion of stem I imposed by the tertiary contact. The

result is likely a decreased incidence of the active conformation, and therefore both a decreased cleavage and ligation rate.

2.1.8 Activity is pH-dependent, [Mg^{2+}]dependent and Sequence-dependent

To test that hammerhead ribozyme catalysis in the context of our embedded single molecule supercoiling assay possessed the same catalytic properties as standard hammerhead ribozyme constructs characterized in solution, we assayed the frequency of cleavage as a function of pH and [Mg^{2+}]. The frequency of cleavage events indeed was found to increase with increasing pH and increasing magnesium ion concentration, consistent with on-pathway hammerhead catalysis.

The effect of metal ion concentration can be seen in both changes in the raw data trace (Figure 7a) dwell times of individual molecules (Figure 7b). Figure 7a compares raw data traces at 4mM Mg^{2+}, 0mM Mg^{2+} , and 0mM Mg^{2+} plus 50 mM EDTA. Later experiment ensures residual Mg^{2+} in the flow cell does not bias the results. The effect of removing divalent ions appears to be an enhancement of cleavage, a decrease in ligation, or both (Nelson 2005). The condition including EDTA appears to slightly enhance the ligation rate, possibly due to the moderate increase in monovalent ions associated with EDTA. These findings are consistent with the aforementioned role of generic positive charge facilitating folding in the hammerhead ribozyme (Martick 2006). In Figure 7b, the dwell times (in supercoiled state) of five representative molecules are compared. In each case, the presence of divalent ions increases population of the supercoiled state.

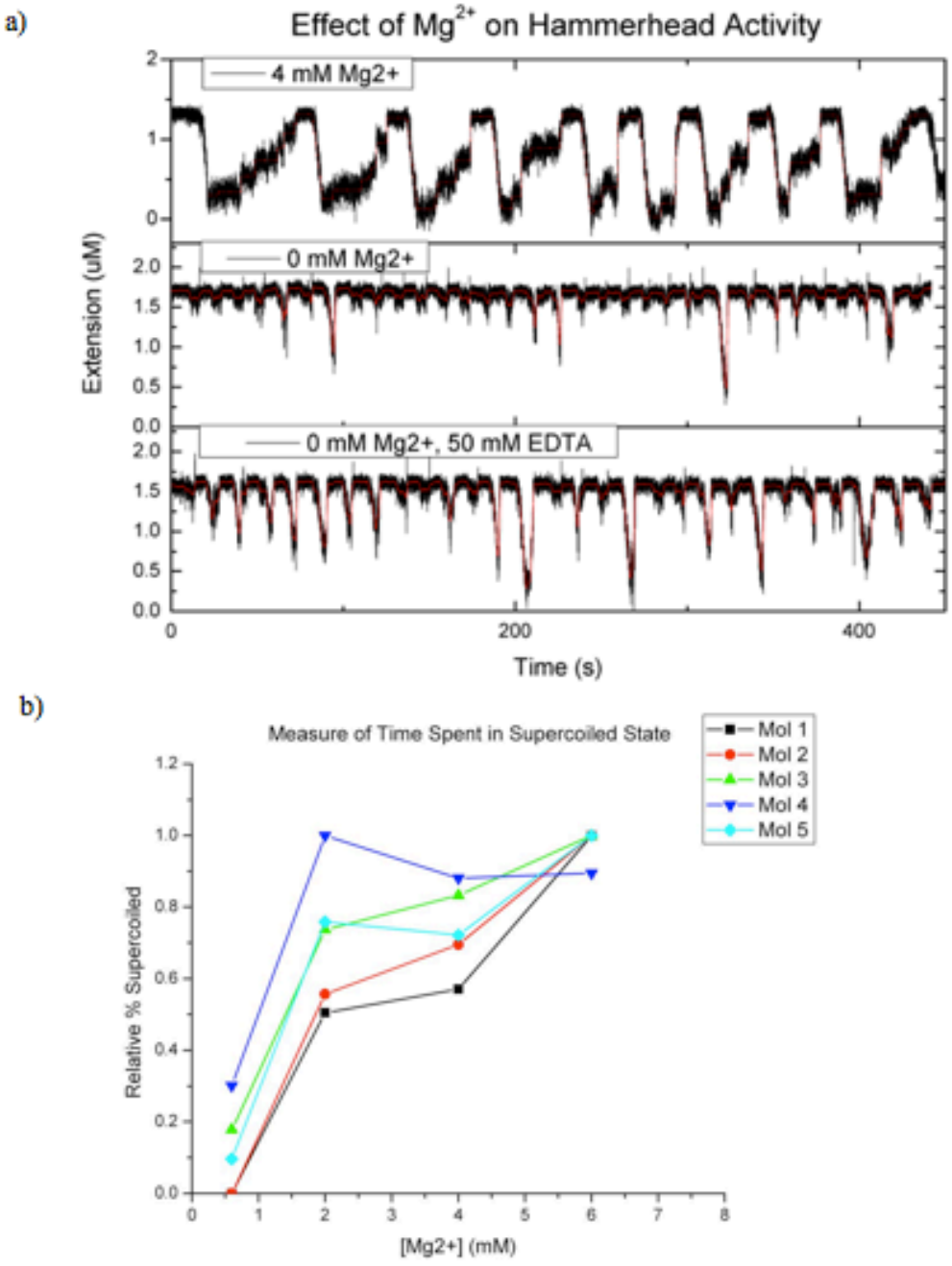

Figure 2.7 Effects of magnesium ion concentration on hammerhead activity. a) Raw data trace compares activity at 4mM Mg^{2+}, 0mM Mg^{2+}, and 0mM Mg^{2+} plus 50 mM EDTA. The EDTA condition ensures removal of residual Mg^{2+} in the flow cell, but introduces millimolar concentrations of monovalent ion that may stabilize folding. b) Comparative dwell time analysis of five separate molecules. Increased divalent ion concentration correlates with an increased population of the supercoiled state. Consistent with the measurement in 7a, a low concentration of divalent ions correlates with an inability to achieve the supercoiled state.

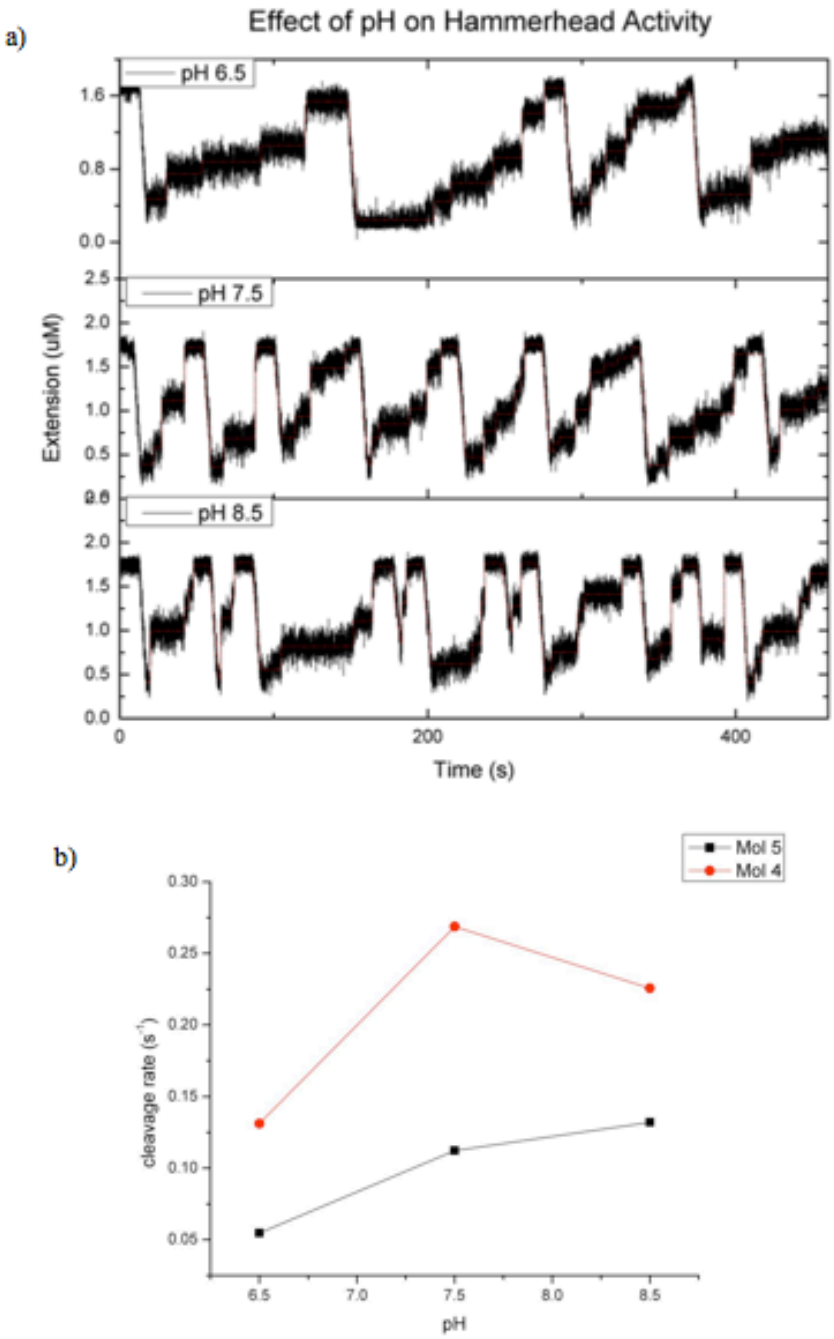

Figure 2.8 pH dependence profile. a) raw data trace, pH titration. Forward rates remains steady while the ligation rate is enhanced at lower pH (top). b) K_{obs} in two different molecules (Mol 5, Mol 4). Kinetic analysis of ~100 cleavage/ligation cycles for each molecule reveals pH profile plateau around 8, in agreement with bulk observations. The deviation in rate between the two molecules reflects static heterogeneity observed in this system.

Consistent with the measurement in Figure 7a, a low concentration of divalent ions correlates with an inability to achieve the supercoiled state. We posit that this is due to an enhanced population of the active conformation under millimolar concentrations of divalent ions (Mcdowell 2010). Discussion of the effects of metal ions and force on the minimal hammerhead are explored later in Chapter 2.

The pH dependence of the full-length hammerhead parallels that of the minimal hammerhead in bulk (log-linear relationship with slope of ~1 at 10mM Mg^{2+}) (Fedor 2009). The pH dependence profile plateaus around 8.0 and is therefore likely indicative of protonation-deprotonation of a functional group with a high pKa (Canney 2004). The single-molecule assay described here closely mirrored these observations in bulk. Specifically, the pH dependence plateaus around 7.5/8 as observed in bulk.

Data collection and cleavage rate measurement are carried out by an automated software program that initiates time zero (T0) when the z-position of the bead crosses a threshold defined by three standard deviations of the bead noise (Figure 5). The second time point is collected when the magnetic bead crosses this threshold

2.2 Instrumentation and Analysis

A discussion below outlines details of instrumentation calibration, dwell-time analysis, automation software, and force-calibration. Additional results are

discussed, including a chiral impact of applied torques, solution effects on activity, and a detailed analysis of the various sequence mutants explored in this study.

2.2.1 Dwell Time Determination

A key step in the development of our instrumentation was the automation of data collection and magnet control. This automated system sets a limit on what we define as a successful supercoiling event for the purposes of calculating cleavage rates. The start of cleavage event timer is when the extension of the molecule is low enough to have a greater than 99% confidence interval that a supercoiling event has occurred (using 5σ based on first 12 seconds of trace). The end of the cleavage event timer is when the mean filtered derivative data passes a threshold of 5σ where the standard deviation is defined by the wait period before the rotation begins (eg first 12 seconds of viewable data on each trace). If no start or finish is detected, that specific supercoil/cleavage attempt is thrown out. If there are no partial relaxation events (where the molecule cleaves and re-ligates before crossing the threshold), the dwell time is a relatively accurate measure of the cleavage rate. Such a system ensures, a) that data analysis was not biased by errors generated by a user manually rotating the magnets and b) that molecules with diminished rates (like the C3 single mutant) could be monitored without a user present. As some dwell times could last 10-20 minutes, this tool became an invaluable asset to ensure consistency of data analysis.

2.2.2 Extension histograms for measurement of chiral impact of applied torques

To generate extension histograms, each cleavage event is analyzed and the software determines if it is in the negative direction or positive direction by referencing the starting rotation position of the dataset and ending rotation position of the dataset. If the last rotation is greater that first (ie in second plot the first point is 800 and the last point is 850), all the data for that event is added to a cumulative data bin for the positive events. So in the end, the software presents separated extension arrays where all of the extensions for negative events are in one array and all the extensions for the positive events will be in a separate array, each represented as a histogram.

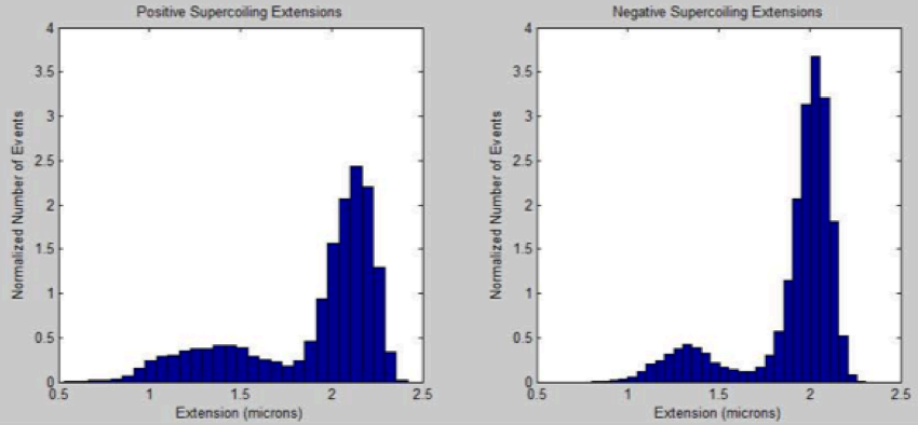

Dwell time Histogram 2.9 Negative supercoiling (right) results in greater population of the fully extended state, reflecting an enhanced cleavage rate and/or decreased ligation rate. Positive supercoiling (left) exhibits a larger population of dwell times in the supercoiled state.

2.2.3 Instrument Calibration

In order to generate an accurate measurement of the length and force applied to the molecule in study, each molecule must be calibrate separately (Oliver 2011).

Slight variations in the optical signature of different magnetic beads, the surface character of different slides, in addition to slight variations in temperature and buffer conditions require the user to compare each active molecule with another magnetic bead that is positioned directly adjacent to the bead under study (Gosse 2002). This "reference bead" can either be stuck to the surface (preferable), or be a nicked inactive tether that maintains a constant length. In any case, we can utilize a Piezo-stepper to decrease the height of the stage in millimeter increments, generating a stack of diffraction pattern images comparable to the signature of a bead changing its height in the Z-position following hammerhead cleavage (Figure 9). In this way, we can observe the change in height of the bead by monitoring the change in interference fringe patterns.

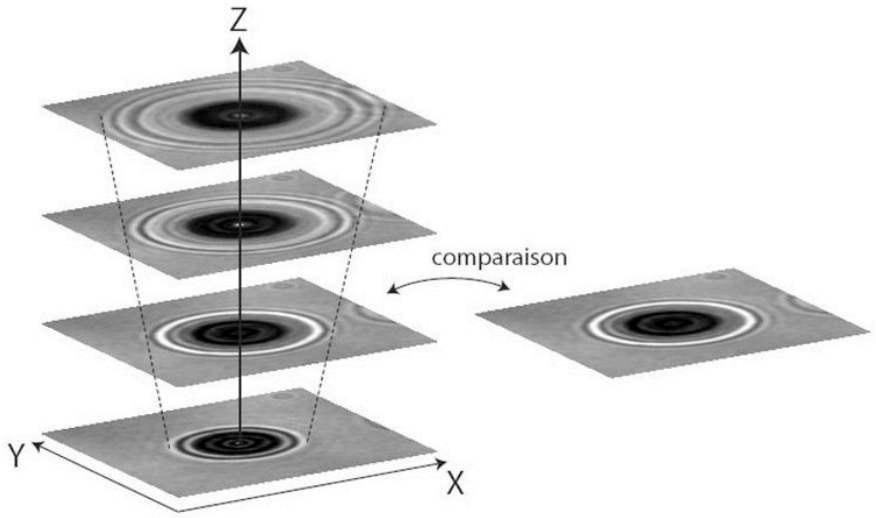

Fiugre: Biophys J 82:6, 3314-29

Figure 2.10 Calibrating the instrument. A Piezo-stepper decreases the height of the microscope stage in millimeter increments, creating a distribution of images representing various Z-positions of a magnet bead suspended above the glass slide. Comparison of a molecule under study to that of a bead permanently fixed to the glass slide enables tracking of Z-position in real time.

2.2.4 Measurement of dsDNA/RNA supercoiling

If a magnetic bead is tethered to the surface by an in tact, double-stranded molecule attached by multiple bonds at each end, the molecule is torsionally constrained and rotating the magnets will twist the DNA and cause it to form plectonemic supercoils (Schöpflin 2012). The twist is initially absorbed by elastic twist deformations, and the torque increases linearly with the number of turns (Figure 10).

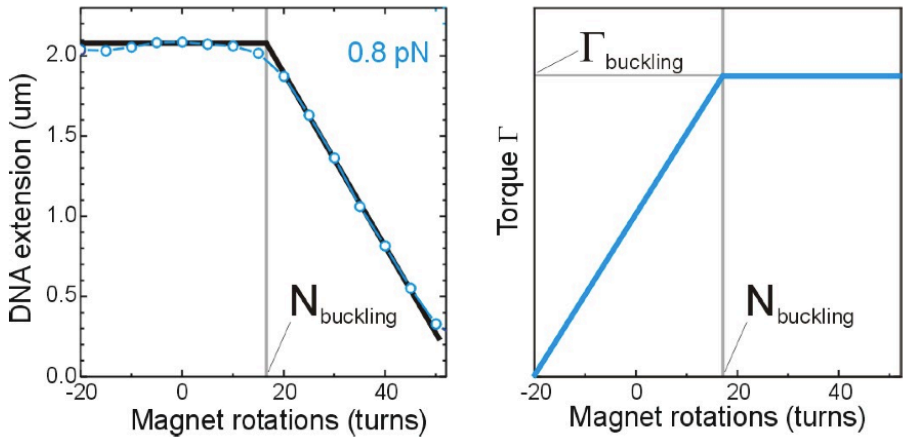

Figure: Bustamante et al., *Nature* 421, 423 (2003)

Figure 2.11 The elastic behavior of supercoiled DNA. Under sufficient torsional strain, a twisted DNA molecule shortens as plectonemic regions are formed. As rotations are transmitted into the molecule, extension remains constant until a buckling transition is reached, after which the molecule contracts linearly with each rotation.

If one continues to rotate the magnets, the molecule undergoes a buckling transition when the energy stored in the elastic twisting deformation is reduced by forming a loop (Marko 2012). In this buckling regime, height of the bead decreases linearly with the number of rotations, and torque remains constant as the energy of each additional rotation is transmitted into plectonemic supercoils (Figure 10) (Schöpflin 2012). In contrast, if the nucleic acid molecule that tethers the bead to the surface is attached only via a single bond at either end or if the molecule is nicked, the molecule will swivel around the single bond and remain torsionally unconstrained, even if the magnets are rotated. Likewise, if a torsionally supercoiled dsDNA molecule has been coiled to the surface and sustains a nick, those supercoils will be relieved, resulting in a rapid increase in height of the magnetic bead (Nöllmann 2007).

Identification of dsDNA/RNA tether that buckles at an appropriate force is indicative of a single tether (Charvin 2003a). Once this has been verified, a force calibration is conducted that measures the response of the molecule to supercoiling under various translational forces. By measuring the variation of a molecule's extension versus the number *n* of extra turns applied to the molecule, and extension curve is generated. At low forces (F= 0.3 pN; red points), the extension curve is symmetric with a maximum at *n=0* (Schöpflin 2012). The decrease in extension from the maximum is due to the molecule buckling to form plectonemes. At intermediate forces (F= ~1pN; blue/green points), buckling occurs when positive turns are added. Denaturation bubbles appear under negative supercoiling, preventing plectoneme

formation. While the majority of our measurements were conducted at the moderate force of .16 pN, at forces nearing 1 pN, our experiments verified that dsDNA/RNA hybrid molecules form denaturation bubbles under negative torque (Figure 11) (Jeon 2010).

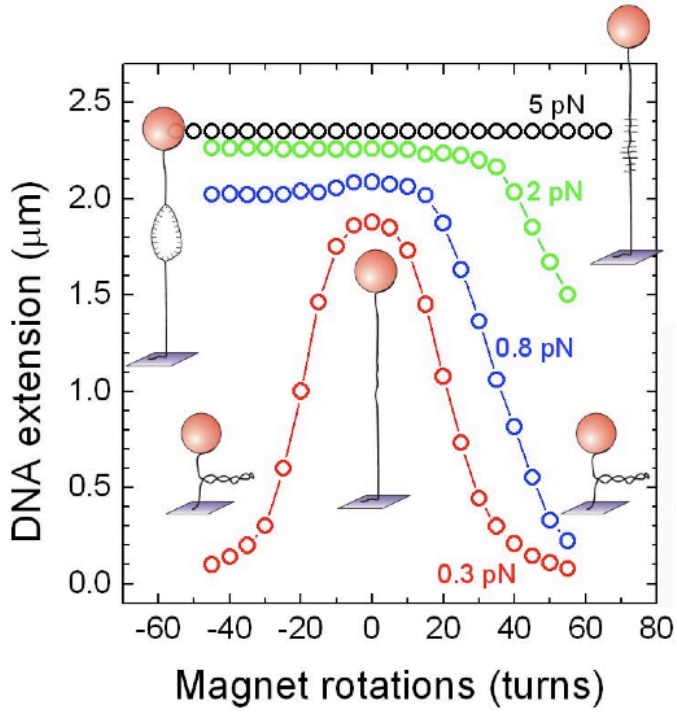

Figure: Croquette, V. et al. Nucl. Acids Res. (2006) 34(15): 4232-4244

Figure 2.12 Response of DNA to supercoiling. Molecule extension versus magnet rotations under positive and negative torque. At low force (F= 0.3 pN; red points), the extension curve is symmetric with a maximum at *n=0.* The decrease in extension from the maximum is due to the molecule buckling to form plectonemes. At intermediate forces (F= ~1pN; blue/green points), buckling occurs when positive turns are added. Denaturation bubbles appear under negative supercoiling, preventing plectoneme formation. At high force (F= 5 pN; black points), denaturation still occurs under both positive and negative torque.

At high force (F= 5 pN; black points), denaturation still occurs under both positive and negative torque. Often, a user will use this knowledge to help differentiate between a single tether and a braid (multiple DNA tethers bound to one paramagnetic bead). Only a single tether will exhibit this asymmetry at high forces, while a braid will always supercoil under either positive or negative torque (Talukder 2011).

2.3 A Magnetic Tweezers Assay for Hammerhead Ribozyme Catalysis

In the discussion below, minimal and full-length activity will be treated separately. Then, the activity of several classic mutants will be analyzed. Finally, an observed chiral impact of applied torques will be presented, in addition to a discussion of observed cruciform structure formation during mechanical annealing.

2.3.1 Single Molecule Minimal Hammerhead Catalysis

We chose to study this molecule first because there were concerns the full-length molecule, with a forward bulk rate of ~1000/min-[1], may be so active that we could not detect changes in z position of the magnetic bead (Martick 2006). We

would have great difficulty differentiating between molecules that were non-specifically nicked and highly active hammerheads if this was the case.

At first glance, the rate of the minimal hammerhead appeared to be greatly diminished relative to its bulk rate. We observed a number of molecules that reported no activity over the course of minutes to hours. In other words, the first observation of minimal hammerheads yielded results that were identical to our all-DNA control molecules. It was difficult, in fact, to determine whether we were observing non-specific surface sticking resulting from beads blocked with too much DNA or simply minimal hammerheads with very slow forward rates. Analysis of the shape of the bell curves indicated that we were in fact observing single, individual tethers (Taneja 2007). Thus, it seemed likely that all of the basic components of the system were appropriately controlled, with either buffer conditions or external force requiring modulation.

Force-titrations did not yield any significant changes. There were no cleavage events observed at any force. As this was the first application of ribozymes to the magnetic tweezer apparatus, we were initially forced to consider the possibility that insertion of the ribozyme into the dsDNA handles had adversely affected its capacity to fold into the active state . After all, almost all natural embedded hammerheads utilize a tertiary contact that serves to facilitate folding (Mcdowell 2010). Perhaps the truncated minimal hammerhead, used for so many years for its ease of use in kinetics studies, was inert in it's embedded form. There is a paucity of bulk data concerning the effect of extending stem I and III in bulk. The only relevant

study extended Stem II alone, and to a maximum length of 7 residues (Uhlenbeck 1995).

Indeed, there was a shift of the internal equilibrium towards ligation reported in this study, suggesting that vastly extending the handles may dampen conformational heterogeneity to such an extent that cleavage is entirely inhibited. On the other hand, several of the other uncontrolled variables may have contributed to this signal. For example, there may have been incomplete deprotection of the RNA after ordering, damage from UV shadowing or heat annealing, faulty ligase activity, or a simple dilution error when making the buffers (Greenfeld 2011). Another possibility is that we were overwinding or underwinding the RNA to such an extent as to render it inoperable. With a growing volume of data suggesting RNA enzymes experience a rugged folding energy landscape (Ditzler 2008), it was not inconceivable that we were forcing the hammerhead into a kinetic trap by inducing too many turns. Thus, we attempted a variety of intermediate supercoiled states to ensure the most gentle conditions were being applied. Still, there were no cleavage events observed.

One significant consideration was the degree to which the hammerhead may be cleaving and degrading in the ligation preparation, which typically runs overnight at room temperature. Steps were taken to reduce the incidence of non-specific cleavage; RNAse inhibitors were included in the ligation prep, and ligation temperatures were maintained at 4 degrees Celcius. Finally, in an attempt to prevent the molecule from cleaving, pH was maintained at pH 6 throughout the entire process. Indeed, the hammerhead ribozyme exhibits a log-linear pH dependence and

the thought was the a majority of molecules would remain uncleaved until introduced to competent conditions on the slide (Shepotinovskaya 2008). However, low pH conditions are also known to disrupt anti-dig/dig surface interactions (Yan 2010).

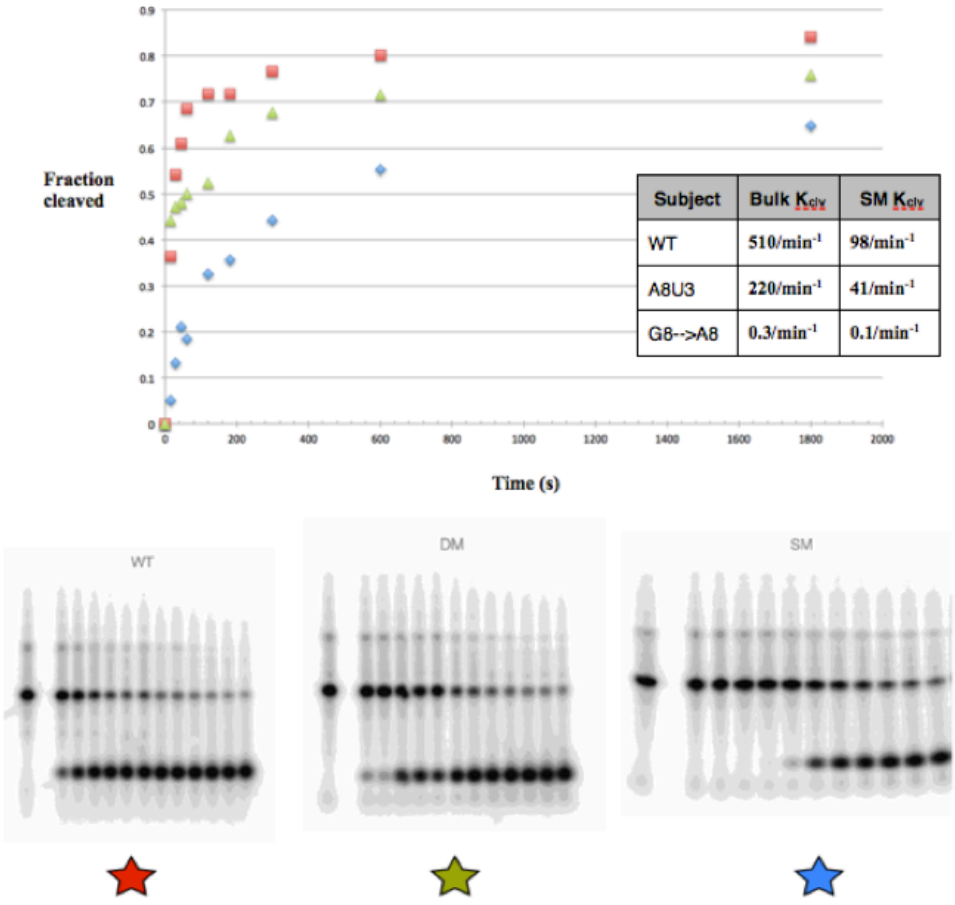

Figure 2.13 Bulk activity assays of wild type (bottom left, 510/min^{-1}), double mutant A8U3 (bottom center, 220/min^{-1}), and single mutant G8-->A8 (bottom right, 0.3/ min^{-1}). Lanes (all gels, bottom): labeled substrate alone (far left lane), time zero (lane 1), 15 seconds (lane 2), 30 seconds (lane 3), 1 minute (lane 4), 5 minutes (lane 5), 10 min (lane 6), 20 min (lane 7), 5 hours (lane 12). Normalized plot of rates (top) agree with documented bulk rates in prior studies. As in the case of the minimal hammerhead, embedding each construct in long DNA handles reduces the cleavage rate. Inset: comparison of average bulk and single molecule rates.

A breakthrough came finally by modulation of ionic strength. We observed the first cleavage event after bringing all buffer conditions to their standard levels with the exception of Magnesium and NaCl (14 mM $MgCl_2$ and 4 M NaCl). A molecule of 2 micron total length supercoiled a distance of 1 micron after an input of 30 turns, remained in the supercoiled state for 3 minutes. After 3 minutes we observed a sudden change of 1 micron of length in the z direction, a signal corresponding to our expectation of a cleavage event.

Three important conclusions were drawn from this event. The first is that the minimal hammerhead did *not* religate after the initial cleavage event. In other words, subsequent cycling of the magnets failed to produce another supercoiling event. This was in line with our predictions from bulk study, and serves as a positive control for the study of full-length hammerhead catalysis. At equilibrium, the internal equilibrium of the minimal hammerhead lies entirely on the products side (minimal reverse reaction) (Canny 2007). In bulk, rapid product dissociation had often been invoked to explain this phenomena. In this case, product dissociation could not occur, but we can infer that conformational heterogeneity of the reactants upon cleavage prevented religation.

The second important finding was that high ionic strength allowed the molecule to take on the active conformation. In bulk, the truncated form cleaves at 1mM $MgCl_2$, a larger than physiological divalent ion concentration (~100 uM), but still 10 times less than is required in the embedded state (Martick 2006). While there are known metal binding sites (namely A9 phosphate) in the hammerhead, the

possibility remained that cleavage would be observed in the absence of metal cations (Kisseleva 2005) (Martick 2008). In this case, metal ions appear critical for folding.

2.3.2 Full-length Hammerhead Catalysis in Single Molecule Format

For many decades, the field was focused on minimal hammerheads greatly truncated from their native sequences (Uhlenbeck 2003). In our bulk studies of the *Schistosomal* hammerhead, the data conformed to previous rates and can be best described as monophasic. As Figure 13 suggests, cleavage kinetics are very fast for the wild type ribozyme, with ~ 40% of cleavage completed within the first 15 seconds of the reaction.

Success with the minimal hammerhead ribozyme was limited by its lack of reversibility, which would enable measurement of more than a single cleavage event per molecule (Fedor 2009). We therefore set out to study *Schistosomal hammerhead* ribozyme, whose internal equilibrium as discussed is ~ 3/1 and should exhibit significant ligase activity (Uhlenbeck 2003). Ligations were performed applying identical conditions as the minimal construct (standard hammerhead conditions, but 4 mM MgCl2).

A mechanical annealing protocol was implement to impart folding homogeneity across the several subjects studied. Mechanical annealing involves completely unravelling the two DNA/RNA strands by imposing thousands of turns in the negative direction until denaturation bubbles form in the DNA backbone (Sheinin

2011). At a critical point, a single tether will completely disassociate its two strands. This was a useful technique in our first trials as we suspected that the ligation may cause the RNA to take on unproductive folds from which it could be liberated by a reannealing protocol (Su 2003). We could try this either by heating and cooling the slide, or by attempting to manually unfold and then refold the two strands in the manner described above (Pereira 2010).

Full-length activity differed from the minimal construct in several respects. First, the rate of cleavage is enhanced relative to the minimal construct, cleaving at about $1/min^{-1}$ under positive torque (versus $.1/min^{-1}$ for the minimal) (Nelson 2008a). Second, the full-length molecule appeared to have altered relaxation dynamics under positive and negative torque. This aspect will be discussed in detail below, but we arrived at this conclusion by comparing the rate of release of the magnet bead relative to that of the minimal construct. Also, one can use the rate of release of an identical DNA molecule in the presence of a single stranded nicking enzyme to measure the rate (Falaschi 2007). Under negative torque, the full-length construct released at a dampened rate, suggesting that a hydrogen bond network may remain in-tact following cleavage. In other words, in our system the tertiary contract acts as a ratchet, slowly releasing torque stored after supercoiling (Bassi 1999). Under negative torque, the rate was similarly knocked down, with minor differences from positive torque.

2.3.3 Active Site Mutations

Crystal structures of the full-length hammerhead reveal two invariant residues in the catalytic core, G8 and C3, which form a tertiary base-pairing interaction that rearranges the active site relative to the minimal hammerhead (Martick 2006). A single C3U or G8A mutation essentially kills ribozyme activity, but when both mutations are made simultaneously, the Watson-Crick interaction is restored, and cleavage activity is rescued to within 200-fold of the wild-type ribozyme (Lee 2008).

We assay both the single and double mutations in the context of our single-molecule construct. These will serve as negative and positive controls, respectively; they are expected to have effects similar to those observed in bulk in solution. However, our single-molecule assay permits us to measure both the cleavage and ligation individual rate constants, and thereby deduce the effect of these mutations upon the internal equilibrium. Figure 13 outlines a comparison of WT, single-mutant, and double-mutant bulk assays employed in this study.

Figure 2.14 G8 & C3 (light blue) form a Watson Crick base pair. The pair stabilizes the active core and orients G8 to act as a general base in the cleavage reaction. Mutation of either G8 or C3 abolishes activity. Restoration of hydrogen-bonding at this position restores activity. Crystal structure of the *Schistosoma Mansoni* hammerhead (2GOZ) includes cleavage site C17 in yellow.

2.3.3a The G8-->A single-mutant abolishes activity

Bulk measurements demonstrated that this particular mutant should effectively kill activity or severely reduce its rate. While this knock-down in activity was significant, it was somewhat more robust than had been previously reported in bulk studies. This may be a consequence of slightly altered annealing protocol, or an stable fold brought on by the DNA residues incorporated just adjacent to the active site. In Figure 13, one can see that at least 1/4 of the hammerhead population remains ligated at equilibrium, suggesting the single-mutant may exhibit a ligase activity that supports supercoil formation. This would represent an important difference between the minimal and full-length molecules observed in this study.

Our predictions for the single mutant proved accurate. First, as in the bulk study, the cleavage rate was significantly diminished (1/10 min^{-1} on average). One can see from the raw data trace in Figure 14 that individual molecules exhibit dwell times or the order of minutes. In addition, single-mutant molecules exhibited reversible cleavage and ligation like as in the WT molecule. We observed several cleavage and religation events for each single-mutant molecule studied. In fact, the single mutant molecule behaved just like the minimal hammerhead, except that it could religate following cleavage(Figure 14) (Tinoco 2006). These observations demonstrate that the observed cleavage and ligation reactions in the single molecule assay were in fact due to standard, on-pathway hammerhead ribozyme catalysis (Lee 2007).

The central pane of Figure 14 shows in input of 15 turns under negative torque, signified by in decrease in rotations on the y-axis. We observed that the single mutant had great difficulty cleaving under positive torque, in line with hypothesis that positive torque depopulates the active conformation of the ribozyme (Mcdowell 2010). Another important observation was that the single mutant molecule would at times becomes lodged in a particular conformation (Bokinsky 2005). Often, we would observe 3-4 successive cleavage events, and then the molecule would become frozen in either the cleaved or ligated state, and would never resume activity. This is consistent with disruption of Watson Crick base pairing at position 3 and 8 (Martick 2006). Both are required to stabilize the active site, and it is reasonable to assume that upon cleavage the hammerhead may revert to a state similar to the cleaved minimal hammerhead, where the energy barrier to ligate is prohibitively large.

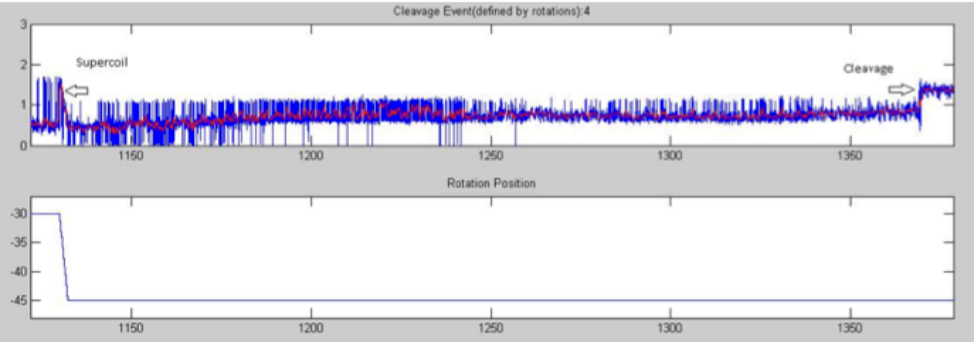

Figure 2.15. Raw data trace, G8-->A. At ~1000 seconds, 15 negative rotations (bottom panel) are introduced, supercoiling the molecule by about 1 micron ("Supercoil," top panel). At about ~1400 seconds (~7 minutes), we observe a cleavage event, signified by a rapid increase in the height of the magnetic bead ("Cleavage," top).

2.3.3b The A8U3 double-mutant restores activity

The A8U3 double mutant was an important control for several reasons. The core residues G5, G8, G12 and C3 in the minimal hammerhead ribozyme are each known to be so fragile that changing even a single exocyclic functional group on any of these abolished catalytic activity (Nelson 2006). The full-length structure demonstrated how G12 and G8 are positioned within the active site - consistent with their previously proposed role in acid-base catalysis (Scott 2007).

A double-mutant that restores this critical base-pair (like A8U3) should restore activity to the hammerhead ribozyme (Link 2007). The activity is expected to be far more robust than the single-mutant, but attenuated relative to the wild type molecule (Thomas 2008). The bulk studies in Figure 13 demonstrate that this trend is observed in ensemble measurements of the identical hybrid molecules employed in the single-molecule study. Unlike the wild type molecule, the A8U3 mutant only displayed about 10% cleavage by the first 15 second time point, resulting in a K_{obs} of ~200/min^{-1} relative to the 500/min^{-1} displayed in the WT molecule. Although all seven other possible Watson-Crick base-pairing combinations between nucleotides 3 and 8 rescue catalytic activity when compared to their corresponding single mutations, none fully restore catalysis as measured in standard solution enzymology assays, suggesting that base-pairing might not be the only factor involved (Lee 2008).

A possible explanation for these variations becomes apparent with the single molecule analysis of the C3U/G8A double-mutant. The rate of ligation is restored to

a greater extent than the rate of cleavage, thus shifting the internal equilibrium further toward reactants.

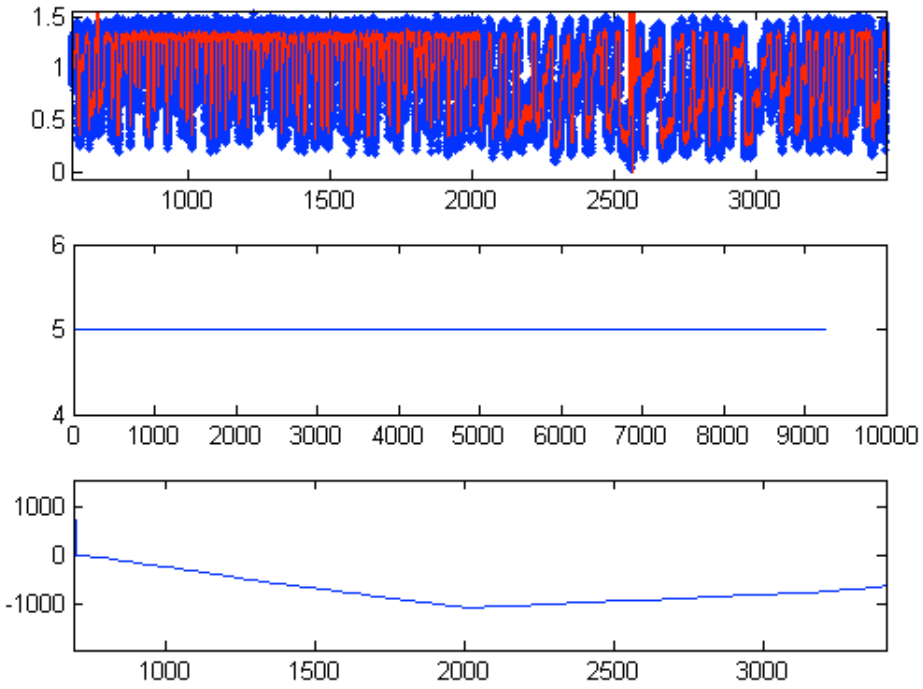

Figure 2.16 A chiral impact of applied torque in A8U3. The raw data trace (top) indicates z-extension in microns, the center pane demonstrates a linear position of 5 mm above the slide (.3 pN), and the bottom pane indicates the sign of magnet rotation. Comparing the top and bottom panes, we find that the A8U3 mutant exhibits longer dwell times under positive torque than negative torque, signifying an enhanced ligation rate under positive torque.

Hence it appears that minor differences due to sequence variations in the active site that nonetheless maintain the hydrogen-bonding structure of the active site

can perturb the internal equilibrium, suggesting that this may well constitute a sensitive regulatory functionality within the context of the natural hammerhead ribozyme, i.e., it may have unmasked the subtle structural fluctuations that are responsible for regulating the nuclease/ligase switch.

Due to its attenuated rate, the double mutant enabled more accurate kinetic measurements and detailed differences in torque effects. In Figure 15, one can see a clear chiral preference displayed by the A8U3 mutant, exhibiting enhanced cleavage under negative torsion. There are two important conclusions drawn from Figure 15: 1) the cleavage rate does not appear to be significantly altered relative to the wild type molecule, 2) there is an increase in partial relaxation behavior under positive torque relative to the wild type. This may signify that the double mutant alters ligation activity rather than cleavage activity, or at least to a greater extent. This is not an observation that could be made in bulk both because rates are averaged in ensemble study, and because supercoiling cannot be controlled in solution (Herbert 2008).

The double mutant in this case is designed to maintain the critical Watson-Crick interaction positioning the putative base at position 8 in an orientation that facilitates abstraction of a proton from the 2'-OH of Cytosine 17. However, the A-U bond that formed is less resilient that the native C-G bond, which contains three hydrogen bonds across its face rather than two for the A-U pair (Przybilski 2007). Thus, it is possible that the Adenine at position 8 either takes on an alternate conformation or simply has access to greater degrees of conformational freedom, and

thereby abstracts the C17 proton with greater frequency.

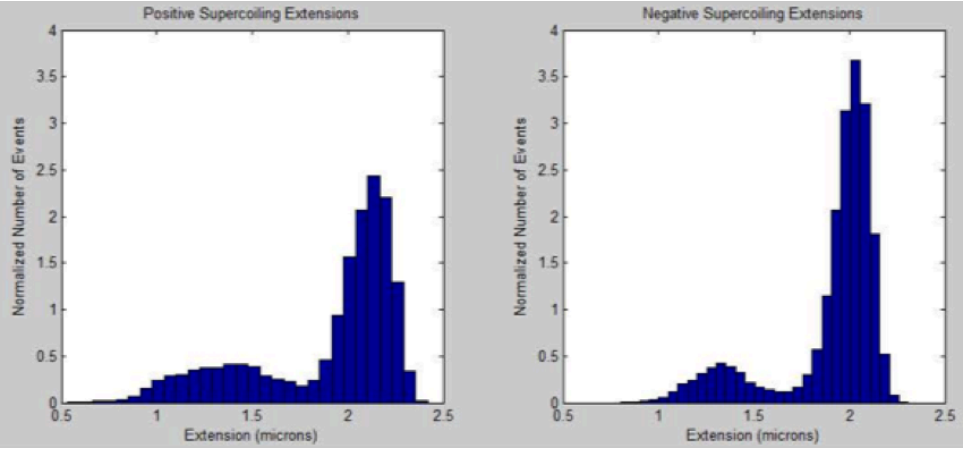

Figure 2.17 Extension histogram of double mutant displaying chiral impact of applied torque. Positively supercoiled A8U3 molecules exhibit extended dwell time in supercoiled state, signified by extension density surrounding ~0.5-1 microns (left), while negatively supercoiled subjects remain in the extended state for a greater proportion of time. The disparity between positive and negative torsion can be attributed to an enhanced population of the active conformation under negative torque.

The extension histogram analysis in Figure 16 clearly shows that positive torque is correlated with longer dwell times in the supercoiled state (.5 micron length). Conversely, molecules spend much less time in the supercoiled state and more in the fully relaxed state when subjected to negative torque.

Because the dampened forward rate of the double mutant enables unencumbered analysis, we focused force, pH and magnesium titrations on this subject. However, simplified data collection did *not* eliminate static and dynamic heterogeneity observed in different molecules. Importantly, we avoided UV

shadowing and extended exposure to elevated temperatures throughout the preparation process in order to provide a homogenous folding population (Li 2007). A relevant study by Greenfeld and colleagues points out that the growing corpus of evidence suggesting RNA is subject to a deeply furrowed folding energy landscape may be biased by damage incurred in preparation. (Greenfeld 2011). With this in mind, we subjected all molecules to the minimal amount of handling possible, avoiding repetitive freeze-thawing and vigorous vortexing, in addition to UV and heat exposure.

2.3.4 Cleavage and Ligation Strongly Favored at High Force

Modulation of tension is fundamental for regulating many different biological processes, especially the activity of enzymes involving DNA wrapping. In our single molecule, we can modulate tension by changing the height of the permanent magnets above the slide. However, changes in the linear position of the magnets alters both the stretching force imposed on the embedded hammerhead (tension), and the torque impinged on the active site (Bryant 2012). By studying torque effects at constant translation force, we can decouple the two effects on hammerhead activity.

FORCE TITRATION (1 Molecule)

force (pN)	kclv (min-1)	klig (min)
0.61	17.5	42253
0.52	13.61	49180
0.45	10.43	36697
0.39	10.13	40678
0.33	8.98	42857
0.29	9.04	40268
0.25	9.05	46692
0.21	6.9	45977
0.18	7.25	56074
0.16	6.93	44444

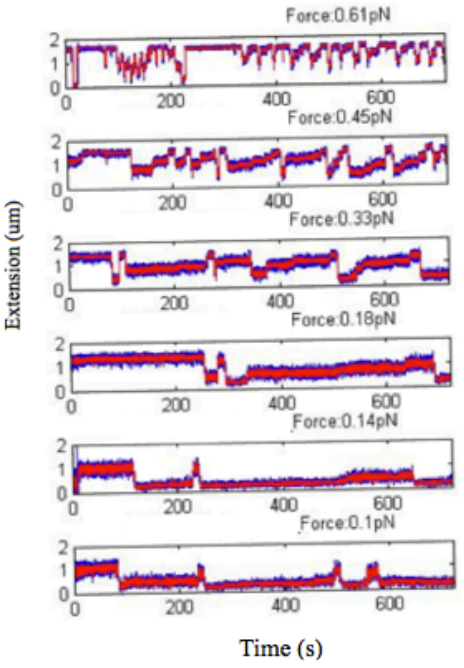

Figure 2.18 Enhanced K_{obs} and fast ligation for A8U3 mutant at elevated translational force. Magnet height ranging from 3-9mm imparts a translational force of 0.1-0.6pN upon A8U3 hammerhead embedded in 2.6kb dsDNA handles. At low forces (bottom, 0.1-0.2pN), we observe average of 6 cleavage events per minute while at high forces (top, 0.6-0.7pN) this rate increases to 17 events per minute. At high forces, the forward rate is so robust that the molecule frequently cleaves before the automated 17 magnet rotations can cause a decrease in extension via plectoneme formation. These effects appear to be independent of torque effects (high forces enhance the cleavage/ ligation rates under both positive and negative torque). (top left) Kclv and Klig versus translational force. Ligation rates are extrapolated from measurable changes in linking number as the extension dynamics of magnetic beads are dominated by drag in the solution following cleavage.

Here, as the translation tension of the molecule is varied from 0.1pN to 0.6pN, the activity of each hammerhead variant changes markedly. Changes in translational force are imparted by changing the height of the permanent magnets positioned above the slide, controlled by a Piezo-stepping device (Lionnet 2012). In the case of both wild type and double-mutant hammerheads, an increase in translational force causes an increase in *both* the cleavage and ligation rate.

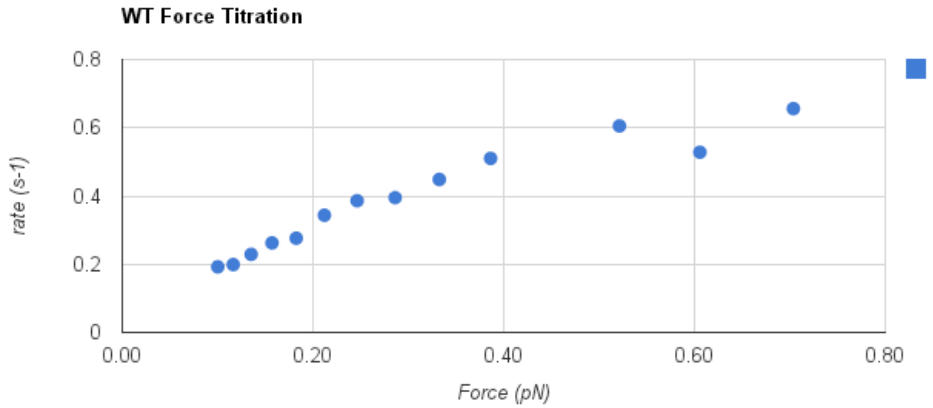

Figure 2.19 Enhanced K_{obs} for wild type hammerhead at elevated translational force. While the rate of cleavage in the wild type molecule is too fast to measure ligation, a near-linear relationship between cleavage rate and force is observable in wild type *Schistosomal* hammerheads. Magnet height ranging from 3-9mm imparts a translational force of 0.1-0.6pN upon a single molecule embedded in 2.6kb dsDNA handles.

The experiments described above show that hammerhead is able to relax (+) and (-) supercoils at both low and high forces. However, the processivity and initiation rate under high forces (~.6 pN) is enhanced under both positive and negative torque. These observations are consistent with findings that undisturbed natural tertiary contacts are associated with dynamic motional sampling that increasingly populate catalytically active conformations (Mcdowell 2010). In our study, it is reasonable to assume that increased translational force orients the stem I and III in a manner similar to tertiary contact formation (Falaschi 2007)(Martick 2006). The result is likely an enhanced population of the active conformation, and therefore both a enhanced cleavage and ligation rate.

2.3.5 pH Profile in Single Molecule Format Mirrors Bulk pH Profile

pH Titrations are amenable to our microscope flow-cell system and comport with our expectations based on bulk measurements. We can easily modulate the pH condition for a given molecule by exchanging fresh buffer through a gravity filtration flow system. As discussed in Chapter 1, the pH dependence of the full-length hammerhead activity parallels that of the minimal hammerhead (Bassi 1999). A log-linear relationship with a slope of ~1 is observed at both 100uM and 10mM Mg^{2+} indicating a mechanism limited by a chemical step (Canny 2004). Single-molecule experiments described herein observed the same trend as observed in bulk, as evaluated at both 100uM and 10mM [Mg^{2+}]. The pH dependence profile of both systems plateaus at around 8.5-9 and are thus likely indicative of a protonation-deprotonation reaction of a functional group with a high pKa.

In bulk format, a 2,6-diaminopurine substitution at positions 8 and 12 converts the pH dependence profile from a log-linear incline with the plateau at pH 8.5-9 (highest measured) to a bell-shaped curve with a peak at pH ~7. Such a change in the curve would be expected if the functional groups at the substituted positions were directly involved in acid-base catalysis. The nucleotide substitution results were consistent with the experiments in which the G8 and G12 were successfully trapped within the crosslinking distance of C17 and N1.1, two nucleotides spanning the active site (Heckman et al., 2005), even though in the minimal hammerhead structures the active site phosphate is located ~16A and ~23A away from the G8 and G12

phosphates, respectively. Although evocative of the nucleobase-catalyzed mechanism, these results could not definitively exclude other possibilities such as structural effects or involvement of functional groups other than nucleobases. The single molecule studied described herein boast the ability to directly assay such structural effects in real time, in stark contrast to bulk measurements.

The ability to observe cleavage and ligation rates separately, in the same assay, is also a powerful tool unavailable in bulk. Low pH (~pH 6.5) causes a marked decrease in K_{obs} in both single molecule and bulk formats (Figure 19)(Figure 20). However, the magnetic tweezers assay can determine whether that decreased rate of product formation is due to a decrease in the cleavage rate, the ligation rate, or both. Figure 18 demonstrates this difference. These findings are consistent with traditional notions of microscopic reversibility (Weinstein 1997).

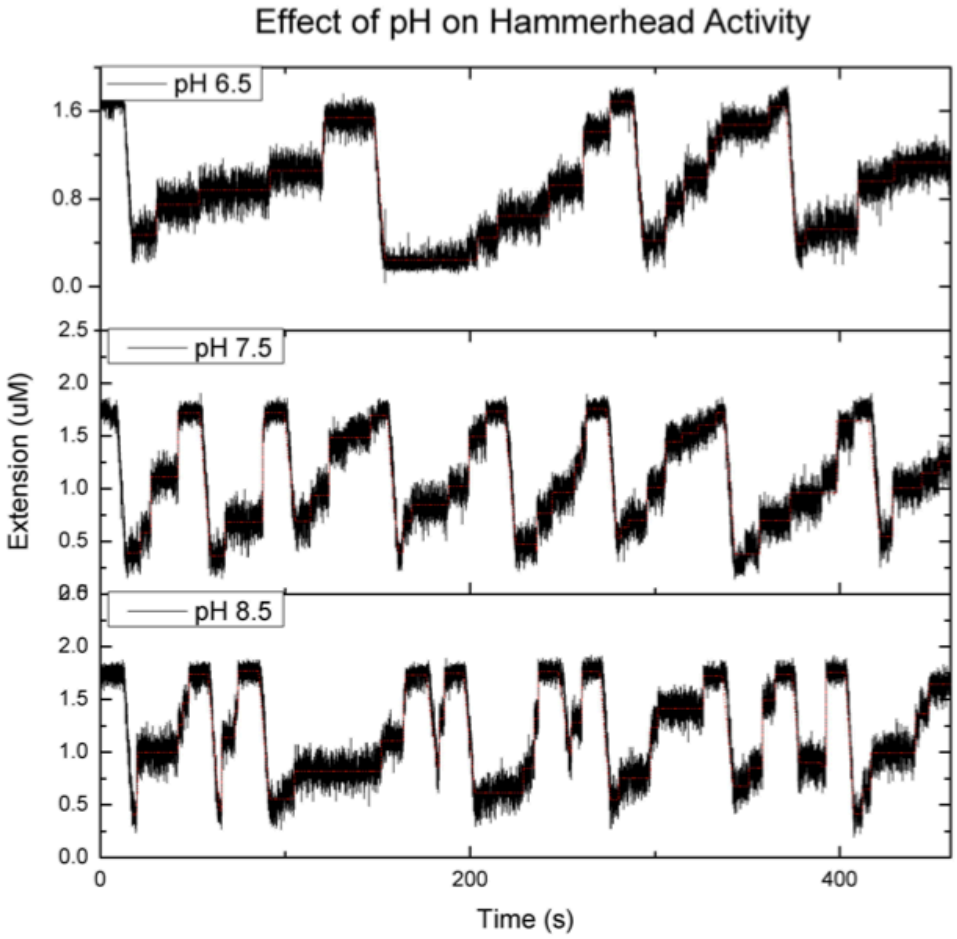

Figure 2.20 Effect of pH on WT Hammerhead activity. Raw data trace, pH titration. Forward rates (K_{clv}) remains steady at all conditions while the ligation rate is enhanced at lower pH (6.5). This finding may lend explanation to observed log linear relationship of pH and K_{clv} in bulk, and highlights an important role for ligation rather than cleavage in producing this effect. For example, in the pH 6.5 condition, ~5 ligation events correspond tp

a)

pH_Translational Force	Kclv (min-1)	# of Events	Standard error
Mol5			
pH 6.5_0.5pN	3.28	*66*	1.79
pH 7.5_0.5pN	6.74	*144*	0.654
pH 8.5_0.5pN	7.92	*136*	0.841
Mol 2			
pH6.5_0.1pN	3.05	*18*	3.46
pH7.5_0.1pN	11.1	*93*	0.417
pH8.5_0.1pN	10.05	77	0.544

b)

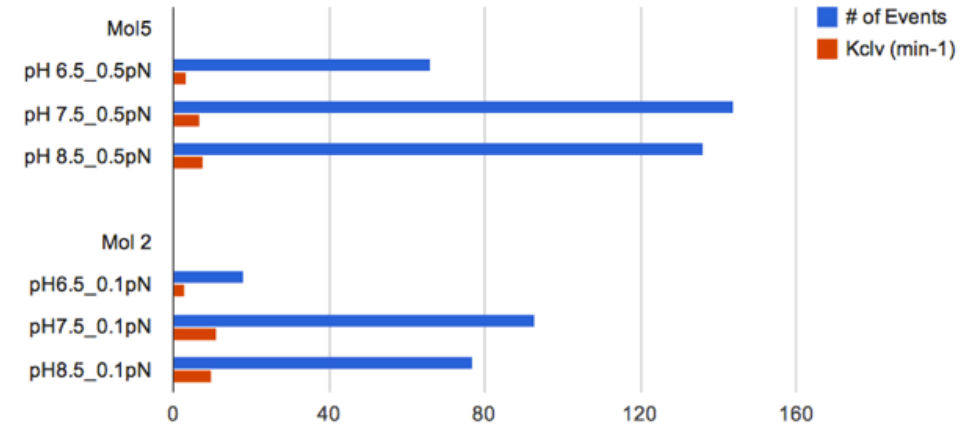

Figure 2.21 Combined pH and tension profile for two A8U3 mutants. a) Molecule 5 (Mol 5) exhibits enhanced relaxation activity at high DNA tension(~0.5pN) and high pH (~8.5). Both the processivity (# of events) and forward cleavage rate (K_{clv}) of Molecule 2 (Mol 2) is reduced relative to Molecule 5, reflecting the effect of increased tension. However, the pH profile of each separate single molecule is independent of tension effects b) Graph depicts correlation of event frequency and forward cleavage rate. In both molecules, the pH profile plateaus around pH8, suggesting a protonation-deprotonation reaction of a functional group with a high pKa.

2.3.6 Bulk Kinetic Analysis of Extended Stems

As discussed, K_{obs} appeared to be greatly diminished in the embedded single-molecule format relative to bulk studies employing truncated stems I and III (Blount 2005). We followed up on this observation with a bulk study employing modified stems much longer than any previous investigation (Nelson 2005). We hypothesized that extension of stem I with dsDNA would mirror the effect of embedding the molecule in 2.6kb handles; namely a attenuating the observable rate of cleavage.

The bulk study involved three sets of minimal hammerheads with an extended stem I. All were extended with dsDNA at stem I, with lengths of 10, 20 and then 40 base pairs, respectively. Standard hammerhead activity assay conditions were employed. Initial results indicated there there was indeed a trend following our expectations; extended stems decreased the rate of cleavage. Activity assays were performed by labeling substrate strand with radiolabeled ATP, and following activity over the course of 5 hours in the presence of saturating enzyme (750 pmole enzyme, 10 pmole substrate) (Figure 19) (Link 2007). This study made exclusive use of denaturing gels so the autoradiograms should only reflect the relative population of substrate and product bands. As shown in Figure 19, extending the base-paired portion of stem I results in decreased K_{obs}. We advance one possible explanation of this phenomena; dampened conformational dynamics in embedded and extended

ribozymes raise the energy barrier to carrying out the forward reaction (Bokinsky 2005).

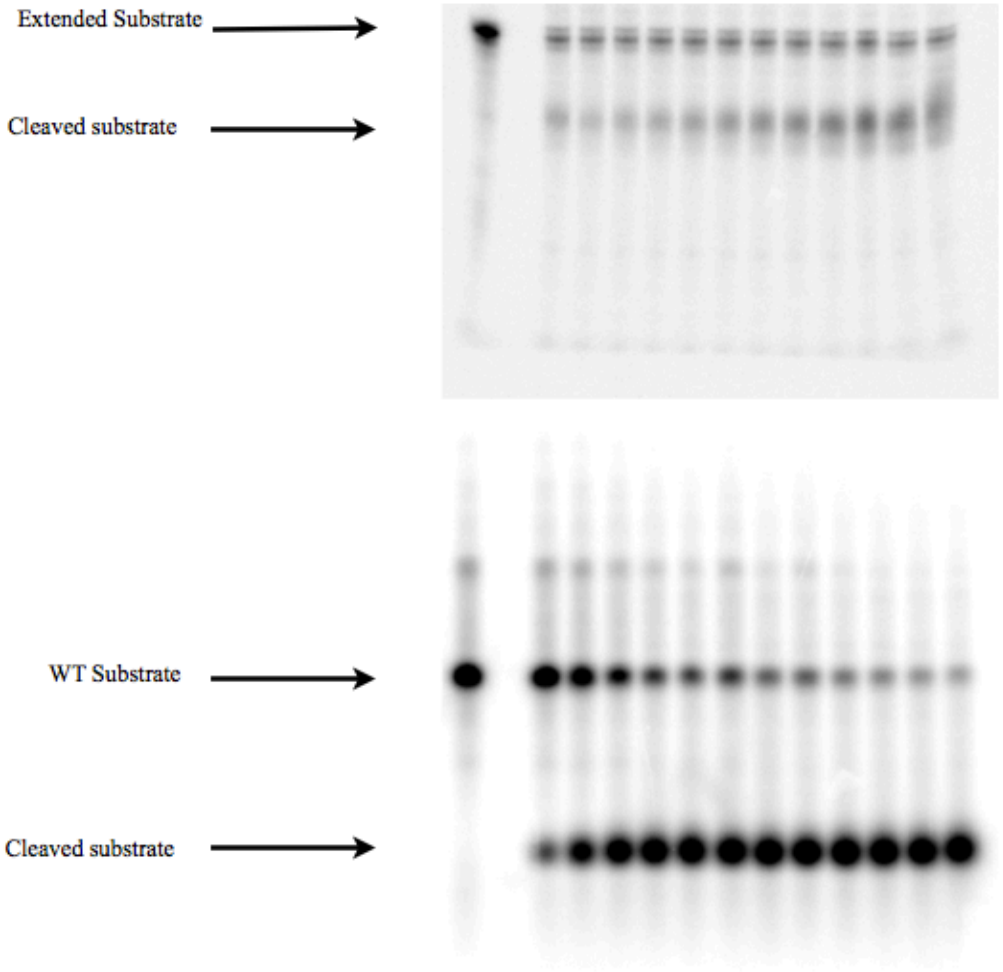

Figure 2.22 Bulk activity assay of minimal hammerhead with 40bp dsDNA extended stem I (top) versus wild type minimal hammerhead activity assay (bottom). Lanes (both gels): labeled substrate alone (far left lane), time zero (lane 1), 15 seconds (lane 2), 30 seconds (lane 3), 1 minute (lane 4), 5 minutes (lane 5), 10 minutes (lane 6), 20 minutes (lane 7), 5 hours (lane 12). Comparison of activity reveals that extension of stem I either enhances the rate of ligation or dampens the rate of cleavage (or both). This is consistent with our observation in single molecule format that conformational dampening enhances the rate of ligation.

2.3.7 Cruciform Structures Revealed via Mechanical Annealing

Alternate DNA folds are common in nature (Ditzler 2008). The single molecule assay described here identified cruciform structure formation when the 2.6 kb dsDNA handle segments were oriented in a "head to head" orientation (complementary sequences arranged in tandem on opposing handles). DNA cruciform structures (Figure 20, a-c) are important for a wide range of biological processes, including replication, regulation of gene expression, and recombination (Brázda 2011). They also have been implicated in the development of diseases including cancer and Werner's syndrome(Brazda 2011). These finings offer a model for future magnetic tweezers studies seeking to probe protein-cruciform DNA interactions.

In the single molecule study here, restriction digests are carried out (Figure 1) in a manner that ensures that identical ends of the digested pUC19 plasmid are ligated to stem I and III of the embedded hammerhead ribozyme. A mechanical unwinding/overwinding cycle induces the characteristic cruciform extension profile displayed in blue (Figure 20 d, bottom) (Myong 2006).

The mechanical annealing protocol involves imposing ~400 rotations in the negative direction, resulting in a dissociation of the two individual strands. A

refolding sequence is then implemented involving the re-introduction of ~400 rotations, re-annealing the two strands (Talukder 2011). While we utilized this phenomenon to impart folding homogeneity across all experimental slides, these findings have implications for future single molecule studies of cruciform-protein interaction (p53 or HMG proteins, for example (Brazda 2011).

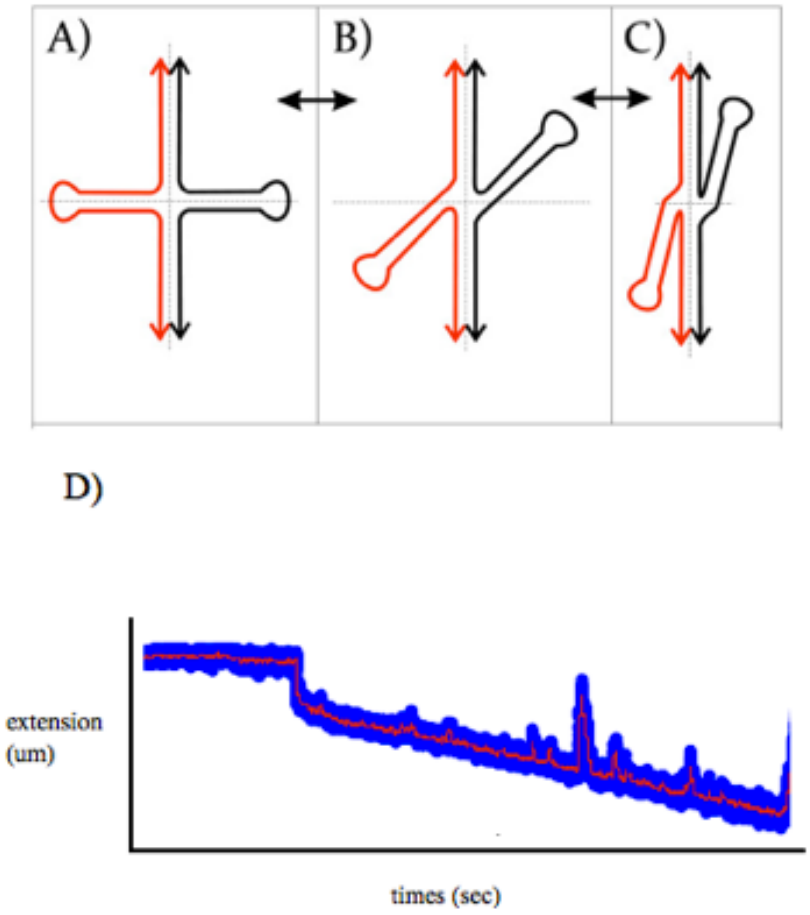

Figure 2.23 Conformations of a cruciform structure. Conformations can vary from a) "unfolded" to b) bent, and to c) "stacked" with 4 chains of DNA in close vicinity. d) In the single molecule format, identical plasmid handles are engineered with "sticky" (restriction site) overhangs (Figure 1) that result in a "head to head" orientation of the two double-stranded 2.6kb segments. A mechanical unwinding/ overwinding cycle induces the characteristic cruciform extension profile displayed in blue (d, bottom).

2.4 A Chiral Impact of Applied Torques

2.4.1 Structural Basis of Chirality Prediction

There are two basic types of hammerhead ribozymes: the minimal hammerhead ribozyme, and the full-length hammerhead ribozyme. The primary difference between the two types is that full-length molecule has a vastly enhanced cleavage rate relative to the minimal hammerhead. The minimal cleaves at a r rate of $1/min^{-1}$ while the full-length variety cleaves at up to $1000/min^{-1}$. A second difference is primarily structural, and was only fully appreciated following the publication of the full-length structure in 2006. (Martick and Scott., 2006). Martick's crystal structure demonstrated that stem I of the full-length hammerhead is unwound relative to the minimal hammerhead.

One prediction drawn from these differences and cross-linking studies discussed in Chapter 1 is that directly unwinding stem I should speed up the cleavage reaction, similar to the effect of the tertiary contact formation (Dunham 2003). Correspondingly, if we overwound stem I we expected a relative decrease in the rate of the reaction. Evidence derived from crystallography is necessarily correlative, and suffers from common drawbacks such as crystal packing effects and the necessity to mutate certain residues in order to increase homogeneity. The magnetic tweezers approach, however, presented the opportunity to directly invoke causation (Nong 2012). If we observed rapid cleavage under negative torque relative to positive torque, our structural and biochemical predictions would be validated.

2.4.2 A chiral impact of applied torques

About 60-70% of all molecules studied displayed a chiral impact of applied torques for part or all of the observation period. In the case of the wild type *Schistosoma* ribozyme, all traces longer than 4 hours exhibited some period of chiral preference, in line with our expectations. While we cannot entirely rule out a molecule with incomplete deprotection or covalent modification leading to these signals, the likely answer is that direct unwinding of stem I forces the enzyme to populate the active conformation (Greenfeld 2011).

A recent smFRET studied of the full-length hammerhead argues that the *Schistosomal* hammerhead tertiary contact is dynamic, that nature has selected for dynamic contacts capable of accessing many different conformations (Mcdowell 2010). Indeed, it is not clear how external twist propagations could transmit to the active site of the hammerhead ribozyme if the tertiary contact was rigid.

But what about the ~40% of observed molecules without a demonstrable chiral preference? Large energy barriers separating misfolded and functional states arising from alternate base pairing are a well-appreciated characteristic of RNA (Pereira 2010). Undoubtedly, molecular heterogeneity is intrinsic the the hammerhead ribozyme subjects in question (Shcherbakova 2008). It should not be surprising that, with an experimental approach that allows the study of thousands of cleavage and ligation cycles, we have isolated persistent functional sub-populations. However, is this observed heterogeneity a product of intrinsic heterogeneity or

covalent RNA modification? A recent work by Herschlag and colleagues reported the removal of such covalent heterogeneity in P4-P6 RNA folding by subverting common steps in RNA preparation such as UV shadowing and heat annealing (Greenfeld 2011)(Woodside 2006).

To ensure that our system was not compromised by the same factors, we avoided UV shadowing entirely and took a moderate approach to our annealing protocol. To purify RNA without exposing the sample to UV shadowing, we ran markers of the target length in parallel with our samples, cut out and stained the gel segment containing markers with ethidium bromide, and then analyzed the gel on a Typhoon scanner. Then, by optimizing the size of paper printout visualizing our marker to the size of translucent gel plate, we could aligned the marker beneath the unexposed gel segment and excise fragments of the appropriate length. Diagnostic gels then confirmed isolation of the target RNA. To probe whether there were alternate populations of incompetent complexes we also conducted a native PAGE gel assay of substrate-labeled complexes with 1:1 molar ratio of enzyme. These assays demonstrated that in each case there was a single migrating band, representing a homogenous population of folded hammerhead molecules.

Having acknowledged the possibility of extant heterogeneity, we shift our focus to chiral preference signal. As discussed, some molecules maintained this preference throughout the entire trace, while others exhibited only a periodic preference for ~30 minutes before shifting into another conformation where a preference was not clear. Under positive twist, K_{clv} is moderate, and each spin cycle

results in supercoiling that reaches the surface of the glass slide. Under negative torque, K_{clv} is very robust, and the molecule supercoils to the surface of the slide very infrequently. This observation aligns with our structural prediction based on differences in stem I twist of the minimal and 2GOZ hammerhead crystal structures (Martick 2006).

Figure 21 clearly shows that the kinetics of the reaction are being affected by the sign of the twisting that we are introducing. In this view, the 900 second trace shows that positive twist (Figure 21 left) is correlated with successful supercoiling events that reach the surface of the slide (extension approaching 0 on the y-axis).

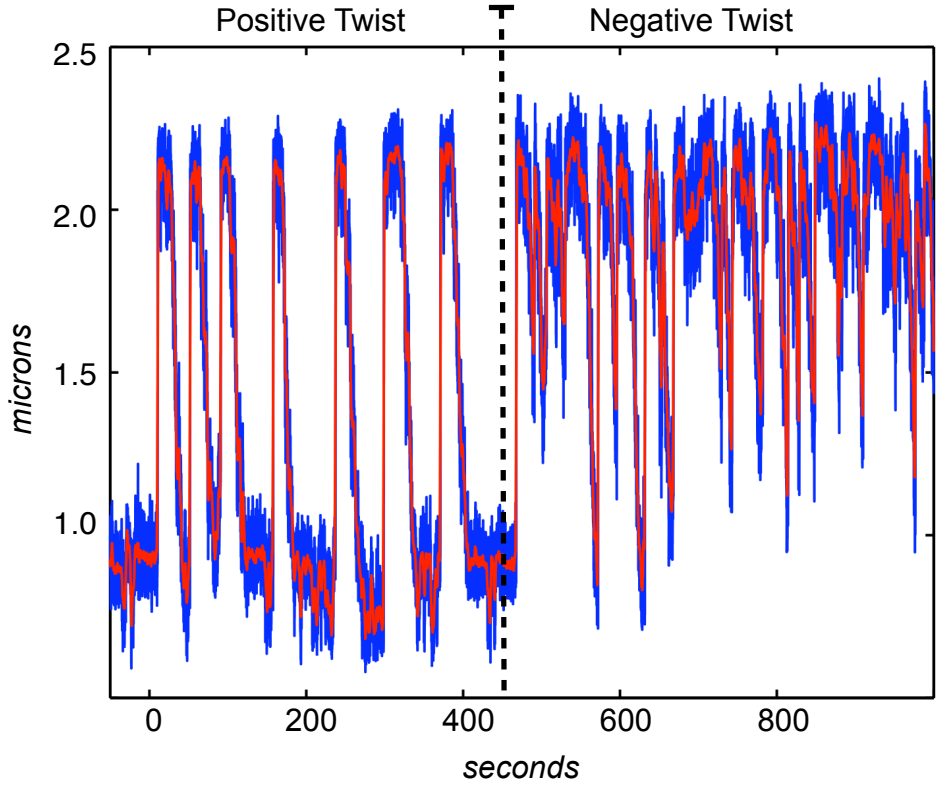

Figure 2.24 Chiral preference of applied torque. K_{obs} is directly dependent on the sign of externally applied magnet rotation. The construct shown in Figure 21 is twisted in the positive (overwinding) direction between 0 sec and 425 sec. Negative (underwinding) supercoils are then applied between 420 seconds and 1000 seconds. Cleavage and ligation occur with greater frequency when negative supercoils (favoring unwinding) are applied versus when positive supercoils are applied.

Conversely, under negative torque (right), K_{clv} is very robust, and the molecule supercoils to the surface of the slide very infrequently. This observation aligns with our structural prediction based on differences in stem I twist of the minimal and 2GOZ hammerhead crystal structures (Martick 2006).

2.4.3 Chirality and Data Analysis

Data analysis of the full-length ribozyme was hampered by a propensity of the molecule to cleave before supercoiling to the surface of the slide. As the preceding description of the analysis software describes, supercoiling events were only considered for "dwell-time" and "extension" analysis if they cross a minimum threshold. Thus, consideration of the raw "extension vs. time" data is often more informative to get a sense of the chiral preference of each molecule. Furthermore, many individual molecules demonstrated short periods of chiral preference within a large trace. These periods are often disguised by a histogram bundling activity for several hours.

Figure 22 shows a characteristic dwell-time analysis trace for the full-length wild type molecule. Looking at the histogram it is clear that dwell times observed under positive supercoils (left) are longer than those for negative supercoils (right). While the difference is modest (average rate of 1event per 5 seconds under positive vs. 1 per 3 seconds for negative), it signifies a chiral preference of applied torques. Recall, however, that all of the shortest events under negative torsion are thrown out because they prevent the molecule from exceeding the minimal threshold. Thus, this graph necessarily fails to show the fastest cleavage events under both positive and negative torsion.

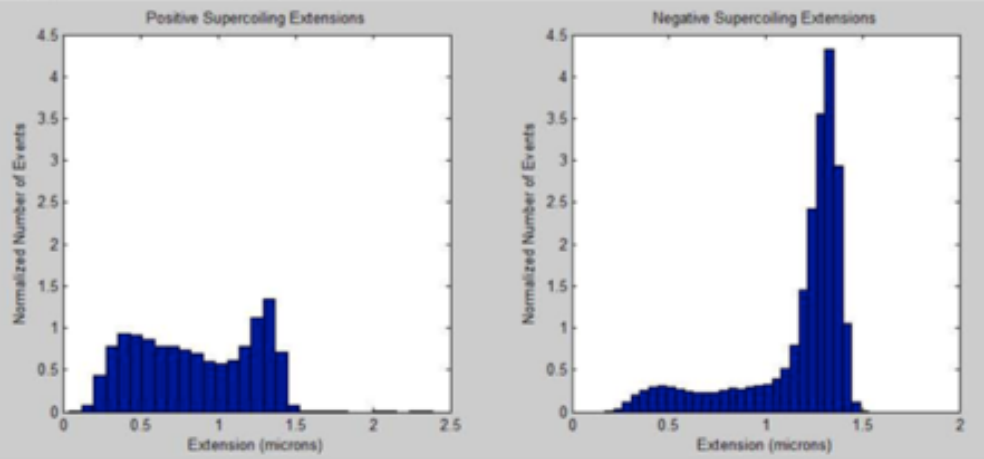

Figure 2.25 Dwell time analysis, wild type full-length hammerhead. Dwell times under positive supercoils (left) are centered about 0.5 microns, indicating a prolonged supercoiled state. Negative supercoils correlate with robust cleavage rates, and consequent occupancy of the fully relaxed state (~1.5 microns).

2.5 T4 Ligase handling during molecule preparation

We carried out ligation of the 5-pieces discussed in Figure 1 at the lowest pH tolerable by T4 ligase enzyme. Doing so ensured that annealed hammerhead would cleave to the least extent possible in the ligation prep (Thomas 2009). Figure 23 shows a pH titration of ligase activity; one can see that T4 DNA ligase tolerates a pH environment as low at 6. To ensure that ligase was inactive during the course of our experiments, we introduced a heat inactivation step prior to observation on the microscope (10 min, 65 degrees Celsius).

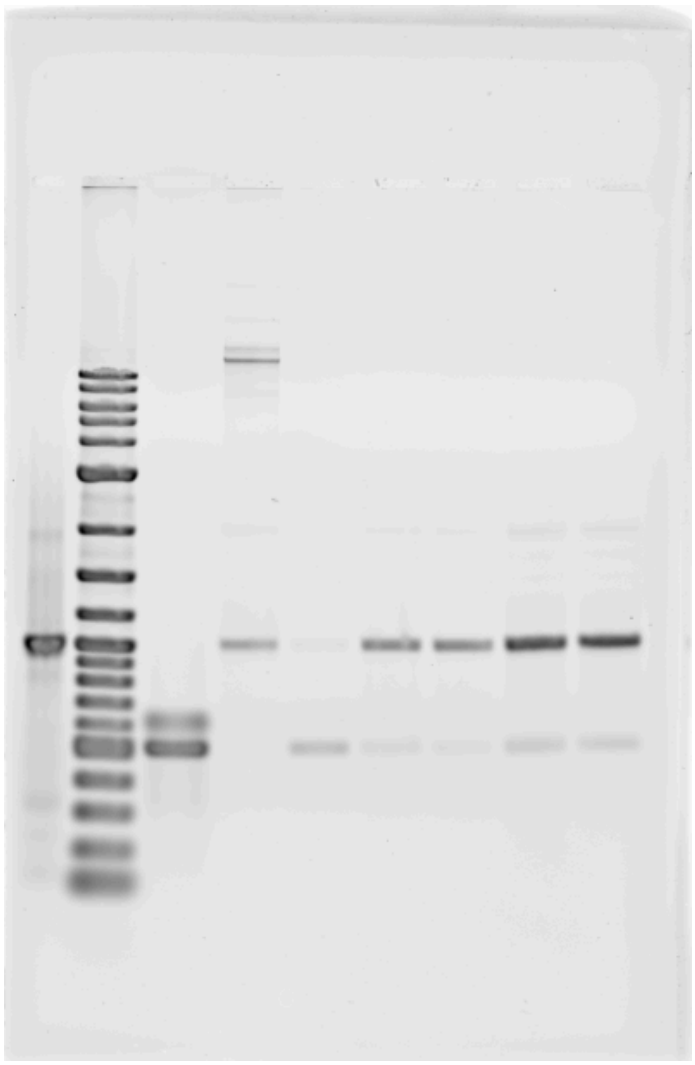

Figure 2.26 T4 DNA Ligase pH titration. All lanes contain 75 ng total material. The 9 lanes from left to right represent: 1)uncleaved PUC19 control (1kb marker), 2) 2 log ladder, 3) unligated 500bp 'BamHI' , 4) 5-piece HH ligation, 5) pH4 ligase buffer, 6) pH5, 7) pH6, 8) pH7, 9) StandardpH 7.5. lanes 5-9 represent two ligated 500bp fragments from lane 3. One can see that T4 DNA ligase tolerates a pH environment as low as pH5.

2.9 Conclusions

First, this study demonstrates that a hybrid dsDNA/RNA structure responds to the external application of torque in a manner identical to dsDNA (Figure 2) (Gosse 2002). Comparable assays have been conducted only with dsDNA (Marko 2012). As demonstrated in Figure 5, we have also shown that the hammerhead ribozyme-embedded dsDNA will dwell in a supercoiled state, cleave, and release stored torque by unravelling to its fully extended, relaxed state. Early critics of this system suggested that the active site hydrogen bond network would impinge release of such supercoils. Thus, we show that supercoiled DNA embedded with a nucleolytic ribozyme with coaxial linking stems acts in much the same way as supercoiled DNA.

The embedded molecules in this assay exhibit two other unique features. Because the two product strands fail to dissociate, they are pre-bound and pre-positioned for the back reaction to take place. The back reaction thus becomes more significant, due to the proximity and effective concentration of the back-reactants (Figure 3). Second, because the ligation reaction becomes much more favorable, we find under the conditions of our assay (an embedded ribozyme experiencing constant torque and force), unlike those in solution with an "idealized" ribozyme construct (Osborne 2005), religation of a cleaved ribozyme becomes spontaneous, permitting us

to suggest that in their natural context, hammerheads may well favor the ligated state, and cleave in response to some form of structural perturbation.

This assay also conforms with the well-described rugged folding landscape of RNA macromolecules (Bokinsky 2005). Our results resonate with a growing corpus of evidence suggesting RNA utilizes greater conformational freedom to overcome limited chemical diversity (Shcherbakova 2008). These observations are also consistent with a dynamic tertiary contact that allows external twist-propagations to transmit to the active site (Mcdowell 2010).

To test that hammerhead ribozyme catalysis in the context of our embedded single molecule supercoiling assay possessed the same catalytic properties as standard hammerhead ribozyme constructs characterized in solution, we assayed the frequency of cleavage as a function of pH and $[Mg^{2+}]$. The frequency of cleavage events indeed was found to increase with increasing pH and increasing magnesium ion concentration, consistent with on-pathway hammerhead catalysis (Figure 7) (Lee 2008a).

A G8A mutation demonstrates that the observed cleavage and ligation reactions in the single molecule assay are in fact due to standard, on-pathway hammerhead ribozyme catalysis.

As a further positive experimental control for non-aberrant hammerhead ribozyme catalysis, we constructed a C3A/G8U double-mutant and demonstrated that it rescues catalysis in the context of the single molecule. Interestingly, the rate of ligation is restored to a greater extent than the rate of cleavage, thus shifting the

internal equilibrium further toward reactants. Hence it appears that minor differences due to sequence variations in the active site that nonetheless maintain the hydrogen-bonding structure of the active site can perturb the internal equilibrium (Canny 2007), suggesting that this may well constitute a sensitive regulatory functionality within the context of the natural hammerhead ribozyme, i.e., it may have unmasked the subtle structural fluctuations that are responsible for regulating the nuclease/ligase switch.

This system also enables the unique opportunity to study the ribozyme in the context of several natural hammerheads that employe a physical separation of enzyme and substrate strands, including the discontinuous hammerhead (Martick 2008).

Finally, reversibility in this assay enables measurement of reaction kinetics, pronounced torque effects, and observation of conformational changes over the course of days. The single-molecule cleavage and ligation supercoiling assay demonstrates that a single natural-sequence hammerhead molecule indeed can undergo hundreds of successive cleavage/ligation cycles, each time regenerating a catalytically competent complex, thus putting to rest the objection that hammerheads (and presumably other self-cleaving RNAs) are not true ribozyme catalysts that exhibit multiple turnover (Leclerc 2010).

Notably, the relatively low-throughput nature of our measurements provide an obstacle to declaring our measurements of cleavage rates, force, and solution titrations to be accurate with statistical certainty. As in many prior single-molecule studies, a small proportion of tethered molecules (5-10%) exhibit the activity measured herein (Nöllmann 2007). Future studies may endeavor to subvert this

obstacle in various ways. First, by ensuring ligation of separate DNA and RNA segments (5 total here) are carried out in a truly 1:1:1 molar ratio. Doing so ensures that there are no excessive "handles" in the ligation preparation which may form braids across several otherwise observable molecules. Second, one may endeavor to purify the entire length of the dsDNA/RNA hybrid molecule by successive ligation and purification and thereby ensure no superfluous DNA segments exist on the slide, though in practice backbone nicking and product loss following purification have proved troublesome. Finally, one must take extreme care to ensure all buffers are pure; the slightest contamination may result in the release of bacterial enzymes that reduce efficacy of slide measurement.

In our single molecule experiment, a second obstacle proved to be a much larger challenge. Namely, methylation of the 2'-OH group of C17 (the nucleophile) in our system fails to abrogate the observed signal for every molecule studied. The mutation, which is predicted to shut down cleavage activity completely, permits an average of 1% of molecules to continue successive cycles of activity. Thus, while the majority of rate calculations, sequence controls, and solution effects agree with our expectations, the low-throughput nature of our active population prohibits an unambiguously convincing statistical analysis in this system. Future studies may avoid this impediment by designing positive control experiments with great care. By imposing translational force and torque, magnetic tweezers may reveal unforeseen properties of RNA and proteins, including off-pathway catalysis and conformational changes that are not necessarily relevant to previous solution studies. It has not

escaped our notice that the specific signals we have observed here may implicate a fundamental mode of supercoil relaxation inherent to RNA rather than the hammerhead ribozyme itself.

CHAPTER 3

A 1.55 Å structure of a full-length Mg^{2+}-bound hammerhead ribozyme

3.1 Introduction

Cationic stabilization remains an important consideration in the study of ribozyme structure and function. Like proteins, ribozyme use a variety of strategies to overcome energetic barriers of chemical reactions (Cochrane and Strobel 2008; Fedor 2009). One of the most ubiquitous of these strategies is the formation of a specific active site that positions solvent and functional groups in the appropriate oreintation to carry out the desired reaction chemistry. Unlike their protein counterparts, RNA has a limited number of polymeric constitutnets (with only 4 common nucleobases) and a highly charged phosphodiester backbone. In order to achieve the complex secondary and tertiary interactions required to carry out catalysis, ribozymes must overcome significant charge repulsion by the polyanionic phosphodiester backbone. RNA frequently depends on the presence of cations to provide a source of charge repulsion for folding and tertiary stabilization.

Divalent metal ions can bind RNA ligands via inner or outer sphere coordination, and often bind site-specifically near the active site, playing a direct role in the chemical mechanism (Sigel and Pyle 2007). Metalloenzymes, including RNaseP and group I introns, utilize divalent metal ions directly in catalysis by positioning to them participate directly the specific chemistry of the reaction (Steitz and Steitz 1993). In contrast to these large ribozymes, several small ribozymes tend to rely much less on divalent metal ions. In fact, four ribozymes are known to function in the absence of divalent metal ions given the presence of high concentrations of monovalent cations (~4M NH^{4+}) (Murray JB, 1998). Among them,

three form critical components of cellular rolling-circle replication machinery in small viruses and virus like RNAs (the hammerhead ribozyme and hairpin ribozyme) (Wedekind and McKay 1998; Rupert 2002; Nakano 2001). These examples demonstrate that RNA folding itself can account for a significant proportion of the catalytic enhancement over backgroud rates. Indeed, a complete understanding of the spectrum of mechanisms utilized by ribozymes has not yet been accomplished, due in significant part to the variety of roles that metal ions can play in ribozyme active sites.

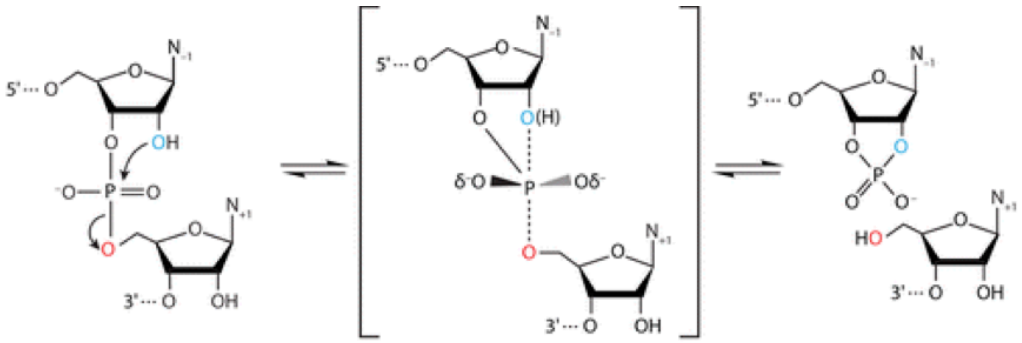

Fedor MJ. 2009. Annu. Rev. Biophys. 38:271-99

Scheme 3.1 Mechanism of RNA self-cleavage. The 2' hydroxyl (blue) serves as the nucelophile once deprotonated, attacking the proximal 3'-phosphate, resulting in a 2', 3'-cyclic phophate and a 5'-OH leaving group. The 5'-OH is the leaving group during cleavage and nucleophile during ligation.

The hammerhead ribozyme is no exception to these challenges. One of the most prevalent ribozyme motifs in biology (DeLaPeña 2010), the hammerhead ribozyme is a member of the type II family of small ribozymes which perform endonucleolytic cleavage of a specific phosphodiester bond via general acid-base

catalyzed nucleophillic attack of a 2'OH on the proximal 3'-phosphate, resulting in a 2',3'-cyclic phophate and a 5'-OH leaving group (Figure1.1) (Cochrane and Strobel 2008; Fedor 2009). Found throughout the Eukaryotic and Bacterial domains, the hammerhead serves as both a model system for understanding RNA catalysis and a novel drug target (De la Peña, 2010). A detailed description of the catalytic mechanism of the hammerhead ribzoyme has been remained challenging to ascertain despite decades of study. This difficulty has stemmed in part from both the hammerhead's non-absolute requirement for divalent metal ions, and in part the from the relatively recent discovery of stabilizing tertiary residues.

One of the most elusive aspects of the hammerhead mechanism is the extent of ion participation in catalysis. The finding that the hammerhead globally folds at moderate divalent ion concentrations, and is activated at higher concentrations suggests that a second metal dependent step may activate the hammerhead ribozyme for catalysis (Kim 2005, Boots 2008). Indeed, folding experiments have also suggested that metal ion identity can influence the achitecture of the active site at medium ionic strength (Boot 2008). The pH profiles of several hammerheads also suggest that coordination mode is dependent on metal ion identity. Reasonable catalytic rates can also be achieved in molar concentrations of monovalent cations alone, hinting at the important roles of nucleobases in the hammerhead ribozyme mechanism (Murray 1998; O'Rear, 2001; Bevilacqua 2004). However, at physiological ionic strengths, the hammerhead requires divalent ions to achieve moderate rates of catalysis; suggesting that the a divalent metal-dependent

mechanism may be a primary mode of catalysis in nature (Khvorova 2003).

Hammerhead ribozymes containing non-conserved interacting tertiary residues are known to promote the formation of the active site, and result in higher observed rates and a substantially lower requirement for divalent metals *in vitro* as well as activity *in vivo* (Khvorova 2003). Recent structures of constructs based on native hammerehads (2GOZ, 2OEU, 2QUS) suggest that a divalent metal may localize to the acitve core of the ribozyme in order to stabilize the close approach of A9 and scissile phosphate groups during the transition state of the reaction (Martick and Scott 2006; Martick 2008; Chi 2008). A structure of the full-length hammerhead in 2008 is consistent with this prediction, demonstrating a Mn^{2+}-binding site located between the A9P and N7 of G10.1 in the active core. Given the wide variety of divalent cations that are known to assist in substrate cleavage (Dahm and Uhlenbeck, 1991), we set out to determine whether more divalent metal-ions sites exist in the full-length structure of *Schistosoma mansoni.* We focused our efforts on Mg^{2+}, not only because it is the most physiologically relevant metal ion, but because outer sphere coordination of Mg^{2+} has been predicted to lower the pKa of the general acid G8, and could potentially position itself act as a proton donor in the catalytic core (RoychowdhurySaha 2006; Thomas 2008).

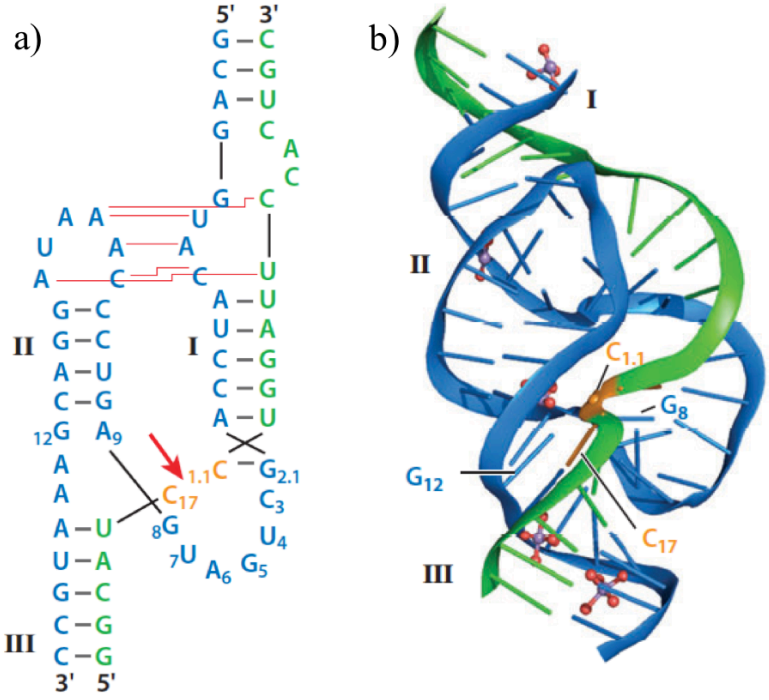

Annu. Rev. Biophys. 2009 38:271-279

Figure 3.1 Sequence and Structure of full-length hammerhead ribozyme. a) Secondary structure of natural hammerhead indicating tertiary interactions (red lines), cleavage site (red arrow), and the relative positions of stems I, II, and III. (pdb 2GOZ) b) Global architecture of a native hammerhead ribozyme (pdb 2GOZ (Martick and Scott 2006)), with enzyme strand in blue and substrate strand in green. The two nucleotides upstream (C17) and downstream (C1.1) of the reactive phosphodiester are gold. and interacting looped regions of stems I and II interact, imparting a significant Solution structure of 2006 showing orientation of the three stems.

It was first proposed in 1994 that a large-scale rearrangement of the minimal hammerhead structure was required to achieve a catalytically active conformation

(McKay 1994). It was subsequently suggrested that two phosphate groups separated by 20Å in the minimal hammerhead (the pro-R phosphate oxygen of A-9 and the scissile phosphate) could come together to form a single metal binding pocket (Wang et al and Herschlag, 1999). In support of this model, simultaneous phosphorothioate substitutions at each position were found to form a binding site for a single thiophillic metal ion in minimal constructs (such as Cd^{2+}) (Wang *et al,* 1999). Phosphorothioate metal rescue was also observed at the same sites in the full-length hammerhead at low ionic strength (Osborne 2005). ^{31}P NMR-detected Cd^{2+} titration studies of substituted full-length constructs suggest that this metal ion association may include an interaction with the 2'-OH nucleophile (Osborne, 2009). NMR experiments have identified A9 as a high affinity metal binding site as well, but there has been little evidence for metal coordiantion to the scissile phosphate (Maderia 2000; Suzumura 2002).

RNA construct	pH	Resolution (Å)	PDB ID
Minimal, RNA-DNA hybrid	6	2.6	1HMH
Minimal, 2'-OCH3 ribose at N_{-1}	6.5	3.1	1MME
Minimal, freeze-trapped RNA	6	3	299D
Minimal, freeze-trapped RNA	5	3	300D
Minimal, tethered between helices I and II	5	2.85	1NYI
Schistosoma mansoni, 2' OCH3 at N_{-1}	5.5	2.99	2GOZ
Schistosoma mansoni, 2' OCH3 at N_{-1}	5.5	2.2	2OEU
Here: *Schistosoma mansoni,* 2' OCH3 at N_{-1}	5.5	1.55	3ZD3

Table 3.1 X-ray crystal structures of hammerhead ribozymes.

The absence of a metal ion bridge between the A-9 and scissile phosphate groups in the 2006 full-length structure might be attributable to the low concentration of Mg^{2+} and binding competition from the high concentration of NH_4^+ employed in the crystallization conditions. On the other hand, Mg^{2+} may serve to simply stabilize the catalytically competent conformation (Penedo 2004). The question of whether Mg^{2+} is required for catalysis in the context of the full-length hammerhead ribozyme therefore remains unresolved. In this study, we probe whether and how many alternate divalent metal-ions binding site(s) exist in the full-length structure.

3.2 Summary of Results

This Chapter examines the 1.55 Å x-ray crystal structure of a natural *Schistosoma mansoni* hammerhead ribozyme demonstrating novel tertiary interactions and Mg^{2+}-bound in three distinct sites (Figure 3.6, Table 3.2). This is the highest resolution structure of any ribozyme to date. Table 1.1 compares the resolution and solution conditions (pH) of severalhammerhead ribozyme crystal structures relevant to this study. The structure presented here reveals modest rearrangements of the active core in addition to well-ordered solvent molecules buried in the active site which may serve to participate in proton transfer during the cleavage reaction. Enzyme and substrate strands have been separated into two strands as in previous experiments (Figure 1.1) (Martick and Scott, 2006). Three Mg^{2+}-binding sites and their coordinated waters are identified as "Site" 1-3 (Figure 3.6, Figure 3.7, and Figure 3.9).

3.2.1 New Contacts at Stems I and II Interface

Like the minimal hammerhead, the full-length *Schistosoma* ribozyme fold comprises a three-way junction resembling a slingshot in which stem II and stem III are coaxially aligned above stem I. The high-resolution Mg^{2+}-bound structure displays a tertiary interaction between the stem II loop/stem I bulge interaction as previsouly observed (Martick and Scott 2006). However, two modest rearrangements in the high-resolution structure reveal novel tertiary interactions between stems I and

II.

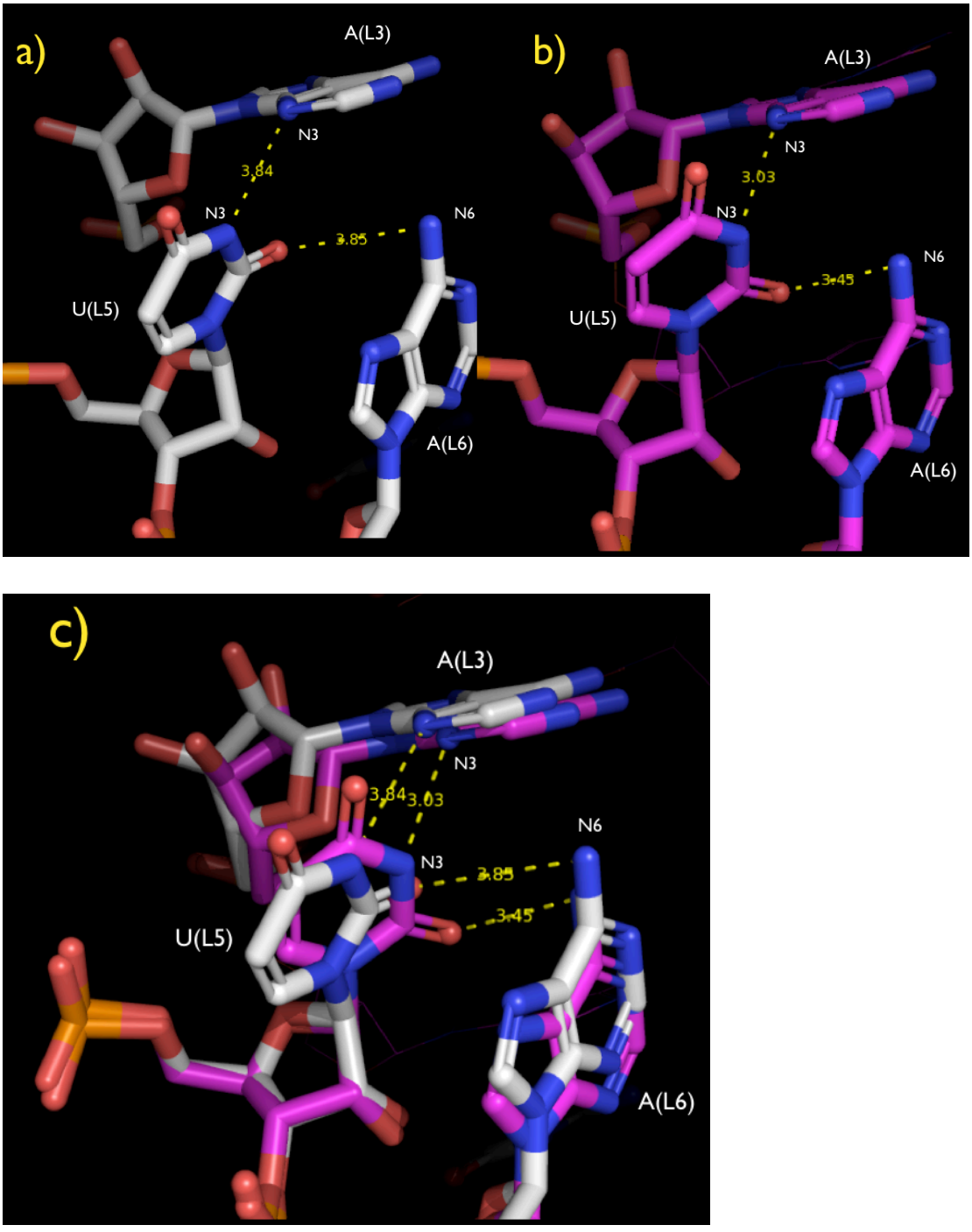

Figure 3.2 New tertiary contacts. a) The 2006 structure and b) Mg^{2+}-bound high-resolution structure display a difference in base angle rotation at U(L5), resulting the assignment of a hydrogen bond between the N3 proton of U(L5) and N3 of A(L3), in addition to a hydrogen bond between the O6 of U(L5) and N6 of A(L6). White= 2GOZ, Magenta =HR2GOZ.

One of the residues that caps stem II, U(L5), experiences a base angle rotation of about 20 Degrees relative to the 2006 structure(Figure 3.3). The rotation forms a hydrogen bond between O6 of U(L5) and N6 of A(L6), resulting in a previously unobserved orientation of the stem I/stem II interface (Figure 3.3b). In addition, a new hydrogen bond is formed between the N3 proton of A(L5) and N3 of A(L3). These rearrangements appear to coincide with a reorientation of the endocyclic ribose oxygen bridging A(L3) and A(L4) (Figure 3.4). The A(L3) base, however, remains in near identical orientation to the 2006 structure.

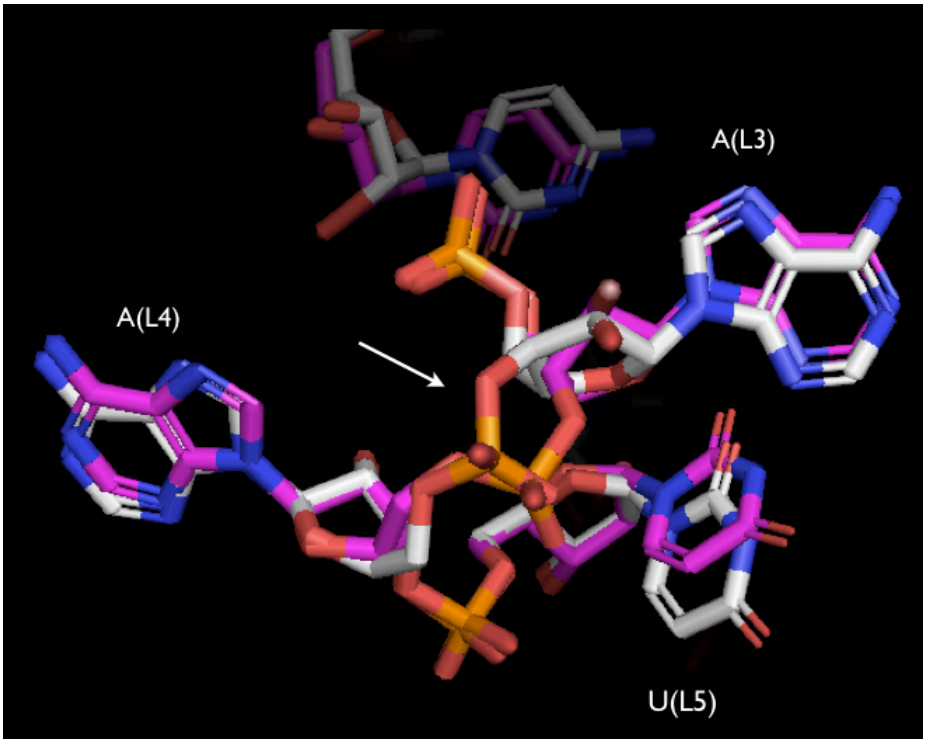

Figure 3.3 New loop/buldge contacts (Figure 3.2) induce a reorientation of the endocyclic ribose oxygen. Superimposed structures of 2GOZ and HR2GOZ display this reorientation of the A(L4) ribose. White= 2GOZ, Magenta =HR2GOZ.

Interestingly, the base angle rotation of U(L5) may modulate the adjacent A(L6)/U(1.7) interaction (Figure 3.5) that forms between the GNRA-like cap of Stem II and U1.7 in the substrate strand. A(L6) represents the final A in the GNRA-like tetraloop capping Stem II. This AU Hoosteen pair between A(L6) and U(1.7) is the only known tertiary interaction involving the substrate strand to be conserved across all tertiary stabilized hammerheads, and is thought to comprise a sensitive regulatory modality in the molecule.

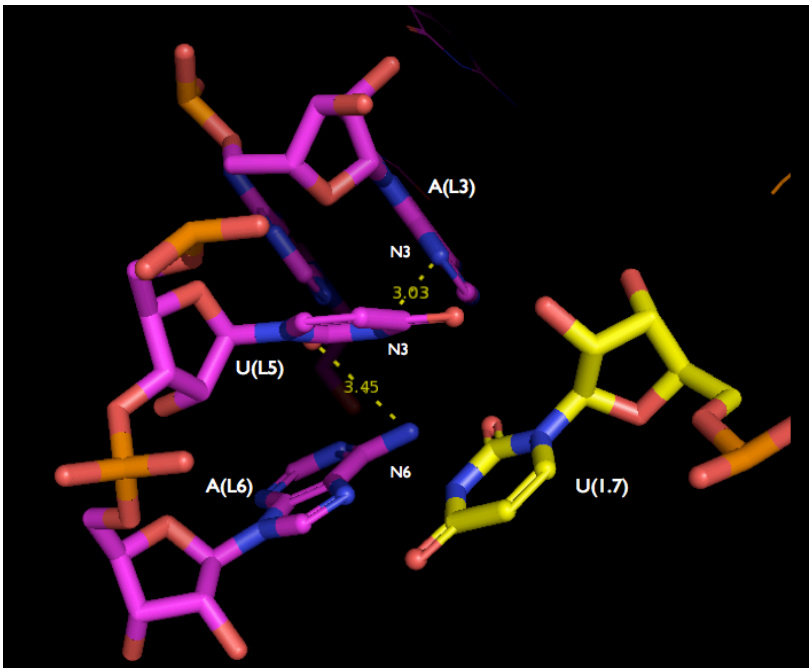

Figure 3.4 Base angle rotation of U(L5) (Figure 3.3) may modulate the A(L6)/U(1.7) interaction. This Hoogsteen interaction formed between the enzyme strand (magenta) at A(L6) and substrate strand (yellow) at U(1.7) represents the only conserved tertiary interaction among all reported hammerhead ribozymes. Rearrangments at U(L5) may be responsible for inducing and stabilizing conformational changes in the active site, and for controlling the cleavage/ligation switch.

As differences in the tertiary contacts between Stems I and II are known to account for differing extents of cleavage in tertiary stabilized hammerheads, the U(L5) rotation may be partially responsible for inducing and stabilizing conformational changes in the active site responsible for catalysis. Furthermore, the fine structure of this interaction at 1.55 Å may enable the hammerhead to modulate its activity between cleavage and ligation.

3.2.2 Three Mg^{2+}-ion-Binding Sites

Three potential Mg^{2+}-binding sites can be identified among the various solvent peaks (Figure 3.6). A Mg^{2+} observed in site 1 and site 3 may stabilize interactions peripheral to the catalytic core of the hammerhead ribozyme, while a Mg^{2+} in site 2 (bound between N7 of G10.1 and the A9 phosphate) may be relevant to the catalytic mechanism of the hammerhead ribozyme reaction. The very high resolution of the crystal structure (1.55 Å) has not only enabled observation of these physiologically relevant Mg^{2+}-bindings sites, but additionally has revealed well-ordered solvent molecules near the active site. One of these ordered solvent molecules takes on a similar orientation to a water found Mn^{2+}-bound in the active core of the 2008 full-length structure (Martick 2008) at position "W73." Both water moelcules are within hydrogen bonding distance of G12 and G8, the putative general base and acid in hammerhead ribozyme catalytic mechanism.

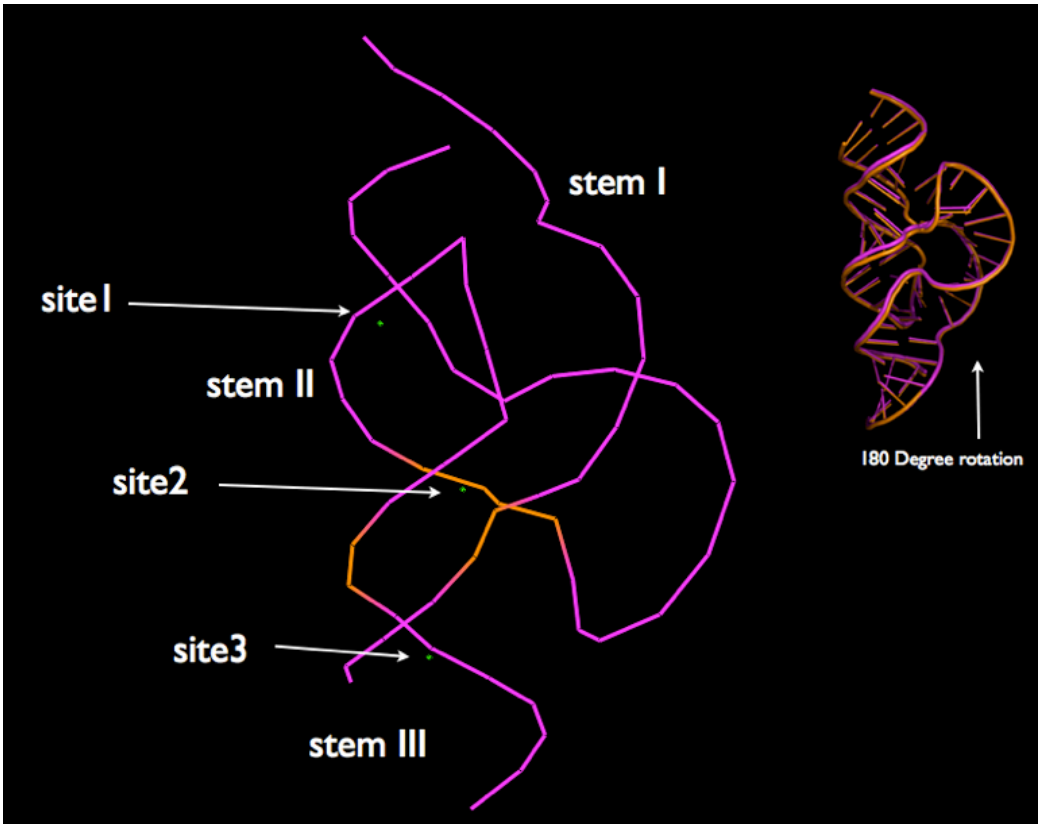

Figure 3.5 Overview of the three Mg^{2+} ion (green star) metal binding sites in the high-resolution full-length hammerhead structure. Site 2 is located in active core(orange), and site 1 and 3 are bound in stems II and III, respectively. Top right: Superimposed ribbon structurse of 2GOZ and HRGOZ rotated 180 Degree rotation relative to enlarged figure.

Mg^{2+}-binding site 1 is positioned near the ribozyme loop/bulge interaction, and site is positioned in Stem III. Site 2 corresponds to a Mn^{2+} ion-binding site identified in stem II of a previously reported hammerhead crystal soaked in 100 mM $MnCl_2$ (Pley 1994), a full-length hammerhead structure bound to Mn^{2+} (Martick 2008), and a Mg^{2+}-ion-binding site in the all-RNA minimal hammerhead structure (Scott 1995).

3.2.2a Site 1

Site 1 most likely corresponds to $Mg(H_20)_5^{2+}$ bound to the N7 group of A(L2) (Figure 3.7). Site 1 may also be associated via the hydration shell with exocyclic nitrogren N6 and nonbridging *pro*-R oxygen of A(L2). The five water ligands form a hydrogen-bonding network with other structural waters and adjacent nucleotides in a manner similar to that formed by a Mn^{2+} ion identified in the loop of stem II in the 2008 Mn^{2+}-bound structure.

Although the A(L2) base is contained in a nonconserved region of the stem II loop, bound Mg(II) influences the network of hydrogen bonds stabilizing the tertiary contact between stem I and stem II. By stabilizing the base-stacking interactions of A(L2) and A(B3), Mg(II) in site 1 reorients the adenine base of A(L2) in a manner that permits hydrogen bonding between the O6 of U(L6) and N3 of A(L2). The proximity of these interactions to U(L5) suggestst Mg^{2+}-binding at site 1 may be linked to the conformational changes discussed previously at the loop/bulge interface (Figure 3.3-Figure 3.5). By reoreinting A(L2) in a manner that permits hydrogen bond formation with U(L6), a Mg^{2+}-ion bound in site 1 may also be partially responsible for inducing and stabilizing conformational changes in the active site.

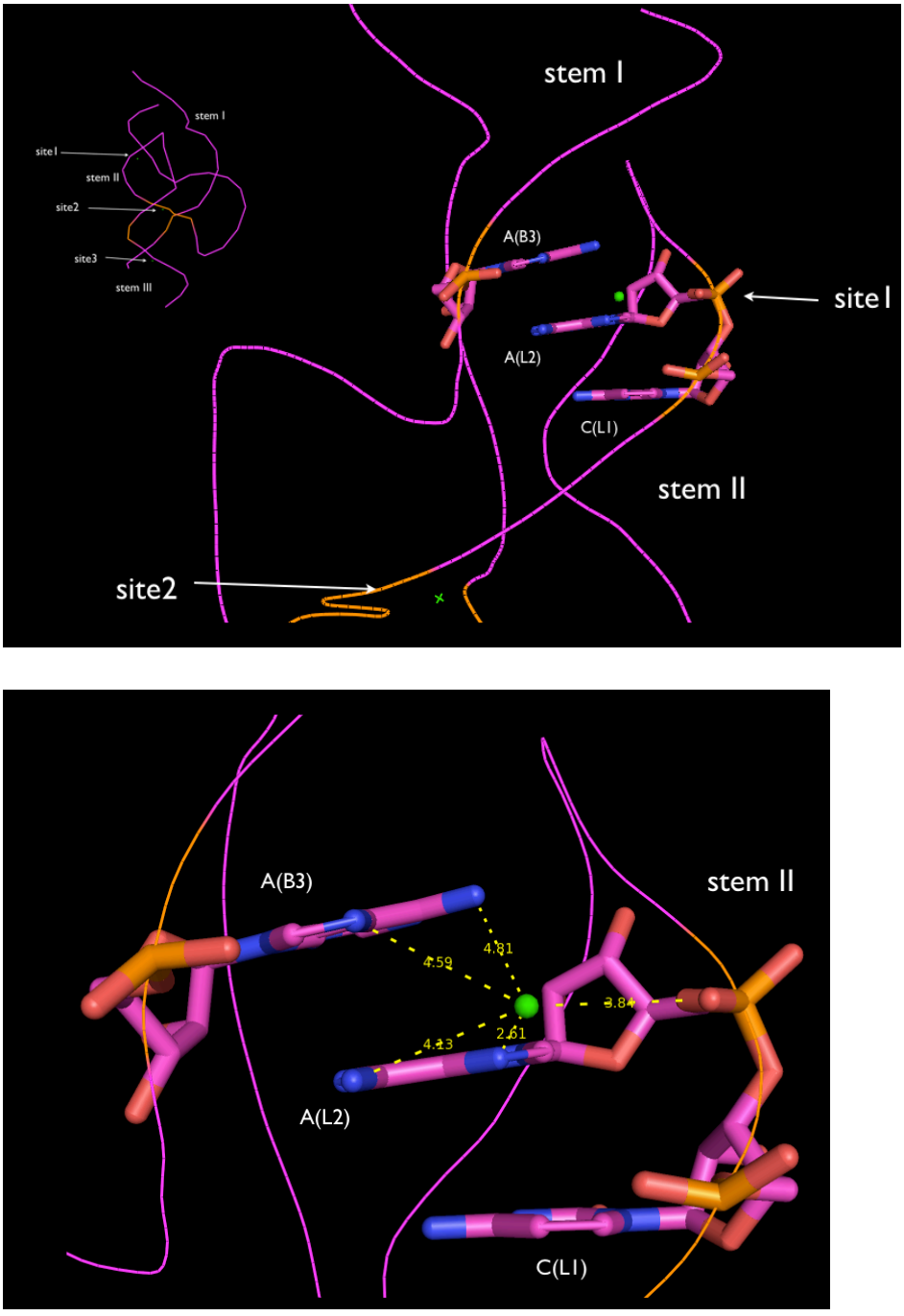

Figure 3.6 Divalent Metal binding site 1. Top: Wide view of metal binding site 1, oriented near the loop/bulge interaction between stem I and II.
Bottom: Site 1 corresponds to a Mg(H20)52+ bound to the N7 group of A(L2). Site 1 may also be associated via the hydration shell with exocyclic nitrogren N6, nonbridging pro-R oxygen of A(L2), N7 of A(B3), and N6 of B(3). The stem II loop residue A(L2) is involved in a stacking interaction with A(B3) of stem I. Distances for all atoms that may bind directly or via hydration shell are shown in yellow. White= 2GOZ, Magenta =HR2GOZ

3.2.2b Site 2

The second peak, corresponding to site 2, likely represents a $Mg(H_20)_4^{2+}$ bound directly to the *pro*-R oxygen of A9 and N7 of G10.1. This Mg^{2+}-ion binding site is identical to a Mg^{2+} site identified in the minimal (Pley 1994; Scott 1996) and full-length (Martick 2008) hammerhead ribozymes (Table 3.1). Minimal hammerhead RNA/DNA hybrid molecules in this study was soaked in 100mM $MnCl_2$, while tertiary stabilized molecules were soaked in either 10mM Mn^{2+} or 10 mM Mg^{2+}. None of these structures showed a divalent metal bridging the A9 and scissile phosphates, which would have strongly implicated a direct participation of Mg^{2+} in the catalytic mechanism (Lee 2007).

A close comparison of the Mn^{2+}-bound and Mg^{2+}-bound structures (Figure 3.8) reveals that both contain a highly-ordered water molecules in the active site, including a solvent molecule bound to the scissile phoshpate (Figure 3.8). This site was occupied in the 2008 Mn^{2+}-bound structure, displaying a binding mode identical to that observed in the original Mn^{2+}-bound minimal hammerhead construct (Kisseleva 2005). In all three structures, the divalent metal binds to the *pro*-R oxygen of A9 and associates with the exocyclic N7 of G10.1. This interaction moderately shifts the lower part of stem II toward stem I in the high-resolution structure (Figure 3.15).

It is intriguing to consider the role of Mg^{2+} bound in site 2; even though the riboyzme takes on the active conformation, the metal group bound at the P9/G10.1 is

~ 6 Å from the active site and does not make contact with functional groups directly involved in catalysis (Figure 3.12). As the only solvent peak located near the catalytic pocket of the hammerhead ribozyme, we must consider the mechanistic implications of Mg^{2+} bound at site 2 (Figure 3.8).

3.2.2b1 Mechanistic Implications of a Mg^{2+}-ion Bound at P9/G10.1

Two models may explain how the the metal ion observed at the P9/G10.1 site may participate in the catalytic mechanism of the hammerhead ribozyme. In the first model, a metal ion may be recruited to the scissile phosphate during the reaction resulting in stabilization of the negative charge of the phosphorane transition state (Wang et al, 1999). This "dynamic model" has been the basis of computational studies which calculate the position of the metal ions during diffrent points along the hammerhead reaction coordinate (Lee et al, 2008). These simulations, based on the crystallographically predicted P9/G10.1 metal site, predict that a slight negative charge build-up results from nucleophile deprotonation. Negative charge buildup is rapid, and results in the recruitment of the P9/G10.1 metal into a bridging coordination mode between the *pro*-R oxygen atoms of the P9 and scissile phosphates (Lee 208; Lee 2009).

a)

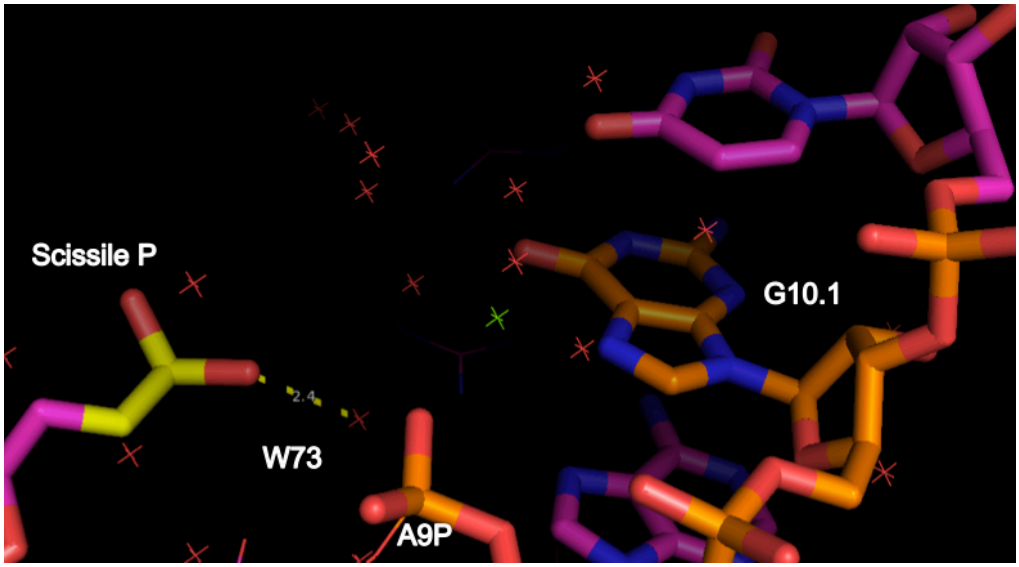

b)

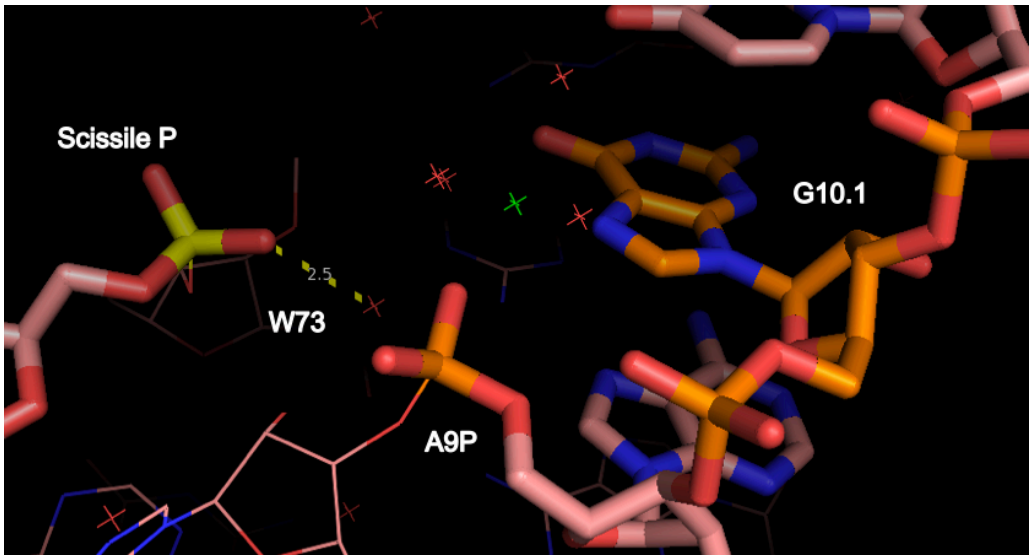

Figure 3.7 View of the active site in a) full-length Mn^{2+}-bound and b) Mg^{2+}-bound hammerhead ribozyme crystal structures. Both structures contain a divalent ion coordinating directly to the scissile phosphate (yellow) ("W73", Martick 2008) at distances of 2.4 A and 2.5 A, respectively. This water molecule can hydrogen bond to G12 (general base) and G8(general acid) (not shown), and therefore may be involved in proton transfer reaction. The Mg^{2+} ion (green star) in site 2 is coordinated by the *pro*-R oxygen of the A9 phosphate (A9P) and the N7 of G10.1, in addition to four water molecules (red stars).

On the other hand, the observed structures may simply represent the most stable states possible under crystal forming conditions, and the positioning of the metal ion may be specific to crystallography. The active form therfore may be different or in equilibrium with the conformation observed in x-ray structures. An "activated ground-state coordination" of the catalytically relevant metal ion to the scissile phosphate could theoretically provide a strong chemical advantage over the dynamic model for several reasons. First, in the ground-state *pro*-R oxygen coordination position, the metal ion could lower the reaction barrier by stabilizing in-line attack geometry, activating the nucleophile via direct or indirect coordination. Second, the metal could withdraw electron density from the phosphate and thereby increase the electrophilicity of the scissile phosphorus. Finally, proximity of the metal ion may lower the pKa of the putative general base and/or nucleophilic 2'-OH. Indeed, in the predicted mechanisms of other metal-dependent ribozymes such as the Group I intron, one or more metal ions are coordinated in the active site of the ribozyme without the need for metal recruitment during the reaction (Frederiksen and Piccirilli 2009).

The Mg^{2+}-binding mode identified in our full-length construct suggests that site 2 represents a divalent metal-binding site in the ground state, and implicates an indirect participation of Mg^{2+} in catalysis. A Mg^{2+} ion at site 2 most likely withdraws some of the accumulating negative charge of the scissile phosphate and may introduce order to the solvent molecules near the cleavage site. This is consistent

with the positioning of site 2 near A9 and G10.1, just out of range of the 2'-oxygen C17. A hydrated divalent metal bound to site 2 (between A9 and G10.1) likely serves both to distribute the build up of negative charge during the transition state and facilitates strand separation before and after cleavage.

A slight local rearrangement of the scissile phosphate, A-9, and G-12 is required to accommodate Mg^{2+} in site 2. However, a solvated water molecule could also make contact to the phosphate oxygen making such a rearrangement unnecessary. Indeed, in both the Mn^{2+} and Mg^{2+}-ion-bound structures, an ordered water molecule is positioned to participate in proton transfer by facilitating deprotonation of G12, and replacement of the proton at the 2'-H of G8 after it has been donated to the 5'-O leaving group (Figure 3.8). In both cases, this ordered water molecule is bound directly to the scissile phosphate (Figure 3.8) and could plainly assist in solvent-mediated proton transfer during the cleavage reaction. We are permitted to make this inference because this water molecule can form hydrogen bonds with G12 (the general base) and the 2'-OH of G8 (putative general acid). Thus, if the binding mode of this water molecule is maintained in the transition state, the Mg^{2+} ion is likely to participate only indirectly by stabilizing accumulating negative charge.

An alternate possibility to a model in which divalent metal participate indirectly in the catalytic step involves a single metal or double metal mechanism. In a single metal mechanism, Mg^{2+} would alter its location from that observed in the high-resolution structure to bridge the A9 and scissile phosphates (Wang 1999). If

this migration takes place, the Mg^{2+} ion would then directly participate in the transition-state charge stabilization interaction, in line with biochemical studies suggesting the importance of the G8 base as a general acid with a pH dependence correlated with metal ion pka (Roychowdhury-Saha and Burke, 2006). In a double-metal mechanism, the Mg^{2+} ion would maintain its position and a second divalent metal would be recruited to bridge the A9 and scissile phosphates. These mechanisms are plausible, but less likely than an indirect mechanism because they involve addition and substration of atoms not observed in the crystal structure.

Binding of a divalent metal in the ground state is consistent with previous crystallographic (Pley 1994; Scott 1996) and biochemical data (Wang 1999). While it does not entirely explain the observed metal-ion dependence of the pKa of the general acid G8 (Roychowdhury-Saha and Burke, 2006), it agrees with recent cadmium rescue experiments on scissile phosphorothioate-substituted hammerheads derived from *Schistosoma mansoni* (De Rose 2012). These later experiments also suggest ground-state coordination (Peracchi et al. 1997; Wang et al. 1999b).

Site 2 in HRGOZ also agrees with an analogous site in the all-RNA minimal hammerhead structure (Scott 1996). However, in the minimal all-RNA structure, a $Mg(H_20)_5^{2+}$ was bound to the *pro*-S oxygen of A9 and, like the hybrid structure, associated with N7 of G10.1 via the hydration shell, rather than a direct bond. While the close agreement of the binding sites in the minimal and full-length structures solidify their identification as conserved binding pockets, it also suggests that the G10.1-C11.1 base pair is conserved in this orientation to maintain the presence of

Mg(II) binding at this site (Figure 3.12). G12, the putative general base in the catalytic cycle, may also be conserved for the purpose of maintaining the Mg^{2+} binding site.

The high concentration of competing monovalent cations in the 2006 full-length structure is likely responsible for the absence of an Mg^{2+} bound at site 2 in that structure. However, under the moderate ionic strength of physiological conditions, the catalytic core would likely permit access to divalent ions in a manner consistent with site 2 of the HRGOZ structure reported here .

a)

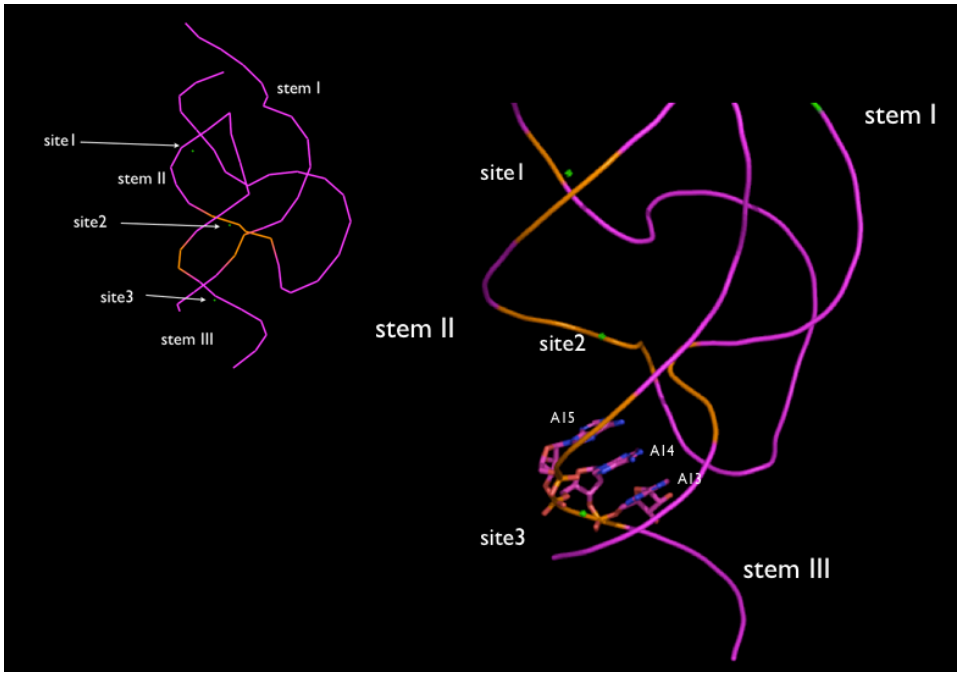

b)

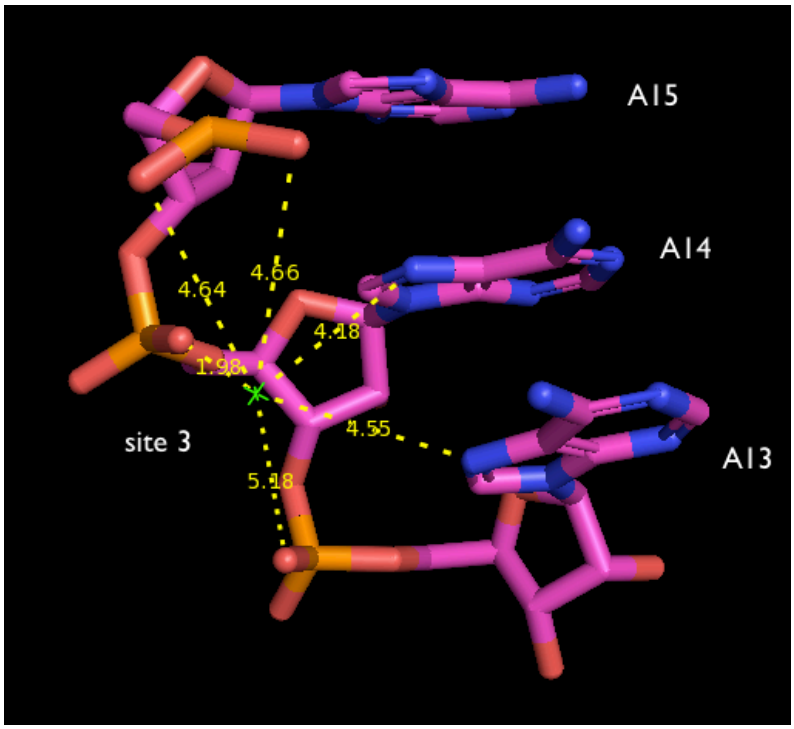

Figure 3.8 Divalent Metal binding site 3. a) Wide view of metal binding site 3, oriented near the loop/bulge interaction between stem I and II.
b) Site 3 corresponds to a $Mg(H_20)_5^{2+}$ bound to the N7 group of A14. Site 1 may also be associated via the hydration shell with atoms displaying distances out to 5.2 Å.

3.2.2c Site 3

Site 3 likely corresponds to $Mg(H_20)_5^{2+}$ bound directly to the *pro*-R oxygen of A14 and associated via the hydration shell with the N7 of A14. This potential Mg^{2+} site may stabilize the stacking interactions between A14 base and A38. The A38 base, in turn, stacks coaxially with the conserved A9 base, and may contribute to a modest reorientation of the A9 phosphate relative to the 2006 structure (Figure 3.11). This rearrangement brings the A9 phosphate ~0.5 Å nearer to and scissile phosphate adjacent to C-17. The closest nonbridging oxygen distance between the two phosphates is now ~3.5 Å, rather than 4.5 Å in the 2GOZ structure and 20 Å in the minimal hammerhead structure. Site 3 closely corresponds to a Mn^{2+}-bound site in the 2008 structure bound to the O2P of A14, stabilizing the junciton of stem II and III.

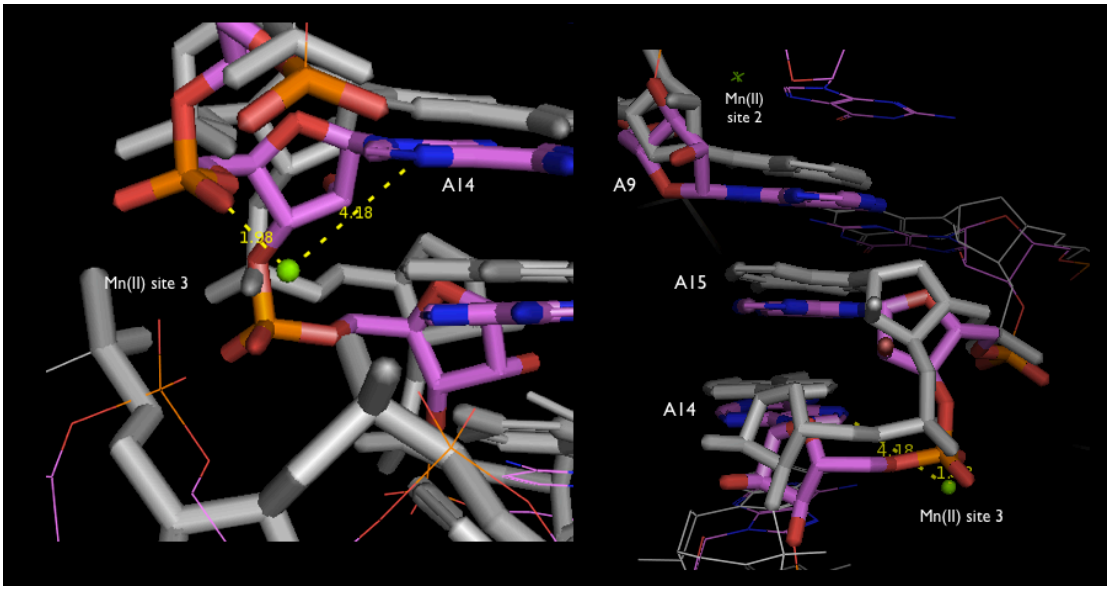

Figure 3.9 Mg^{2+} binding Site 3 superimposed with 2006 crystal structure. left: In stem III, a $Mg(H_20)_5^{2+}$ is bound directly to the pro-R Oxygen of A14 and associates via a hydration shell (not shown) with the N7 of A14. right: This potential Mg^{2+} site may stabilize the stacking interactions between A14 base and A38. The A38 base, in turn, stacks coaxially with the conserved A9 base. Mg(II) binding site 2(top) and 3(bottom) may act cooperatively to impart a subtle rearrangement of the active core. White= 2GOZ, Magenta =HR2GOZ.

3.2.3 Subtle Active Site Rearrangement

The minimal hammerhead lacks tertiary interactions and predominantly occupies an "open" conformational state that requires a rearrangmenet to a "closed" or active state to achieve the catalytic fold. Consistent with evidence from prior work showing that the conserved catalytic nucleotides form a more compact arrangement in a Mg^{2+}-bound "closed" state (NewbyLambert 2006), the Mg^{2+}-bound structure displays close compaction of exocyclic G5 and G6 functional groups. This closer compaction in the presence of Mg^{2+} is also refelcted in the interaction of G12 and A9 bases, which shift ~0.5 Å closer in the 1.55 Å structure.

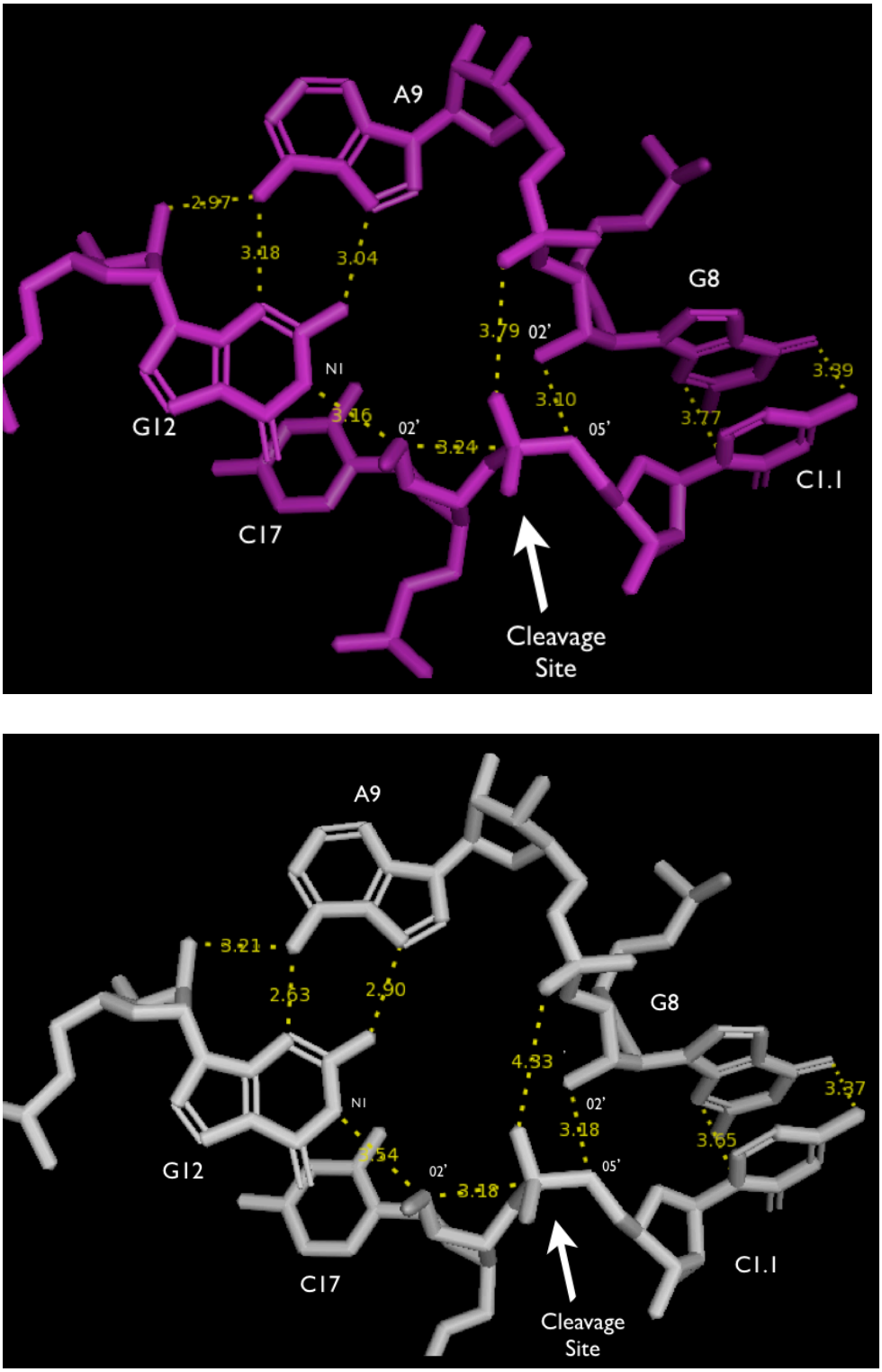

Figure 3.10 Subtle rearrangement of the Active Site.
2GOZ (bottom) and HRGOZ (top). Improved base-stacking between C1.1 and G-8 and a modest distancing of A-9 and G-12 reposition the active site for optimal in-line attack.

The nucleophilic 2' oxygen of C17 is brought within 3.18 Å of the scissile phosphorus due to steric repulsion of the G-5 and G-6 groups. As a result of this shift, the 2'-OH of C17 is also brought to within hydrogen-bonding distance (3.16 vs. 3.54 A) to N1 of G12 (the putative general base). Improved base-stacking between G8 and C1.1 also brings the 2'OH of putative general acid G8 to within ~3.1 Å of the leaving group, supporting its role as a general acid involved in charge stabilization following cleavage. (Figure 1.1, Figure 3.11). Thus, G8 and G12 are ideally positioned to participate in proton transfer, reinforcing their putative roles as general acid and base, respectively. These modest rearrangements in the presence of Mg^{2+} provide an active core that more closely resembles the trigonal bipyramidal transition-state phosphate configuration characteristic of a phosphodiester isomerization taking place via an in-line attack.

A single magnesium bound between the A9 phosphate and the exocyclic nitrogen of G10.1 undoubtedly contributes to this reorientation of the catalytic pocket (Figure 3.8). The A9 and scissile phosphates shift from a distance of 4.33 Å in the Mg^{2+}-free structure to 3.79 Å in the Mg^{2+}-bound structure, indicating a subtle shift that rearranges the active site to reflect an improved geometry amenable to catalysis (Figure 3.11)

Data Collection:	Overall
Resolution limits (A)	20.39 - 1.55
Minimum (Fobs/Sigma_Fobs)	1.34
R value	0.23
Total number of reflections	26447
Number of reflection (non-anomalous)	26447
Completeness	97.48%
Multiplicity	
Crystallographic Refinement	
R Value (Working + Test Set)	0.1985
R Value (Working Set)	0.1959
Free R Value	0.231
Free R Value Test Set Size	7.57
Free R Value Set Count	2002
Error Estimates	
Coordinate Error (Maximum-likelihood based)	0.24
Phase Error (Degrees, maximum-likelihood based)	24.38
Rmsd from Ideal Value	
Bond	0.005
Angle	0.835
Chirality	0.063
Planarity	0.009
Dihedral	17.51
Min Nonbonded Distance	1.93

Table 3.2 X-ray Data Collection and Crystallographic Refinement

3.3 Detailed Discussion: Natural Hammerhead Structure at 1.55 Å and the Role of Mg^{2+}-ion-binding Sites

3.3.1 Background

3.3.1a The Role of Metal Ions in Ribozyme Folding and Catalysis

The precise role played by metal ions is unknown in many ribozymes, including the VS and Hammerhead ribozymes (Fedor 2009). In both of these examples, the molecules can cleave in the absence of divalent metal ions, casting doubt on the idea of a metal ion-mediated mechanism (Krasovska 2005). While by 1998 it was known that divalent ions were not an absolute requirement for hammerhead catalysis, a large body of biochemical and structural evidence suggested participation of divalent ions in folding and catalysis of full-length molecules under physiological conditions (Feig 1999). A high-resolution structure of a full-length hammerhead displaying an active-site architecture with only a 4.3 Å separation of the A9 and scissile phosphates also suggested a divalent metal ion may be required to disperse electrostatic repulsion of the phosphate oxygens (Martick and Scott 2006). Subsequent metal-soaking studies revealed five Mn^{2+} binding sites in natural *Schistosomal hammerhead*, despite the absence of bound metals in the 2006 structure (Martick 2008). In the present study, we probe whether the natural hammerhead also binds Mg^{2+}, perhaps the most physiologically relevant of the divalent metals.

Relative to the 2006 salt conditions, we increase the concentration of magnesium ions (from 1mM to 10mM) while maintaining the monovalent concentration (1M NH4+).

The resulting high-resolution crystal structure of the *Schistosoma* hammerhead reported here shows a Mg(II) metal ion ideally positioned to stabilize the transition state, take part in the chemical step of the reaction and/or to facilitate folding. This work discusses the implications of structural observations in the high-resolution structure, including a discussion of active site architecture, global rearrangements, agreement of divalent binding sites with previous structural and biochemical studies, and finally the catalytic mechanism of cleavage and ligation.

3.3.2 Mg^{2+}-ion-binding Site 2 Highlights Role of Core Nucleotides in Proton Transfer

3.3.2a General Base catalysis & G12

Examination of the Mg^{2+}-bound high-resolution structure reveals repositioning of core residues previously implicated in proton transfer (Martick and Scott 2006). For example, N1 of G12 is within approximate hydrogen bonding distance of the 2'-O of C17 (3.26 Å in the Mg^{2+}-bound structure). This represents a modest rearrangement relative to the Mg^{2+}-free structure (3.55 Å). If G12 functions as a general base, it is most likely that the 2'-proton would be abstracted by a deprotonated N1.

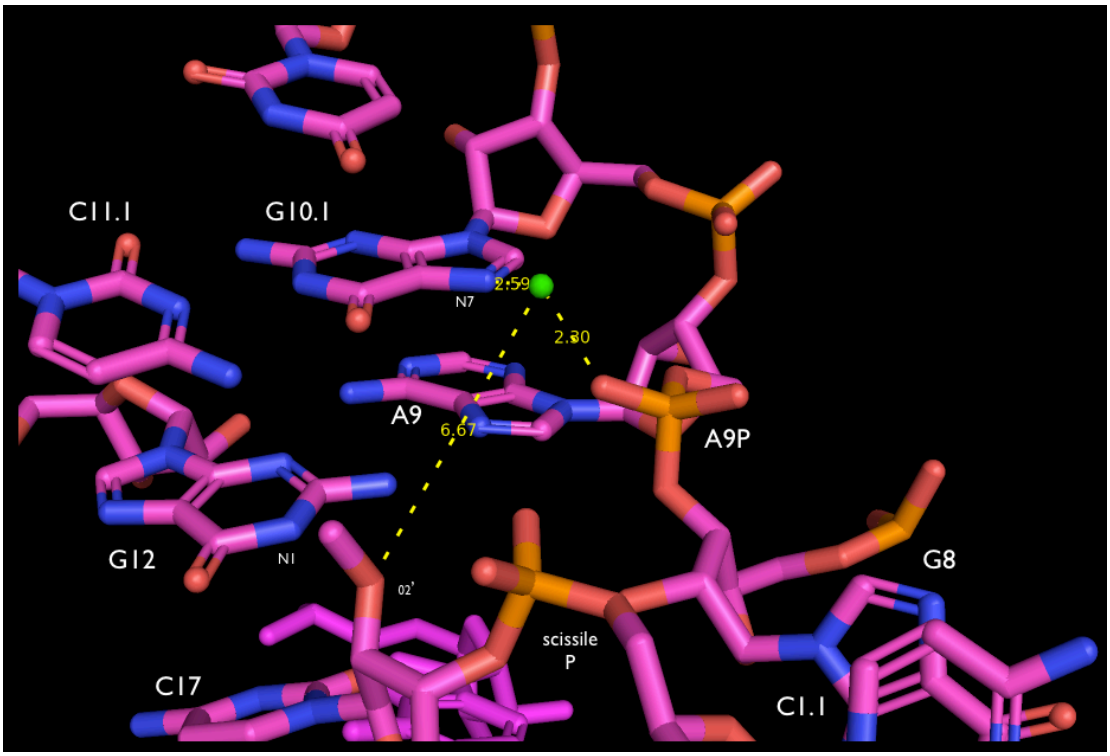

Figure 3.11 Orientation of Mg^{2+}-ion-binding site 2 in active site. Mg^{2+} binding site in the catalytic core. A slight structural rearrangement relative to the 2006 structure and a Mg^{2+} metal bound to the pro-R oxygen of A9 and N7 of G10.1 in site 2 brings putative catalytic groups G12 and G8 into alignment. The Mg^{2+} is too distant from catalytic site (6.67 A) to directly participate in catalysis, but may participate by an indirect mechanism involving proton transfer of well-ordered solvent molecules in the active site. The C11.1/G10.1 Watson-Crick pair orients the N7 group of G10.1 to coordinate the Mg^{2+} bound in site 2, and may be highly conserved for this purpose.

Previous kinetics experiments also support this model. For example, the apparent pKa of the hammerhead ribozyme reaction is 8.5, suggesting involvement of two groups with high pKas in the protonation/deprotonation events of catalysis. Indeed, substitution of G12 with groups of different pKas, such as inosine (pKa 8.7), 2,6-diaminiopurine (pKa 5.1), or 2-aminopurine (pKa 3.8), shifts the reaction rate profile in a manner consistent with G12's suggested role in general base catalysis

(Ham and Burke, 2005; RoychowdhurySaha 2006). N1 of the guanosine nucleotide has also been proposed to play a role of a general base in the context of hairpin ribozyme catalysis (Han 2005). The pH profiles of imidazole-substituted hairpin ribozymes show altered pH dependence consistent with a direct role of N1 of G in proton transfer (Wilson et al 2006). However, the apparent pKa of the hammerhead reaction, 8.5, is considerably lower than the pKa of a guanosine (9.4). As discussed, photocrosslinking experiments and mutational data further support a role of the N1 of G12 as a general base, consistent with a transition into an active conformation (Heckman 2005).

The Mg^{2+}-bound structure reported here comports with kinetics studies and biochemical experiments, reinforcing the role of G12 in proton transfer (Osborne 2005). In the high-resolution structure, G12 demonstrates the closest reported approach of N1 of G12 to the nucleophillic 2'OH of C17 of any reported crystal structure (3.16 A). This observation enables the definitive assignment of hydrogen bond between these residues, supporting a model wherein the 2'-proton of the nucleophile is readily abstracted by N1 of G12. Thus, the active site architecture of the high-resolution structure is in close agreement with previous studies implicating G12 as the general base.

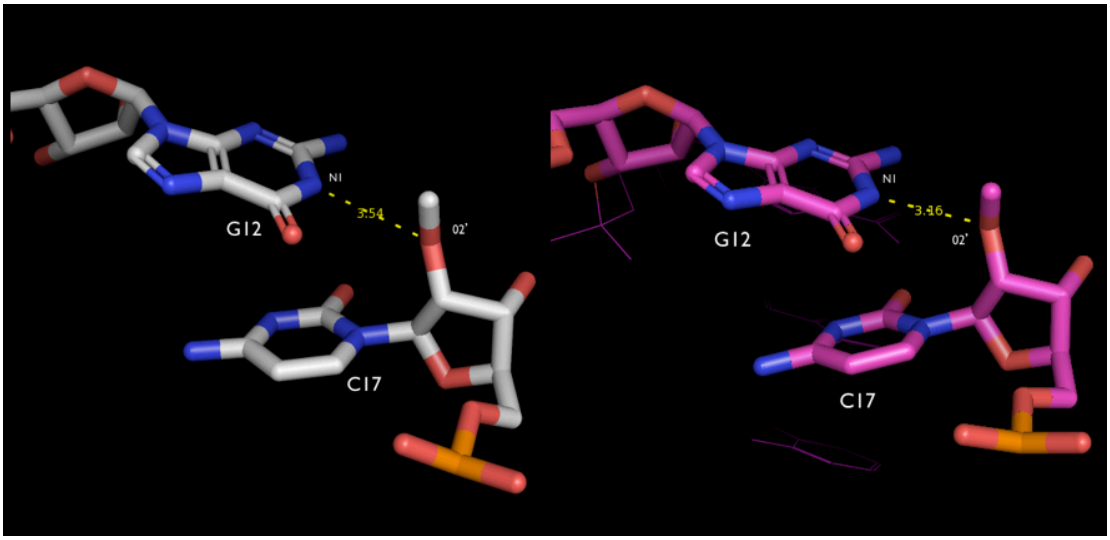

Figure 3.12 Approach of 2'OH of C17 and N1 of G12 to hydrogen bonding distance in the high-resolution structure. Magenta = High-res, White= 2006 structure.

3.3.2b General Acid Catalysis, and the Critical G8:C3 Base Pair

Mutation experiments suggest that G8 and C3 are critical for catalytic activity, yet the precise role of each residue was not clear from the minimal hammerhead structure (McKay 1996). In both the high-resolution and 2006 structures of the *Schistosome* hammerhead, the G8 & C3 pair to form an important component of the hydrogen bond network stabilizing the active conformation (Martick and Scott 2006). These solution structures support a model in which both minimal and full-length hammerheads partition between two folds- an inactive state similar to the minimal structure and an active fold characterized by interactions between nucleobases G8 and C3. Because we know that the full-length molecule exhibits a 500-fold enhanced

forward rate over the minimal ribozyme, the minimal hammerhead is likely to adopt the G8-C3 pair only transiently (~1% of the time).

Previous biochemical analyses (Han and Burke, 2005) have implicated G8 as a general acid in the hammerhead ribozyme cleavage reaction. These experiments suggested a model where a proton on the N1 of G8 is labile and can be donated to the 5'-oxygen leaving group in the cleavage reaction as it is displaced from the scissile phosphate. However, in the original and now the high-resolution crystal structure, the base of G8 is paired with C3, and it is the 2'-OH of G8 that is observed to hydrogen bond (3.18 A in Mg^{2+}-free, 3.51 A in Mg^{2+}-bound structures) to the 5'-O leaving group. The Mn^{2+}-bound and Mg^{2+}-bound structures are in near-perfect agreement with respect to the Mg^{2+}-ion bound at site 2.

If G8 functions as a general acid in the cleavage reaction, either it must break its pairing with C3 and reorient toward the leaving group, or it is the 2'-OH of G8 that is the relevant functional group in acid catalysis. To test between these hypotheses in previous studies, the base pair can be switched to C8 and G3. Indeed, it was observed that the G8C + C3G double mutant (k_{obs} = 0.22 min-1 at pH 7.5) rescues the deleterious effects of the single G8C mutation (k_{obs} < 0.0001 at pH 7.5), demonstrating that the base pair, when reestablished, restores catalysis and that it is not the endocyclic nitrogen but the 2'-OH of G8 that is the relevant participant in proton transfer (Lee 2008). Thus, our findings reinforce a catalytic model in which G8 and C3 form a critical base pair in the active core, positioning the 2'OH of G8 to act as a general acid in the hammerhead cleavage reaction.

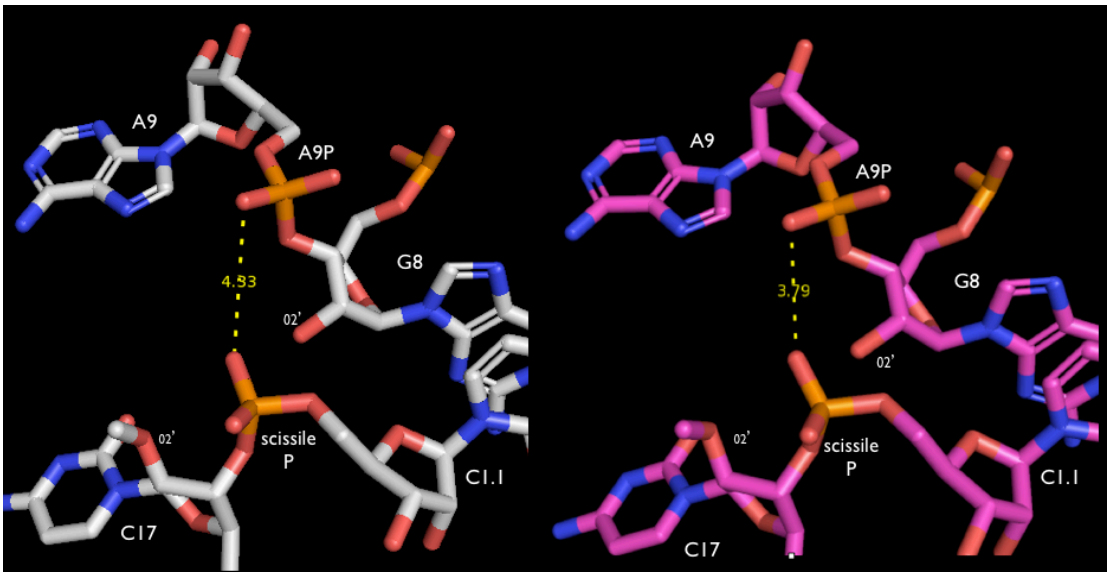

Figure 3.13 Approach of A9P and scissile phosphate is ~.5 A closer in the full-length hammerhead. Magenta = High-res, White= 2006 structure.

3.3.3 Mg^{2+} Sites in Partial Agreement with Reactant-state MD Simulations

The positioning of the three Mg^{2+} binding sites is also consistent with recent reactant-state simulation of the hammerhead predicting the presence of Mg^{2+} binding sites. In nearly all such simulations, the Mg^{2+} localizes near A9 and N7 of G10.1. These observations are consistent with the the minimal structure, the Mn^{2+}-bound structure and our high-resolution structure where a Mg(H20)42+ site is found to be bound directly to the pro-R oxygen of A9 and N7 of G10.1.

However, twelve separate molecular dynamics (MD) simulations of the reactant state (with and without a Mg^{2+} ion), in addition to early and late transition

state mimics, support a model in which a divalent ion *bridges* the A9 and scissile phosphates (Lee 2008; Lee 2007). Our results demonstrate that the Mg^{2+} binding site *does not* bridge the A9 and scissile phosphates, despite their close approach (3.79 A). Instead, the binding site coordinates the N7 of G10.1 with a nonbridging phosphate oxygen at A9.

While a Mg^{2+} spends significant time associated with the 2'OH of G8 in all twelve aforementioned MD simulations, only in the "early" and "late" transition-state (TS) simulations does the Mg^{2+} ion position closer to the leaving group oxygen (Lee 2007). However, no Mg^{2+} ions were observed in the original full-length crystal structure under nonphysiological monovalent salt (~1 M NH4+) and physiological divalent (1 mM Mg^{2+}) concentrations. Here, the Mg^{2+} metal ion bound in site 2 comports with "early" and "late" modeled MD simulations, binding in close proximity (~2.5 A) of the leaving group oxygen. As discussed above, thio/rescue effect experiments have also suggested that a single metal bound at the P9/G10.1 site interacts with the scissile phosphate during formation of the TS. The occupation of the P9/G10.1 site with Mg(II) in our structure, in addition to these findings, suggest that a divalent ion interacts with the 2'OH of G8 in "early" conformational states, and in "late" states the G8 2'OH is hydrogen bonded to the leaving group and oriented in an ideal conformation to act as a general acid catalyst. Thus, MD simulations largely comport with our recent crystallographic and previous biochemical data.

3.3.4 Close Agreement of 2012 and 2006 Structures Reinforces Relevance of Intermediate Structures

The crystallographic observation of various trapped reaction intermediates shows that the hammerhead can undergo significant conformational changes, yet raises the question of whether those changes represent on-pathway structures. Given the divergent orientation of conserved functional residues near the active core in "trapped" intermediate hammerhead crystal structures, the possibility remains that these structures resulted from alteration of local conformational dynamics rather than relevant on-pathway conformations (Bravo 1999). These intermediates include an uncleaved hammerhead in close agreement with the G8-A13 "inactive" fold, the secondary structure of an "early" conformational intermediate, and a "later" intermediate captured by the creation of a "kinetic bottleneck" at the bond-breaking point along the reaction pathway (Bolduc 1995; Moffat and Henderson 1995). The later ribozyme incorporated an unaltered nucleophile and a leaving group that prevents cleavage (Beigelman 1995).

The high activation energy (~20 kcal mol^{-1}) for hammerhead catalysis contributes to this view, because trapping a conformation near the transition state under such conditions would be very difficult. This view was also reinforced by the crystal structure of a helical tether displaying a *decreased* cleavage rate in the crystal lattice relative to cleavage of the unmodified form of the crystal (Dunham 2003). If

this structure truly represented a catalytic intermediate, one would expect this rate to *increase*. Finally, the fact that all known crystal structures of the hammerhead up to this point adhered to a identical unit cell and space group, suggested that the observed conformations may be significantly impacted by the energetic preference for this particular crystalline form.

The active site represented in the 2006 full-length structure may therefore represented a subset of conformations captured only upon crystallization under the specific conditions employed, rather than a long-lived ground state structure. Small chemical or ionic changes could alter this structure in a manner unrelated to the catalytic mechanism. In our study, however, the revelation of a high-resolution structure in very close agreement with the 2006 structure and Mn^{2+}-bound structure undermines this view. Our structure most closely resembles the in-line "later" intermediate structure, with the exocyclic G5 and G6 functional groups oriented toward the ribose, and the cleavage base C17 oriented at a right angle to their plane. As in the original full-length structure, this orientation of the cleavage base appears to be the result of a conformational change in the scissile phosphate, which rotates out of its helical position in the "early" and "inactive" structures (Sigurdsson 1995). Furthermore, a significant change in divalent ion concentrations (1 mM to 10 mM Mg^{2+}) did *not* substantially alter the the Mg^{2+}-bound structure, strengthening the contention that the observed positioning of conserved nucleotides is relevant to the catalytic mechanism. The high-resolution structure therefore validated the predicted reaction pathway derived from "early" and "late" trapped conformational

intermediates, undermining the view that the natural hammerhead crystal structure represented a subset of conformations unrelated to the catalytic mechanism.

3.3.5 A Compact Mg^{2+}-bound Structure

Crosslinking studies tethering G5 and helix III suggested that hammerheads containing tertiary contacts exhibit a more compact structure of the hammerhead (Han 2005). They also revealed that increasing concentrations of magnesium ions also bring helix I closer in space to helix II. The high-resolution structure reported here agrees with these findings, exhibiting close packing of stems I and II in the presence of elevated Mg^{2+} concentrations relative to the 2006 structure (10 mM v. 1 mM Mg^{2+}).

Corroborating these findings, EPR studies demonstrated that a bound Mn^{2+} is displaced from the minimal hammerhead upon binding of neomycin B, but not from full-length hammerhead constructs (Kisselva 2005). As the primary difference between these subjects is the presence of two interacting external loops, the suggestion was advanced that the full-length fold traps Mn^{2+} in a tightly bound conformation. The stability of this tightly-bound conformation can reasonably be said to have resulted in the highly-ordered, high-resolution structure in the present case (1.55 A resolution). While generic charge stabilization in the previous full-length crystal structure may have been sufficient to enable formation of the active conformation, it is probably less ordered than the present structure due to the absence of bound Mg^{2+} (Martick and Scott 2006).

Solution FRET studies analyzing the effects of various metal ions on global folding suggest that the identity of the divalent metal (whether Ca2+, Mg^{2+}, Mn^{2+}, or Sr2+), has little effect on the global folding of the *Schistosoma* hammerhead, indicating these folding effects may be generalizable (Pardi 2008). The Figure below shows a surface map of the superimposed 2006 and 2012 high-resolution structures. The predominance of orange coloring (representing the 2006 structure) indicates a more compact fold near stems I and II of the high-resolution structure (magenta surface density).

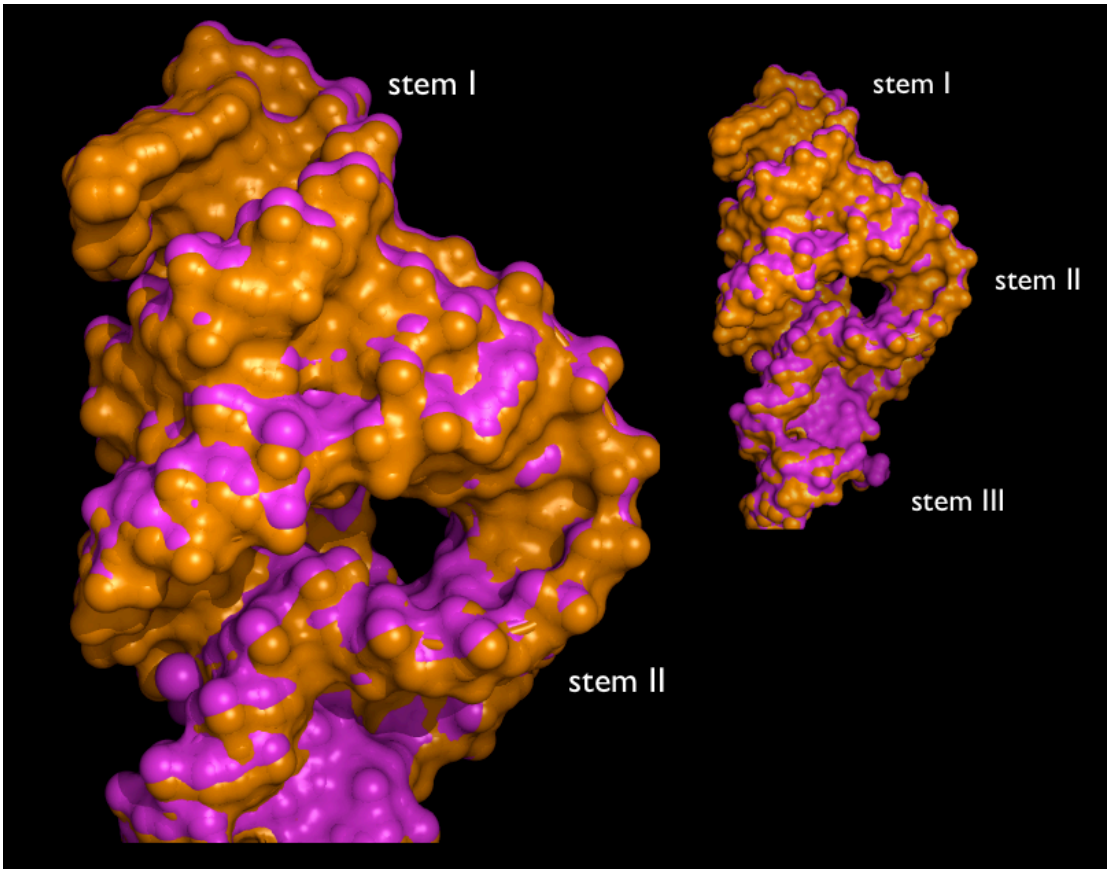

Figure 3.14 Close packing of stem I and II in the high-resolution structure (Surface map of the superimposed 2006 and 2012 high-resolution structures). The predominance of orange coloring (signifying the 2006 structure) indicates a more compact fold near stems I and II of the high-resolution structure.

3.3.6 The Mg^{2+}-bound Structure Agrees with Previous Biochemical Experiments

Electron paramagnetic resonance (EPR) spectroscopy and FRET studies have been employed to study the effects of divalent mental binding in full-length hammerhead constructs (Edwards 2005; Lee 2007a). These findings are in close agreement with recent full-length structures which identify a Mg^{2+} and Mn^{2+}-binding site at the A9/G10.1 position in active core of the *Schistosoma* hammerhead. While the 2006 natural hammerhead crystal structure did not identify this divalent magnesium binding site, an elevated concentration of Mg^{2+} (10mM vs. 1 mM) employed in this study permitted observation of a peak in close agreement with these findings.

EPR studies were carried out in order to compare Mn^{2+} binding in minimal and full-length constructs (Kisseleva 2005). These measurements have suggested a single high-affinity binding site in both full-length and minimal hammerhead constructs, located between bases A9 and G10.1 of the sheared G:A tandem base pair. Notably, the K_D determined for the minimal site was two orders of magnitude smaller than that identified by continuous wave EPR measurements (K^D of < 10nM) in the full-length hammerhead. Neither dissociation constant changes upon decreasing the NaCl concentration. One explanation for high dissociation constant in the full-length molecule is that the positively charged ammonium groups of neomycin B cannot compete with Mn^{2+} in the context of a tight global fold.

The high-affinity Mn^{2+} site was also found to be displaced from the minimal hammerhead upon binding of neomycin B, but not from full-length hammerhead constructs (Schiemann 2003). As the primary difference between the minimal and full-length structures is two interacting external loops, a model in which the full-length hammerhead traps a Mn^{2+} in a tightly bound conformation was reinforced.

In line with EPR experiments, the extended ribozyme folds at lower concentrations of Mg^{2+} as compared to the minimal hammerhead (Penedo 2004; Kim 2005). FRET studies of noncleavable hammerheads also indicate accelerated rates of cleavage at elevated Mg^{2+} concentrations (Pardi 2008). Taken together, these results indicate that the loop-loop interactions dramatically increase the affinity for binding of a divalent metal, with affinities near the A9/G10.1 site that suggest a highly optimized metal-binding site.

The suggestion that the full-length ribozyme active site possesses a single high-affinity divalent metal binding site that is much weaker in the minimal also parallels the observation that the full-length hammerhead is catalytically active at physiological salt concentrations whereas the the minimal is not (Khvorova 2003). The lowered ionic strength of the buffer conditions likely facilitates magnesium binding as points of negative charge in the ribozyme are no longer screened by monovalent ions.

Evidence from recent single molecule FRET studies of the *Schistosomal* hammerhead maintaining the putative A9/G10.1 divalent binding site similarly impute an important role for divalent metals near the active core (Mcdowell 2010).

This study compared hammerhead variants with wild-type, partially disrupted, and fully disrupted loop-loop interaction sequences, finding that undisturbed natural tertiary interactions lead to dynamic motional sampling in the presence of increasing concentrations of Mg^{2+}. As in bulk FRET studies, increased concentrations of Mg^{2+} led to enhanced catalytic activity (Murray 2000).

The observation of magnesium bound between bases A9 and G10.1 in the present study aligns with these observations. In the Mg^{2+} bound structure, the nucleophillic 2‘oxygen is brought within 3.2 A of the scissile phosphorus due to steric repulsion This subtle shift of the active core reinforces EPR and FRET experiments that suggest the presence of a divalent metal at the A9/G10.1 position is correlated with enhanced catalytic activity. Given that in the presence of Mg^{2+}, N1 of G12 is now within hydrogen bonding distance of the 2‘OH of C17 and that the global structure of the molecule exhibits a very compact fold, we can extrapolate that the enhanced activity is likely due to improved folding rather than direct participation in catalysis. This contention is supported by the finding that the bound metal does not bridge the A9 and scissile phosphates, but maintains a distance of ~6 A from the active site. Thus, the new high-resolution structure verifies the presence of a bound divalent metal in the active core of the *Schistosoma* hammerhead, as predicted by several structural and biochemical studies.

3.3.7 High-resolution Structure Reveals Novel Tertiary Interactions

Interactions loops 1 and 2 of the hammerhead ribozyme (Figure 1.1) increases the catalytic activity of the hammerhead ribozyme. Crystal structures of *Schistosoma mansoni* and tobacco ring spot virus satellite RNA (sTRSV) provide important information regarding how major grooves of loops 1 and 2 contact each other (Khvorova 2003). Mutations that disrupt the structures or change key nucleotides in the loop-loop contacts have a strong effect on both catalytic activity *in vitro* and viroid replication *in vivo*. Together with structural comparisons, mutagenesis data indicates that the three-dimensional structures of loops 1 and 2 are conserved, giving rise to a tertiary interaction motif that is likely shared by a significant franction of natural hammerheads despite relatively weak sequence conservation (Gago 2005; Dufour 2009).

Indeed, the only structural feature shared by all known hammerheads is the presence of a conserved AU Hoosteen pair bewtween A(L6) and U(1.7) (Wedekind 1998). A(L6) is the final A in the sequence of the GNRA-like tetraloop capping Stem II. In both the sTRSV and high-resolution hammerhead tertiary contact, the structure of the GNRA tetraloop rearranges relative to the minimal structure so that the A forms a Hoogsteen base pair with U1.7 (Nelson 2005). However, the new high-resolution structure reveals a novel interaction of the R residue directly adjacent to the A which may serve to stabilize the conserved tertiary interaction. In the original full-length structure, N3 of U(L5) was too distant from the A(L3) base to form a hydrogen bond

(3.84 A), but in the high resolution structure a base angle rotation of U(L5) brings the proton of N3 within hydrogen bonding distance of N3 of A(L3) (3.03 A), likely forming a hydrogen bond. In addition, the rotation brings the exocyclic O6 of U(L5) within hydrogen bonding distance of the N6 of A(L6) where these atoms were could not form a bond in previsous structure (3.45 v. 3.85 A).

This new orientation of the stem I/stem II interface is significant as it may have unveiled a sensitive regulatory switch modulating interaction of the highly conserved A(L6) and U(1.7) groups (Figure 3.16). This "switch" may turn the hammerhead ribozyme from the inactive to the active state. Mutations that disrupt this switch are predicted to have strong effects on the catalytic activity of the ribozyme *in vitro* and likely on the infectivity of hammerhead-containing viroid *in vivo.* In addition, the agreement between the high-resolution and 2006 structures with respect to the interaction between A(L5) and U(1.7) also reinforces that this interaction is highly conserved in nature. That the A(L6): U(1.7) interaction remains unperturbed despite this point of flexibility at U(L5) also highlights its identification as a conserved tertiary interaction.

Considering the emergence of several pathogenic hammerhead subjects, this novel interactions may serve as an important drug target in the future (Flores 2005). Given the crucial link between teritary contact formation and catalysis, in addition to the fact that this interaction represents the *only* conserved tertiary interaction among all known hammerheads, the new U(L5)/A(L6) interaction serves as an appropriate target for small molecule, mAb, or RNA antisense inhibitors.

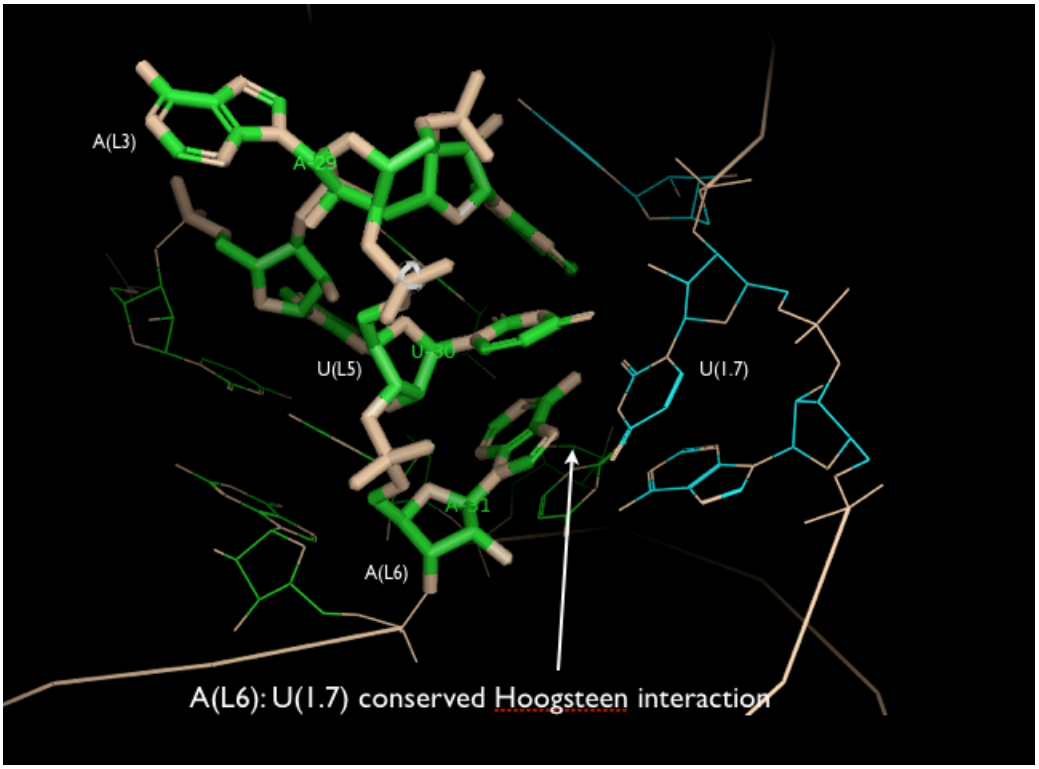

Figure 3.15 Bond angle rotation of U(L5) stabilizes the highly conserved Hoogstein interaction between A(L6) and U(1.7).

3.3.8 High-resolution Structure Resolves Disagreements Between Biochemical and Structural Data

3.3.8a Clarifying Functional Roles of the 13 Conserved Nucleotides

Substitution of any of the 13 core conserved residues was known by 1996 to significantly abrogate cleavage (McKay 1996). Similar to solution studies introducing abasic nucleotides in the conserved core of the minimal hammerhead, mutation of any of the 13 conserved core residues of the *Schistosoma* hammerhead results in large decreases in the extent of catalysis. The effects of these mutations are independent of temperature or the addition of polyamines, in contrast to the effects observed with protein enzymes and large ribozymes.

The pronounced sensitivity of the hammerhead to structural perturbation contrasted sharply with the behavior of protein enzymes and large ribozymes. (Peracchi 1996). In proteins, mutation within a small subset of 'catalytic' residues typically yield a large decrease in activity. This disparity is likely attributable to the fact that a small RNA catalyst like the hammerhead lacks the structural redundancy present in protein enzymes of similar molecular mass. For example, RNase T1 has a comparable molecular mass to that of the ribozyme (~11 v. ~10 kDa for a minimal hammerhead) and also catalyzes a phosphodiester cleavage reaction identical to the hammerhead. Of the 20 different mutations characterized near the active site of the

enzyme, only two positions decreased K_{cat} by more than 100-fold. Similarly, mutations at only two positions in cytosolic gultathione S-transferase (17 kDa) produced decreases in K_{cat} of >100-fold.

In comparison, 23 of 33 mutants in a previous hammerhead study displayed activity decreases of >100-fold (Blount and Uhlenbeck, 2005). The functional significance of mutations at positions G8, G5, C3 and G12 were particularly contentious, as numerous studies suggested a catalytic role for these nucleotides despite conflicting structural data. Indeed, mutation of each were found to decrease K_{cat} by $>10^3$-fold, despite being entirely solvent exposed in the crystal structure and/ or displaying nonfunctional positions in the active core (Martick and Scott 2006). Reexamination of these disparities in light of the high-resolution *Schistosoma* confirms their previously predicted roles in structure stabilization, folding and catalysis.

In the high-resolution structure, both the 2'-hydroxyl and G5 form part of the network of hydrogen bonds stabilizing the rearranged core. Disruption of this network could reasonably be expected to abrogate cleavage & ligation activity. Furthermore, the 2'-hydroxyl group of G8 and the hydrogen bonding face of G12 are positioned near the scissile phosphate in the full-length structure. This positioning suggests that both of these elements facilitate proton transfer in support of cleavage of the substrate strand. This model agrees with findings that derivatives of G8 or G12 with altered pKas change the pH dependence of the ribozyme (Han and Burke, 2005).

However, it is difficult to ascertain whether such modifications disrupt catalysis by preventing proton transfer or by altering the functional fold of the molecule.

Nevertheless, the high-resolution structure reinforces the finding that that 13 conserved residues in the high-resolution structure form a single cooperative network of hydrogen bonds. Mutation or even minor structural variation of these residues can be expected to substantially dampen the forward rate of cleavage, in agreement with previous biochemical findings. While the active conformation may be populated only transiently, its stable isolation under divergent divalent ion concentrations in the 2006 and high-resolution full-length structures also makes the catalytic mechanism of the hammerhead more clear. Nearly identical positioning of G8, G12, C17 and the other ultra-conserved residues in both structures solidifies their predicted functional roles.

3.3.8b Conformational Isomerization

A number of disagreements between the structural and functional data resulted in a debate regarding the extent of conformational isomerization of the full-length molecule in solution. While there exists a relative paucity of structure-function experiments conducted on the *Schistosome* hammerhead itself, one may assume that the large corpus of data assessing the kinetics of minimal hammerheads is applicable to the full-length molecule, as they necessarily share the same cleavage mechanism.

Structural data have suggested that hammerhead conformational changes are rather limited (Han 2005; Edwards 2005). For example, the conformations of freeze-

trapped hammerhead intermediates showed only modest structural changes in near the active core in metal ion-free structures (Table 3.1) (Bravo 1999). The addition of Mg^{2+} results in only a slight translation of C17 out of the CUGA turn and a modest rotation of the scissile phosphate in the active core. Furthermore, the finding that the hammerhead is capable of cleaving within the crystalline lattice suggested that large-scale structural changes were not required in order for the molecule to assume the active conformation. The rate of cleavage in the crystal was in fact fivefold faster than the same molecule in solution. Indeed, a large body of work implied the presence of very limited structural changes distal to the cleavage site, despite numerous conserved residues that were presumably peripheral to the active site.

Biochemical data suggest extensive conformational isomerization of the ribozyme, in stark contrast to structural experiments. Metal ion rescue experiments employing phosphorthioate substitutions at A9 and the scissile phosphate suggested that the two domains interact closely with one another during the transition state, coordinating the same divalent metal despite a 20 Å separation in the minimal crystal structure (Maderia 2000). Consistent with a model involving close approach of stems I and II, a hydroxy-radical footprinting experiment suggested a compact structure at moderate divalent ion concentrations (<10 mM) (Han 2005). Crosslinking experiments demonstrating cleavage capacity despite the linkage of two distal residues separated by 40 Å also support a model in which helices I and II undergo significant conformation isomerization in solution (Heckman 2005). In these experiments, crosslinking of G8 and G12 residues of the minimal hammerhead

suggested that the functionally important nucleobase G5 can interact with two different sites in the hammerhead. The first is the cleavage site. The second site is the distal segment of helix III; approximately 10 Å distant from G5 in the minimal crystal structure. These results implicate a high degree of conformational flexibility for the molecule to sample a wide range of conformational space. Finally, the revelation that the loops of stems I and II interact in most naturally occurring hammerheads contrasts with suggestions that conformational isomerization is limited in minimal hammerheads.

The high-resolution crystal structure reported here displays significant unwinding of stem I relative to the minimal structure, and a more compact structure. This suggests that the conformational change during cleavage must be different than that seen in the original crystal structures of minimal and likely involves a close interaction of domains 1 and 2 within the core. In both tertiary-stabilized hammerheads, interactions between loops I and II drastically enhance the forward rate. In addition, a significant structural rearrangement observed in both the 2006 and high-resolution crystal structures involves the approach of the phosphate at position P9 to within 4 A˚of the cleavage site phosphate P1.1. This positioning of the two phosphates, predicted by phosphorothioate experiments, provides very strong support for a dynamic isomerization model (Hunsicker 2000). Indeed, these phosphates are separated by 20A˚in the minimal hammerhead, suggesting the requirement for a major underwinding of stem I to achieve rearrangement in the active conformation. Thus, the high-resolution structure of the *Schitosoma* hammerhead reinforces the

notion that substantial conformational isomerization is required to achieved the active conformation. This finding aligns with a substantial body of biochemical evidence and comports with the notion that natural tertiary contacts may enhance conformational dynamics.

3.3.9 Conclusion

The hammerhead is an ideal system to study RNA catalysis. An deep understanding of the hammerhead mechanism and the role of divalent ion binding sites may facilitate understanding more complex RNA machinery such as the ribosome, and ultimately may assist in the design of new medical therapies. An expanding repertoire of therapeutic antisense hammerhead agents and the emergence of several pathogenic hammerhead ribozymes raises the issue of what role divalent metal play in the structure of the full-length hammerhead at ion concentrations that more closely resemble physiological conditions.

Our report details the highest-resolution structure of any reported hammerhead ribozyme to date (1.55 A resolution). With this improved resolution, new local rearrangements and hydrogen bonding interactions within the loop/bulge region are clear. In addition, the new structure demonstrates that a divalent metal ion does indeed occupy the A9/G10.1, in addition to two peripheral sites in Stem I and III.

Given the stability of the tertiary conformation, in addition to the proximity of the A9 and scissile phosphate oxygens in full-length hammerhead crystal structures, a bridging coordination mode between the A9 and scissile phosphates appeared plausible given in the ground state of these structures. However, previous crystallographic models locate a divalent ion only in the nearby P9/G10.1 coordination site (Martick 2008), or at least not strongly localized in the case of Mg^{2+} (Martick and Scott, 2006; Chie 2008). In strong agreement, the data presented in this report supports a ground-state metal coordination to the P9/G10.1 coordination site, suggesting an indirect catalytic role of divalent metals bound in the active core.

Crystal soaking experiments were not able to detect a metal ion at site 2 in the 2006 structure. Its present identification suggests that a divalent metal may stabilize global folding of the hammerhead and provide charge neutralization during the cleavage reaction. Finally, the high-resolution structure confirms the large-scale conformational changes observed in the 2006 structure. The observation of these global changes aids in the resolution of several disagreements between biochemical and structural data.

3.4 Experimental Methods

3.4.1 Reaction Conditions

RNA oligos were purchased from Dharmacon, and 2'-protecting groups were removed by incubation in 100mM acetic acid adjusted to pH 3.8 with TEMED. Crystals grew in hanging-drop vapor diffusion plates using RNA concenrations of 8-10 mg/mL and previsouly reported conditions. Reservoir conditions were identical to those previously reported in the 2OEU structure, except Mg^{2+} at 10 mM MgCl2 was subsituted for Mn 2+, and pH was maintained at 5.5. Additional salts included 100 mM MES (pH 6.5) and 0.5 M (NH4)2SO4. The data analyzed in this work displays unusually high resolution (1.55 A) relative to current PDB depositions of RNA structures. The full-length motif was based upon a well-characterized sequence from the *Schistosoma* hammerhead (Canny *et al,* 2004; Khvorova *et al.,* 2003). The sequence was divided into separate enzyme and substrate strands similar to those previously published (Khvorova et al., 2003). The complex was formed by incubating the mixture at 95C for 2 min., at 65C for 2 min., and finally at 27C for 5 min. The enzyme strand was in vitro transcribed from a DNA template containing a double-stranded T7 polymerase promoter. The enzyme DNA template, as well as the substrate RNA, was synthesized using an Expedite 8900. Five base-pair switches were engineered in non-essential regions to facilitate crystallization. The substrate strand contains a 2'-OMe C-17 at the active site to prevent cleavage.

The full-length *Schistosoma* hammerhead ribozyme formed monoclinic (C2) crystals having one molecule per asymmetric unit. An Br-phased 2.0 MAD map permitted tracing of the molecule prior to refinement. The crystal lattice is stabilized by stacking interactions between helical ends of the molecules, van der Waals interactions between adjacent helices, and two intermolecular nucleotide interactions described below. We assigned hydrogen bonds to donor and acceptor atoms separated by less than 3.5 Å that obeyed the angular criteria of Baker and Hubbard.

References

1. Aggarwal A, Rudnick J, Bruinsma RF, Klug WS. Elasticity theory of macromolecular aggregates. Phys Rev Lett 2012, Oct 5;109(14):148102.

2. Amiri KM, Hagerman PJ. Global conformation of a self-cleaving hammerhead RNA. Biochemistry 1994, Nov 15;33(45):13172-7.

3. Astrachan L, Volkin E. The absence of ribonucleic acid in bacteriophage t2r+. Virology 1956, Oct;2(5):594-8.

4. Bassi GS, Møllegaard NE, Murchie AI, Lilley DM. RNA folding and misfolding of the hammerhead ribozyme. Biochemistry 1999, Mar 16;38(11):3345-54.

6. Beaudry D, Busière F, Lareau F, Lessard C, Perreault JP. The RNA of both polarities of the peach latent mosaic viroid self-cleaves in vitro solely by single hammerhead structures. Nucleic Acids Res 1995, Mar 11;23(5):745-52.

7. Benyo B, Biro JC, Benyo Z. Codes in the codons: Construction of a codon/amino acid periodic table and a study of the nature of specific nucleic acid-protein interactions. Conf Proc IEEE Eng Med Biol Soc 2004;4:2860-3.

8. Blount KF, Uhlenbeck OC. Internal equilibrium of the hammerhead ribozyme is altered by the length of certain covalent cross-links. Biochemistry 2002, May 28;41(21):6834-41.

9. Bokinsky G, Rueda D, Misra VK, Rhodes MM, Gordus A, Babcock HP, et al. Single-molecule transition-state analysis of RNA folding. Proc Natl Acad Sci U S A 2003, Aug 5;100(16):9302-7.

10. Bokinsky G, Zhuang X. Single-molecule RNA folding. Acc Chem Res 2005, Jul; 38(7):566-73.

11. Brázda V, Laister RC, Jagelská EB, Arrowsmith C. Cruciform structures are a common DNA feature important for regulating biological processes. BMC Mol Biol 2011;12:33.

12. Breaker RR. Riboswitches and the RNA world. Cold Spring Harb Perspect Biol 2012, Feb;4(2).

13. Bryant Z, Oberstrass FC, Basu A. Recent developments in single-molecule DNA mechanics. Curr Opin Struct Biol 2012, Jun;22(3):304-12.

14. Burke JM. Hairpin and hammerhead ribozymes: How different are they? Biochem Soc Trans 2002, Nov;30(Pt 6):1115-8.

15. Buzayan JM, Hampel A, Bruening G. Nucleotide sequence and newly formed phosphodiester bond of spontaneously ligated satellite tobacco ringspot virus RNA. Nucleic Acids Res 1986, Dec 22;14(24):9729-43.

16. Canny MD, Jucker FM, Kellogg E, Khvorova A, Jayasena SD, Pardi A. Fast cleavage kinetics of a natural hammerhead ribozyme. J Am Chem Soc 2004, Sep 8;126(35):10848-9.

17. Charvin G, Bensimon D, Croquette V. Single-molecule study of DNA unlinking by eukaryotic and prokaryotic type-ii topoisomerases. Proc Natl Acad Sci U S A 2003, Aug 19;100(17):9820-5.

19. Clouet-d'Orval B, Uhlenbeck OC. Hammerhead ribozymes with a faster cleavage rate. Biochemistry 1997, Jul 29;36(30):9087-92.

20. Crick FH. The origin of the genetic code. J Mol Biol 1968, Dec;38(3):367-79.

21. Crouse GF, Fodor EJ, Doty P. The specificity of in vitro chromatin transcription. Nucleic Acids Res 1979, Jan;6(1):371-83.

22. Curtis EA, Bartel DP. The hammerhead cleavage reaction in monovalent cations. RNA 2001, Apr;7(4):546-52.

24. Dahm SC, Derrick WB, Uhlenbeck OC. Evidence for the role of solvated metal hydroxide in the hammerhead cleavage mechanism. Biochemistry 1993, Dec 7;32(48):13040-5.

25. de la Peña M, García-Robles I. Ubiquitous presence of the hammerhead ribozyme motif along the tree of life. RNA 2010, Oct;16(10):1943-50.

26. De Vlaminck I, Dekker C. Recent advances in magnetic tweezers. Annu Rev Biophys 2012;41:453-72.

27. De Vlaminck I, van Loenhout MT, Zweifel L, den Blanken J, Hooning K, Hage S, et al. Mechanism of homology recognition in DNA recombination from dual-molecule experiments. Mol Cell 2012, Jun 8;46(5):616-24.

28. De Vlaminck I, Henighan T, van Loenhout MT, Burnham DR, Dekker C. Magnetic forces and DNA mechanics in multiplexed magnetic tweezers. PLoS One 2012;7(8):e41432.

29. Ditzler MA, Rueda D, Mo J, Håkansson K, Walter NG. A rugged free energy landscape separates multiple functional RNA folds throughout denaturation. Nucleic Acids Res 2008, Dec;36(22):7088-99.

30. Doherty EA, Doudna JA. Ribozyme structures and mechanisms. Annu Rev Biochem 2000;69:597-615.

31. Duckett DR, Murchie AI, Clegg RM, Bassi GS, Giraud-Panis MJ, Lilley DM. Nucleic acid structure and recognition. Biophys Chem 1997, Oct;68(1-3):53-62.

32. Epstein LM, Gall JG. Transcripts of newt satellite DNA self-cleave in vitro. Cold Spring Harb Symp Quant Biol 1987;52:261-5.

33. Falaschi A, Abdurashidova G. Molecular mechanics and DNA replication regulation. HFSP J 2007, Nov;1(4):215-9.

34. Ferguson A, Boomer RM, Kurz M, Keene SC, Diener JL, Keefe AD, et al. A novel strategy for selection of allosteric ribozymes yields riboreporter sensors for caffeine and aspartame. Nucleic Acids Res 2004;32(5):1756-66.

35. Garrett TA, Pabón-Peña LM, Gokaldas N, Epstein LM. Novel requirements in peripheral structures of the extended satellite 2 hammerhead. RNA 1996, Jul;2(7): 699-706.

36. Gosse C, Croquette V. Magnetic tweezers: Micromanipulation and force measurement at the molecular level. Biophys J 2002, Jun;82(6):3314-29.

37. Greenfeld M, Solomatin SV, Herschlag D. Removal of covalent heterogeneity reveals simple folding behavior for P4-P6 RNA. J Biol Chem 2011, Jun 3;286(22): 19872-9.

38. Guerrier-Takada C, Gardiner K, Marsh T, Pace N, Altman S. The RNA moiety of ribonuclease P is the catalytic subunit of the enzyme. Cell 1983, Dec;35(3 Pt 2): 849-57.

39. Hammann C, Lilley DM. Folding and activity of the hammerhead ribozyme. Chembiochem 2002, Aug 2;3(8):690-700.

40. Han J, Burke JM. Model for general acid-base catalysis by the hammerhead ribozyme: PH-activity relationships of G8 and G12 variants at the putative active site. Biochemistry 2005, May 31;44(21):7864-70.

41. Hartig JS, Famulok M. Screening of molecular interactions using reporter hammerhead ribozymes. Methods Mol Biol 2008;429:251-63.

42. Heus HA, Pardi A. Structural features that give rise to the unusual stability of RNA hairpins containing GNRA loops. Science 1991, Jul 12;253(5016):191-4.

43. Hirose T, Shu MD, Steitz JA. Splicing-dependent and -independent modes of assembly for intron-encoded box C/D snornps in mammalian cells. Mol Cell 2003, Jul;12(1):113-23.

44. Hutchins CJ, Rathjen PD, Forster AC, Symons RH. Self-cleavage of plus and minus RNA transcripts of avocado sunblotch viroid. Nucleic Acids Res 1986, May 12;14(9):3627-40.

45. Jeon JH, Adamcik J, Dietler G, Metzler R. Supercoiling induces denaturation bubbles in circular DNA. Phys Rev Lett 2010, Nov 12;105(20):208101.

46. Kauert DJ, Kurth T, Liedl T, Seidel R. Direct mechanical measurements reveal the material properties of three-dimensional DNA origami. Nano Lett 2011, Dec 14;11(12):5558-63.

47. Khvorova A, Lescoute A, Westhof E, Jayasena SD. Sequence elements outside the hammerhead ribozyme catalytic core enable intracellular activity. Nat Struct Biol 2003, Sep;10(9):708-12.

48. Kim NK, Murali A, DeRose VJ. Separate metal requirements for loop interactions and catalysis in the extended hammerhead ribozyme. J Am Chem Soc 2005, Oct 19;127(41):14134-5.

49. Koizumi M, Ozawa Y, Yagi R, Nishigaki T, Kaneko M, Oka S, et al. Design and anti-hiv-1 activity of ribozymes that cleave HIV-1 LTR. Nucleic Acids Symp Ser 1995(34):125-6.

50. Kruger K, Grabowski PJ, Zaug AJ, Sands J, Gottschling DE, Cech TR. Self-splicing RNA: Autoexcision and autocyclization of the ribosomal RNA intervening sequence of tetrahymena. Cell 1982, Nov;31(1):147-57.

51. Kulczyk AW, Tanner NA, Loparo JJ, Richardson CC, van Oijen AM. Direct observation of enzymes replicating DNA using a single-molecule DNA stretching assay. J Vis Exp 2010(37).

52. Leclerc F. Hammerhead ribozymes: True metal or nucleobase catalysis? Where is the catalytic power from? Molecules 2010, Aug;15(8):5389-407.

53. Li PT, Bustamante C, Tinoco I. Real-time control of the energy landscape by force directs the folding of RNA molecules. Proc Natl Acad Sci U S A 2007, Apr 24;104(17):7039-44.

54. Li W, Sun ZQ, Xie P, Dou SX, Wang WC, Wang PY. Elastic response and length change of single DNA molecules induced by a combination of cisplatin and transplatin. Phys Rev E Stat Nonlin Soft Matter Phys 2012, Feb;85(2-1):021918.

55. Lionnet T, Allemand JF, Revyakin A, Strick TR, Saleh OA, Bensimon D, Croquette V. Magnetic trap construction. Cold Spring Harb Protoc 2012, Jan;2012(1): 133-8.

56. Lipfert J, Kerssemakers JJ, Rojer M, Dekker NH. A method to track rotational motion for use in single-molecule biophysics. Rev Sci Instrum 2011, Oct;82(10): 103707.

57. Markley JC, Godde F, Sigurdsson ST. Identification and characterization of a divalent metal ion-dependent cleavage site in the hammerhead ribozyme. Biochemistry 2001, Nov 20;40(46):13849-56.

58. Marko JF, Neukirch S. Competition between curls and plectonemes near the buckling transition of stretched supercoiled DNA. Phys Rev E Stat Nonlin Soft Matter Phys 2012, Jan;85(1-1):011908.

59. McDowell SE, Jun JM, Walter NG. Long-range tertiary interactions in single hammerhead ribozymes bias motional sampling toward catalytically active conformations. RNA 2010, Dec;16(12):2414-26.

60. McKay DB. Structure and function of the hammerhead ribozyme: An unfinished story. RNA 1996, May;2(5):395-403.

61. Mehraeen S, Spakowitz AJ. Intrinsic fluctuations lead to broad range of transduced forces in tethered-bead single-molecule experiments. Phys Rev E Stat Nonlin Soft Matter Phys 2012, Aug;86(2-1):021902.

62. Nash KL, Alexander GJ, Lever AM. Inhibition of hepatitis B virus by lentiviral vector delivered antisense RNA and hammerhead ribozymes. J Viral Hepat 2005, Jul; 12(4):346-56.

63. Neuman KC, Nagy A. Single-molecule force spectroscopy: Optical tweezers, magnetic tweezers and atomic force microscopy. Nat Methods 2008, Jun;5(6): 491-505.

64. Neuman KC. Single-molecule measurements of DNA topology and topoisomerases. J Biol Chem 2010, Jun 18;285(25):18967-71.

65. Nong EX, DeVience SJ, Herschbach D. Minimalist model for force-dependent DNA replication. Biophys J 2012, Feb 22;102(4):810-8.

66. O'Rear JL, Wang S, Feig AL, Beigelman L, Uhlenbeck OC, Herschlag D. Comparison of the hammerhead cleavage reactions stimulated by monovalent and divalent cations. RNA 2001, Apr;7(4):537-45.

68. Oddershede LB. Force probing of individual molecules inside the living cell is now a reality. Nat Chem Biol 2012, Nov;8(11):879-86.

69. Oliver PM, Park JS, Vezenov D. Quantitative high-resolution sensing of DNA hybridization using magnetic tweezers with evanescent illumination. Nanoscale 2011, Feb;3(2):581-91.

70. Orgel LE. Evolution of the genetic apparatus. J Mol Biol 1968, Dec;38(3):381-93.

71. Penedo JC, Wilson TJ, Jayasena SD, Khvorova A, Lilley DM. Folding of the natural hammerhead ribozyme is enhanced by interaction of auxiliary elements. RNA 2004, May;10(5):880-8.

72. Penedo JC, Wilson TJ, Jayasena SD, Khvorova A, Lilley DM. Folding of the natural hammerhead ribozyme is enhanced by interaction of auxiliary elements. RNA 2004, May;10(5):880-8.

73. Pereira MJ, Behera V, Walter NG. Nondenaturing purification of co-transcriptionally folded RNA avoids common folding heterogeneity. PLoS One 2010;5(9):e12953.

74. Pley HW, Flaherty KM, McKay DB. Three-dimensional structure of a hammerhead ribozyme. Nature 1994, Nov 3;372(6501):68-74.

75. Prody CA, Zevin-Sonkin D, Gnatt A, Goldberg O, Soreq H. Isolation and characterization of full-length cdna clones coding for cholinesterase from fetal human tissues. Proc Natl Acad Sci U S A 1987, Jun;84(11):3555-9.

76. Rios AC, Tor Y. Model systems: How chemical biologists study RNA. Curr Opin Chem Biol 2009, Dec;13(5-6):660-8.

77. Romero-López C, Díaz-González R, Barroso-delJesus A, Berzal-Herranz A. Inhibition of hepatitis C virus replication and internal ribosome entry site-dependent translation by an RNA molecule. J Gen Virol 2009, Jul;90(Pt 7):1659-69.

78. Rueda D, Wick K, McDowell SE, Walter NG. Diffusely bound mg2+ ions slightly reorient stems I and II of the hammerhead ribozyme to increase the probability of formation of the catalytic core. Biochemistry 2003, Aug 26;42(33):9924-36.

79. Salerno D, Tempestini A, Mai I, Brogioli D, Ziano R, Cassina V, Mantegazza F. Single-molecule study of the DNA denaturation phase transition in the force-torsion space. Phys Rev Lett 2012, Sep 14;109(11):118303.

80. Sarkar K, Meister K, Sethi A, Gruebele M. Fast folding of an RNA tetraloop on a rugged energy landscape detected by a stacking-sensitive probe. Biophys J 2009, Sep 2;97(5):1418-27.

81. Sawata S, Shimayama T, Komiyama M, Kumar PK, Nishikawa S, Taira K. Enhancement of the cleavage rates of dna-armed hammerhead ribozymes by various divalent metal ions. Nucleic Acids Res 1993, Dec 11;21(24):5656-60.

82. Schlingman DJ, Mack AH, Mochrie SG, Regan L. A new method for the covalent attachment of DNA to a surface for single-molecule studies. Colloids Surf B Biointerfaces 2011, Mar;83(1):91-5.

83. Schöpflin R, Brutzer H, Müller O, Seidel R, Wedemann G. Probing the elasticity of DNA on short length scales by modeling supercoiling under tension. Biophys J 2012, Jul 18;103(2):323-30.

84. Shcherbakova I, Mitra S, Laederach A, Brenowitz M. Energy barriers, pathways, and dynamics during folding of large, multidomain rnas. Curr Opin Chem Biol 2008, Dec;12(6):655-66.

85. Sheinin MY, Forth S, Marko JF, Wang MD. Underwound DNA under tension: Structure, elasticity, and sequence-dependent behaviors. Phys Rev Lett 2011, Sep 2;107(10):108102.

86. Stancik AL, Brauns EB. Rearrangement of partially ordered stacked conformations contributes to the rugged energy landscape of a small RNA hairpin. Biochemistry 2008, Oct 14;47(41):10834-40.

87. Starzyk RM, Schimmel P. Construction of intra-domain chimeras of aminoacyl-trna synthetases. J Biomol Struct Dyn 1989, Oct;7(2):225-34.

88. Su LJ, Brenowitz M, Pyle AM. An alternative route for the folding of large rnas: Apparent two-state folding by a group II intron ribozyme. J Mol Biol 2003, Dec 5;334(4):639-52.

89. Sun LQ, Cairns MJ, Saravolac EG, Baker A, Gerlach WL. Catalytic nucleic acids: From lab to applications. Pharmacol Rev 2000, Sep;52(3):325-47.

90. Sun Z, Tikhonova EB, Zgurskaya HI, Rybenkov VV. Parallel lipoplex folding pathways revealed using magnetic tweezers. Biomacromolecules 2012, Oct 8;13(10): 3395-400.

91. Talukder S, Chaudhury P, Metzler R, Banik SK. Determining the DNA stability parameters for the breathing dynamics of heterogeneous DNA by stochastic optimization. J Chem Phys 2011, Oct 28;135(16):165103.

92. Taneja B, Schnurr B, Slesarev A, Marko JF, Mondragón A. Topoisomerase V relaxes supercoiled DNA by a constrained swiveling mechanism. Proc Natl Acad Sci U S A 2007, Sep 11;104(37):14670-5.

93. Vlijm R, Smitshuijzen JS, Lusser A, Dekker C. NAP1-Assisted nucleosome assembly on DNA measured in real time by single-molecule magnetic tweezers. PLoS One 2012;7(9):e46306.

94. Volkin E, Astrahcan L. Intracellular distribution of labeled ribonucleic acid after phage infection of escherichia coli. Virology 1956, Aug;2(4):433-7.

95. Wang S, Karbstein K, Peracchi A, Beigelman L, Herschlag D. Identification of the hammerhead ribozyme metal ion binding site responsible for rescue of the deleterious effect of a cleavage site phosphorothioate. Biochemistry 1999, Oct 26;38(43): 14363-78.

96. Weinstein LB, Jones BC, Cosstick R, Cech TR. A second catalytic metal ion in group I ribozyme. Nature 1997, Aug 21;388(6644):805-8.

97. Wilcox JL, Ahluwalia AK, Bevilacqua PC. Charged nucleobases and their potential for RNA catalysis. Acc Chem Res 2011, Dec 20;44(12):1270-9.

98. Winardhi RS, Fu W, Castang S, Li Y, Dove SL, Yan J. Higher order oligomerization is required for H-NS family member mvat to form gene-silencing nucleoprotein filament. Nucleic Acids Res 2012, Oct 1;40(18):8942-52.

99. Woodson SA. Taming free energy landscapes with RNA chaperones. RNA Biol 2010;7(6):677-86.

100. Yan X, Cao Z, Lau C, Lu J. DNA aptamer folding on magnetic beads for sequential detection of adenosine and cocaine by substrate-resolved chemiluminescence technology. Analyst 2010, Sep;135(9):2400-7.

101. Yarus M. How many catalytic rnas? Ions and the cheshire cat conjecture. FASEB J 1993, Jan;7(1):31-9.

102. Yeo M, Rha SY, Jeung HC, Hu SX, Yang SH, Kim YS, et al. Attenuation of telomerase activity by hammerhead ribozyme targeting human telomerase RNA induces growth retardation and apoptosis in human breast tumor cells. Int J Cancer 2005, Apr 10;114(3):484-9.

103. You H, Iino R, Watanabe R, Noji H. Winding single-molecule double-stranded DNA on a nanometer-sized reel. Nucleic Acids Res 2012, Jul 5.

104. Zamaratski E, Trifonova A, Acharya P, Isaksson J, Maltseva T, Chattopadhayaya J. Do the 16 mer, 5'-GUGGUCUGAUGAGGCC-3' and the 25 mer, 5'-GGCCGAAACUCGUAAGAGUCACCAC-3', form a hammerhead ribozyme structure in physiological conditions? An NMR and UV thermodynamic study. Nucleosides Nucleotides Nucleic Acids 2001;20(4-7):1219-23.

CONCLUSIONS

In summary, the single molecule study and high resolution structure together present novel insights into the unique mechanochemical properties of the hammerhead ribozyme, one of the most prevalent autocatalytic motifs in nature. The single-molecule study, while describing the first important steps in developing a magnetic tweezers based study of hammerhead kinetics, was limited by the low-throughput nature of the assay. Thus, the structural studies described in CH2 represent the most important contribution to the field. The Mg^{2+}-ion-bound structure presented represents the highest resolution crystal structure of a hammerhead ribozyme to date (Table 3.1). The 1.55 Å structure reveals novel tertiary contacts

resulting from rotation of U(L5) which may be partially responsible for inducing and stabilizing conformational changes in the active site. Rotation of U(L5) may modulate the conserved AU Hoogsteen interaction (Figure 3.5), enabling the hammerhead to switch its activity between cleavage and ligation.

Prior to solution of the high-resolution *Schistosoma* structure, biochemical and structure experiments suggested a divalent metal ion was bound at the AP9/G10.1 site under physiological conditions (Kisseleva 2005; Lee 2007). However, crystal soaking experiments were not able to detect a metal ion at this site in the 2006 structure. In previous studies, the observation that several extended hammerheads cleaved at rates comparable to the minimal hammerhead in monovalent ions also suggested that divalent metals were primarily required to maintain the active fold.

In agreement with biochemical a structural findings, the new Mg^{2+}-bound structure demonstrates that a divalent metal ion does indeed occupy the A9/G10.1 position at a solution concentration of 10 mM Mg^{2+}. This finding confirms both structural (Scott et al. 1995) and spectroscopic measurements (Maderia et al. 2000b; Vogt et al. 2006; Osborne et al. 2009) indicating a higher-affinity population of the P9/G10.1 metal ion site in the tertiary stabilized hammerhead ribozyme. A bound magnesium in the A9/G10.1 site is also in agreement with coordination sites previously identified (Martick 2008; Martick and Scott, 2006; Chie 2008). In addition, both the Mn^{2+}-bound and Mg^{2+}-bound structure reveal well-ordered solvent molecules in the active site positioned to take part in proton transfer. Together, these data suggests an indirect catalytic role of divalent metals bound in site 2.

Furthermore, coordination to the P9/G10.1 site leads to a subtle rearrangement of the active core, clarifying the catalytic roles of several conserved functional groups.